FOURTH ANNUAL
CLIMATE ASSESSMENT
1992

U.S. DEPARTMENT OF COMMERCE
National Weather Service
National Meteorological Center
Climate Analysis Center

Climate Analysis Center
Camp Springs, Md
March 1993

FOURTH ANNUAL
CLIMATE ASSESSMENT
1992

EDITORS: M. S. Halpert
C. F. Ropelewski

TECHNICAL ASSISTANCE:
J. D. Kopman

U. S. DEPARTMENT OF COMMERCE
NATIONAL OCEANIC AND ATMOSPHERIC ADMINISTRATION
NATIONAL WEATHER SERVICE
NATIONAL METEOROLOGICAL CENTER

TABLE OF CONTENTS

LIST OF FIGURES

CONTRIBUTORS

Air Resources Laboratory/ERL/NOAA

J. Angell

Center for Ocean-Land-Atmosphere Interactions, Univ. of Maryland

B. E. Doty

Climate Analysis Center/NMC/NWS/NOAA

A. N. Basist
G. D. Bell
J. M. Chaplin
R. H. Churchill
D. R. Garrett
M. E. Gelman
M. S. Halpert
J. E. Janowiak
J. D. Kopman
V. E. Kousky
C. S. Long
A. J. Miller
D. Miskus
E. A. O'Lenic
C. F. Ropelewski
P. Sabol
P. A. Schultz
T. M. Smith
R. J. Tinker
H. M. Van den Dool

Climate Monitoring and Diagnostics Laboratory/ERL/NOAA

J. Peterson
E. Dutton

Climatic Research Unit, University of East Anglia, (UK)

P. D. Jones

Coupled Model Project/NMC/NWS/NOAA

A. Leetmaa
M. Ji
R. W. Reynolds

Hadley Centre for Climate Prediction and Research, (UK)

D. E. Parker

Johnson Research Center, University of Alabama in Huntsville

J. R. Christy

NASA Marshall Space Flight Center

R. W. Spencer

National Climatic Data Center/NESDIS/NOAA

R. R. Heim Jr.
T. R. Karl

Satellite Research Laboratory/NESDIS/NOAA

L. L. Stowe

South African Department of Environment Affairs

M. Laing

PREFACE

This report is designed to present a timely summary of recent observations of the global climate system and an early assessment and interpretation of the major climate anomalies of the past year. Our priority is to present the summary of data as soon as possible and to serve as a spur to further investigation. Subsequent research publications will undoubtedly revise and expand this brief descriptive volume. Our focus is on the global scale, with only limited attention to regional issues. We hope that this global perspective will support more detailed local and regional analyses.

ACKNOWLEDGMENTS

This assessment would not have been possible without the cooperation and contributions from several scientists representing a cross-section of the NOAA climate community. We also wish to acknowledge the contributions from several scientists outside of NOAA. Each of the contributors has our sincere thanks for their very timely and useful input. A special note of appreciation goes to Brian Doty of the Center for Ocean-Land-Atmosphere Interactions at the University of Maryland, for his invaluable help with much of the color graphics. We also thank the reviewers (D. Rodenhuis, V. Kousky, L. Mannello, P. Arkin, T. Karl, and M. Coughlan) for their comments and useful suggestions. This report is partially supported by the Climate and Global Change/Global Climate Perspectives System (GCPS) Project.

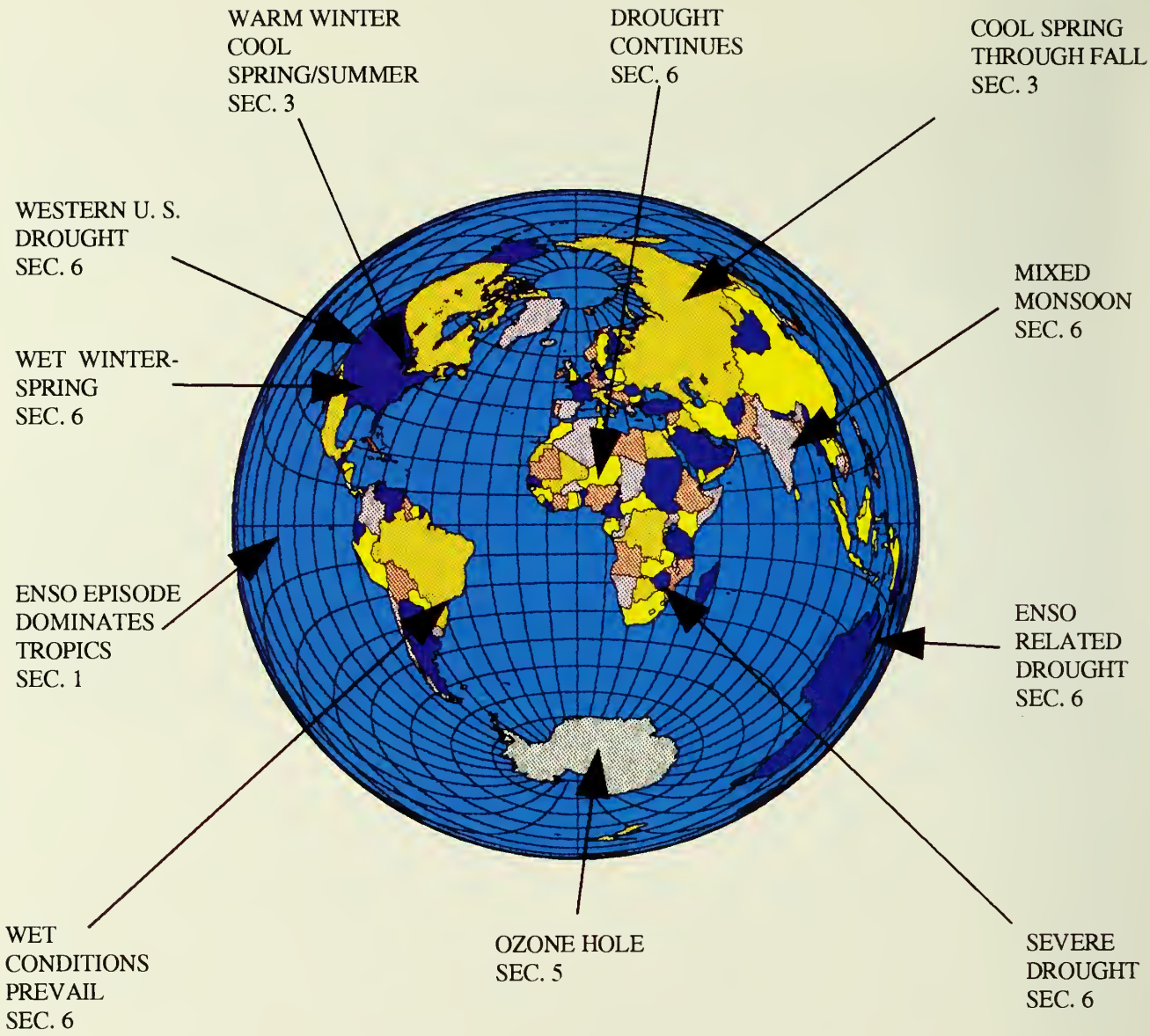

Fig. 1. Schematic depicting major climate events during 1992.

EXECUTIVE SUMMARY

Natural events such as the Mt. Pinatubo eruption in the Philippines and the El Niño/Southern Oscillation (ENSO) episode in the tropical Pacific Ocean had a major impact on the Northern Hemispheric climate in 1992. During the first part of the year, the 1991-92 ENSO episode contributed to much above normal temperatures in the Northern Hemisphere, while cooling during the latter part of the year was associated with the aerosol cloud that was produced by the eruption of Mt. Pinatubo in June 1991. By the spring of 1992, the stratospheric aerosol cloud had extended from the tropics well into the Northern Hemisphere. As the aerosol cloud spread throughout the Northern Hemisphere during a time of increasing solar radiation, the surface temperature anomalies responded by decreasing over much of the hemisphere. This cooling contributed to surface temperatures during 1992 being estimated as the coolest year since 1986. It was still, however, one of the warmest years in the historical surface record. Temperatures cooled dramatically throughout the troposphere as observed by radiosondes and satellites, while increasing in the lower stratosphere.

Significant precipitation anomalies during 1992 were also related to the long-lived ENSO episode (**Fig. 1**). The devastating drought over southeastern Africa was reported to be the worst in this region in over 100 years. Precipitation was generally lighter than normal in the monsoon regions of India and Australia. In North America, extremely wet conditions occurred in the southwestern United States during the December 1991 - May 1992 period. The resurgence of the ENSO late in the year was associated with much needed precipitation along the drought-stricken west coast of the United States.

The presence of volcanic aerosols in the stratosphere may have further depleted the already seriously reduced ozone concentrations over the polar regions of the Southern Hemisphere. 1992 ozone values during the springtime in the Antarctic stratosphere were the lowest ever observed, while the area of the ozone hole was larger than ever recorded, more than 50% larger than in 1991 and 1987, the previous maximum years of record. The depth of the ozone hole also increased during 1992, extending from altitudes of 14 to 18 km.

1. EL NIÑO/SOUTHERN OSCILLATION (ENSO)

The Southern Oscillation is the major mode of interannual climate variability. Since 1990, the ocean/atmosphere system has been involved in various stages of an unusually long-lived warm (ENSO) episode. Furthermore, the interpretation of the climate of 1992 has been complicated by the fact that the 1991/92 ENSO demonstrated a resurgence in the latter half of the year.

Weak warm episode conditions were observed in the tropical Pacific from early 1990 through mid-1991, featuring positive sea surface temperature (SST) anomalies in the western equatorial Pacific (**Fig. 2**, bottom), slightly enhanced convection in the same region (**Fig. 3**, bottom), and weaker than normal equatorial 850 mb easterlies throughout the Pacific (**Fig. 4**). Winds and heights in the troposphere are derived from the NMC operational Global Data Assimilation System (GDAS). During that period the warmest equatorial water in the Pacific was located between 160°E and 170°E (**Fig. 2**, top). Beginning in mid-1991 the warmest water gradually shifted eastward, crossing the date line in late 1991 and reaching as far east as 160°W by March 1992. This was accompanied by a similar eastward shift of the strongest equatorial convection [associated with outgoing longwave radiation (OLR) values less than 220 Wm^{-2}, **Fig. 3**, top] and an increase in the magnitude of the negative OLR anomalies in the central equatorial Pacific (**Fig. 3**, bottom and **Fig. 5**).

During December 1991 through April 1992, precipitation anomalies in many tropical and subtropical regions were consistent with those generally observed during the mature phase of a warm episode (**Fig. 6**). Excessive rainfall was observed over central South America, over northern Mexico and over the western gulf states of the United States. During January, heavy rains extended into southern California where severe flooding occurred. Flooding was also observed throughout much of the December through April period in eastern Texas. In contrast, severe drought plagued southeastern Africa, the Philippines, northern Australia and the Caroline Islands in the western Pacific.

By March 1992, which is close to the maximum in the mean annual cycle of SST in the eastern equatorial Pacific, anomalous convection extended eastward to the South American coast (**Fig. 3**, bottom). SST anomalies along the coast reached values greater than +2°C and were reported to be locally greater than +4°C at stations along the northern coast of Peru, as El Niño conditions developed in that region. During the period from late May to mid-July, SST and OLR anomalies rapidly decreased in the eastern equatorial Pacific (**Fig. 2**, bottom and **Fig. 5**) as the equatorial cold tongue became reestablished. From mid-July through December, 1992 SST anomalies returned to weak warm episode conditions, similar to those observed from 1990 to mid-1991, characterized oceanic and atmospheric anomaly fields.

The evolution of the subsurface oceanic thermal field along the equator from mid-1991 to mid 1992 was, in many respects, similar to that observed during the 1986-1987 warm episode. Data used in monitoring the subsurface thermal structure are derived from an analysis system which assimilates oceanic observations into an oceanic general circulation model (*Leetmaa and Ji, 1989*). Between August 1991 and October 1991, the thermocline depth increased in the central and eastern equatorial Pacific (**Fig. 7**), resulting in temperature anomalies of greater than

+6°C near 120 m depth in the region around 140°W (**Fig. 8**). At the same time, the thermocline was shoaling in the western portion of the basin (**Figs. 7 and 8**). From October 1991 through March 1992, there was a steady eastward propagation of the subsurface temperature anomaly pattern (**Figs. 8 and 9**), as the thermocline continued to deepen in the eastern equatorial Pacific and the shoaling spread from the western Pacific into the central Pacific. By May 1992, the thermocline was abnormally shallow throughout much of the equatorial Pacific, which resulted in negative subsurface temperature anomalies at 100 m that dominated the region from the western Pacific eastward to near 110°W. Subsurface conditions changed very little along the equator from May through September 1992 (**Figs. 9 and 10**). However, beginning in October and continuing through December the thermocline again deepened in the central and eastern equatorial Pacific, and subsurface temperature anomalies increased to greater than +4°C near 120 m depth in the region around 130°W. Thus, at the end of 1992, aspects of the subsurface thermal field resembled that observed during the mature phases of the 1986-1987 and 1991-1992 warm episodes.

Similarly, at the end of 1992 atmospheric fields also exhibited characteristics typical of a warm episode. Sea level pressure was anomalously low (high) over the central and eastern tropical Pacific (over Indonesia) and the Southern Oscillation Index (SOI) was near -1.0 (**Fig. 11**). Enhanced convection developed along the equator near the date line (**Fig. 3**, bottom), as equatorial easterlies remained weaker than normal throughout the Pacific (**Fig. 4**).

During the period 1990-1992, the low-level equatorial easterlies have been weaker than normal (westerly anomalies) (**Fig. 4**), convection has been enhanced in the western equatorial Pacific (**Fig. 3**, bottom) and SST has been anomalously warm in the central equatorial Pacific (**Fig. 2**, bottom). Throughout this period, negative (positive) sea level pressure anomalies have dominated the eastern (western) equatorial Pacific, and the SOI has been predominantly negative (**Fig. 11**). The most recent warm episode featuring a similar prolonged period of negative values of the SOI was 1939-1941. A more comprehensive comparison between that period and the present warm episode is not possible due to the lack of SST data during World War II.

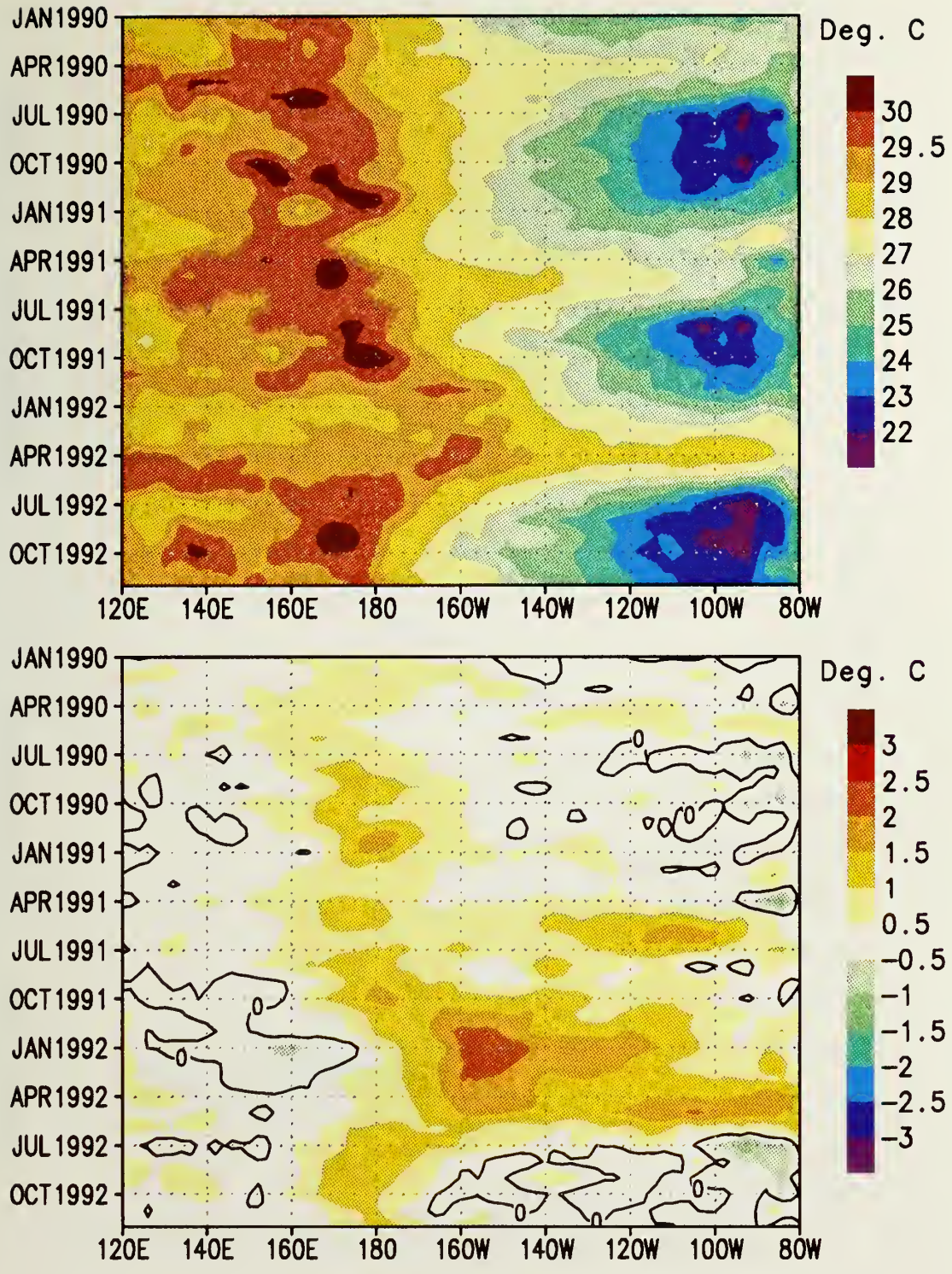

Fig. 2. Time-longitude section of mean (top) and anomalous (bottom) sea surface temperature (SST) averaged from 5N-5S. Anomalies are departures from the COADS/ICE climatology (Reynolds, 1988). (Data provided by R. Reynolds.)

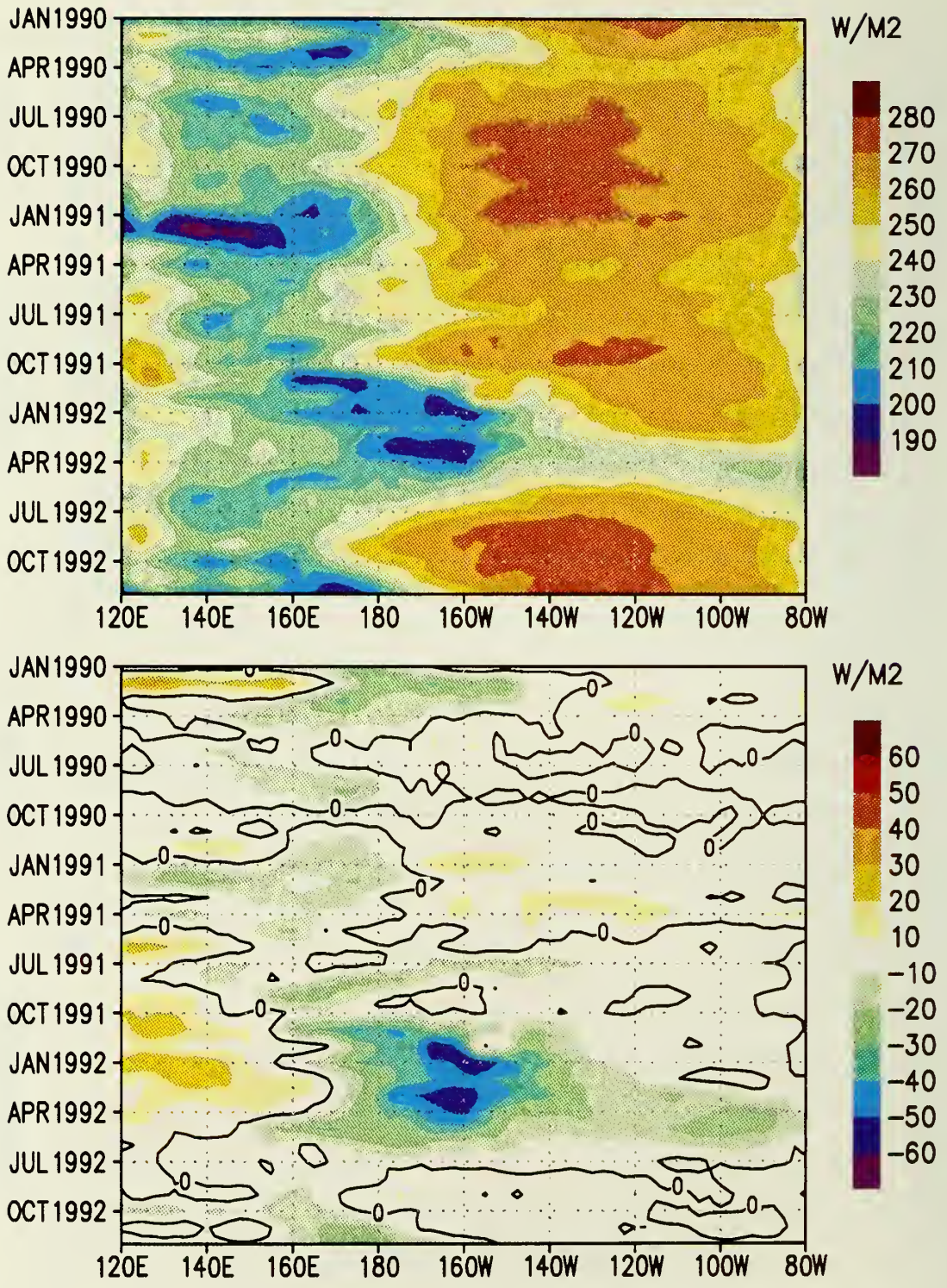

Fig. 3. Time-longitude section of mean (top) and anomalous (bottom) outgoing longwave radiation (OLR) averaged from 5N-5S. (Source: CAC)

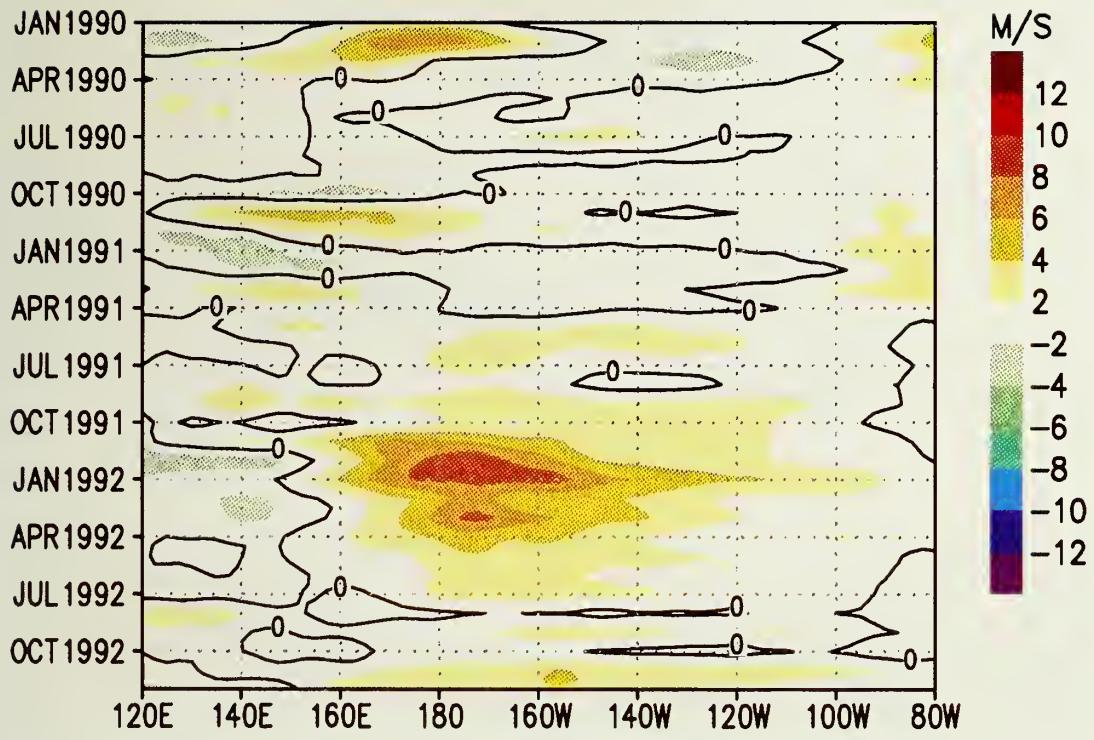

Fig. 4. Time–longitude section of monthly anomalous 850 mb zonal wind averaged from 5N–5S. Anomalies are departures from the 1979–1988 base period monthly means. (Source: CAC)

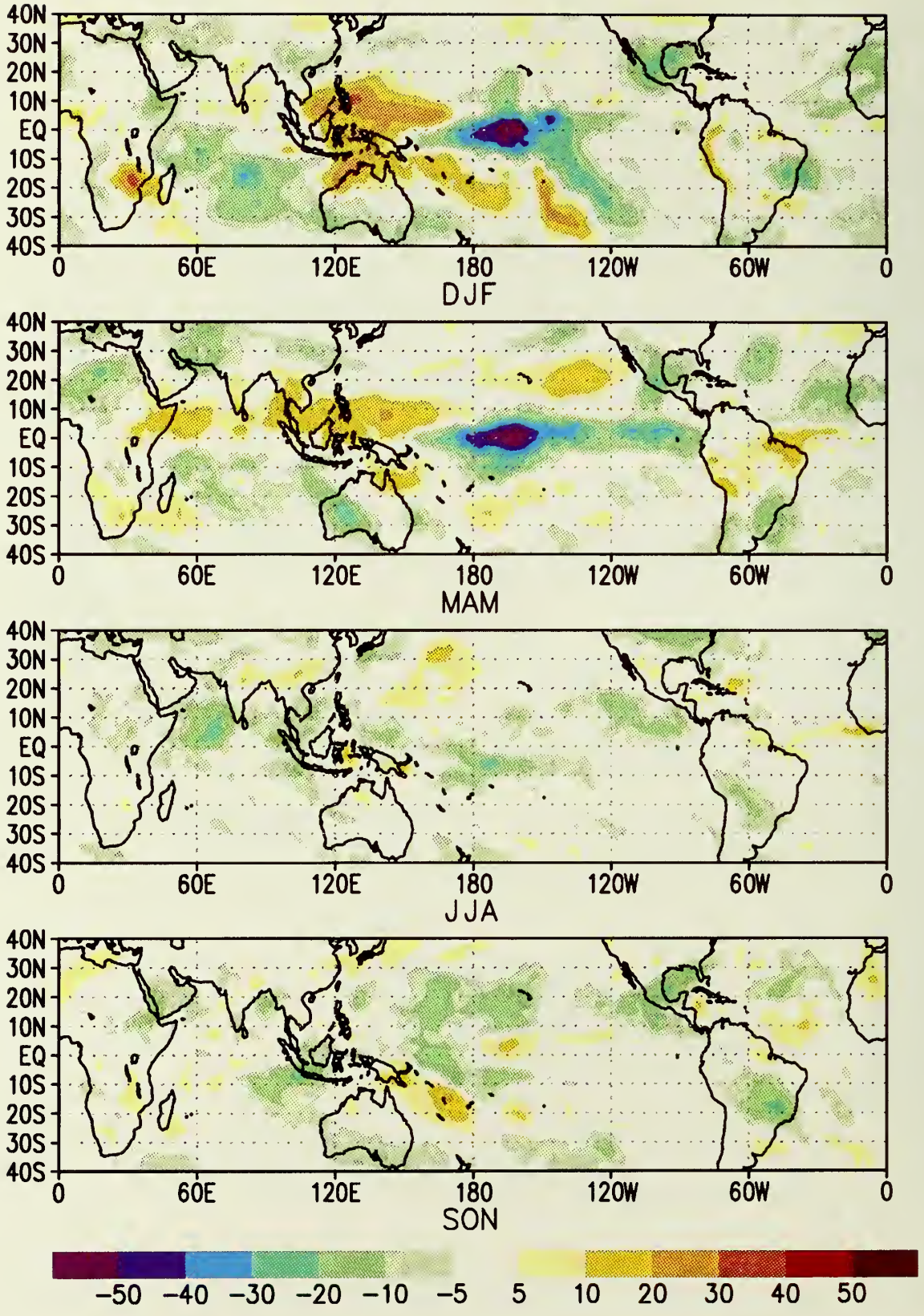

Fig. 5. Seasonal outgoing longwave radiation (OLR) anomalies (W/M2) computed relative to the 1979–1988 base period mean.

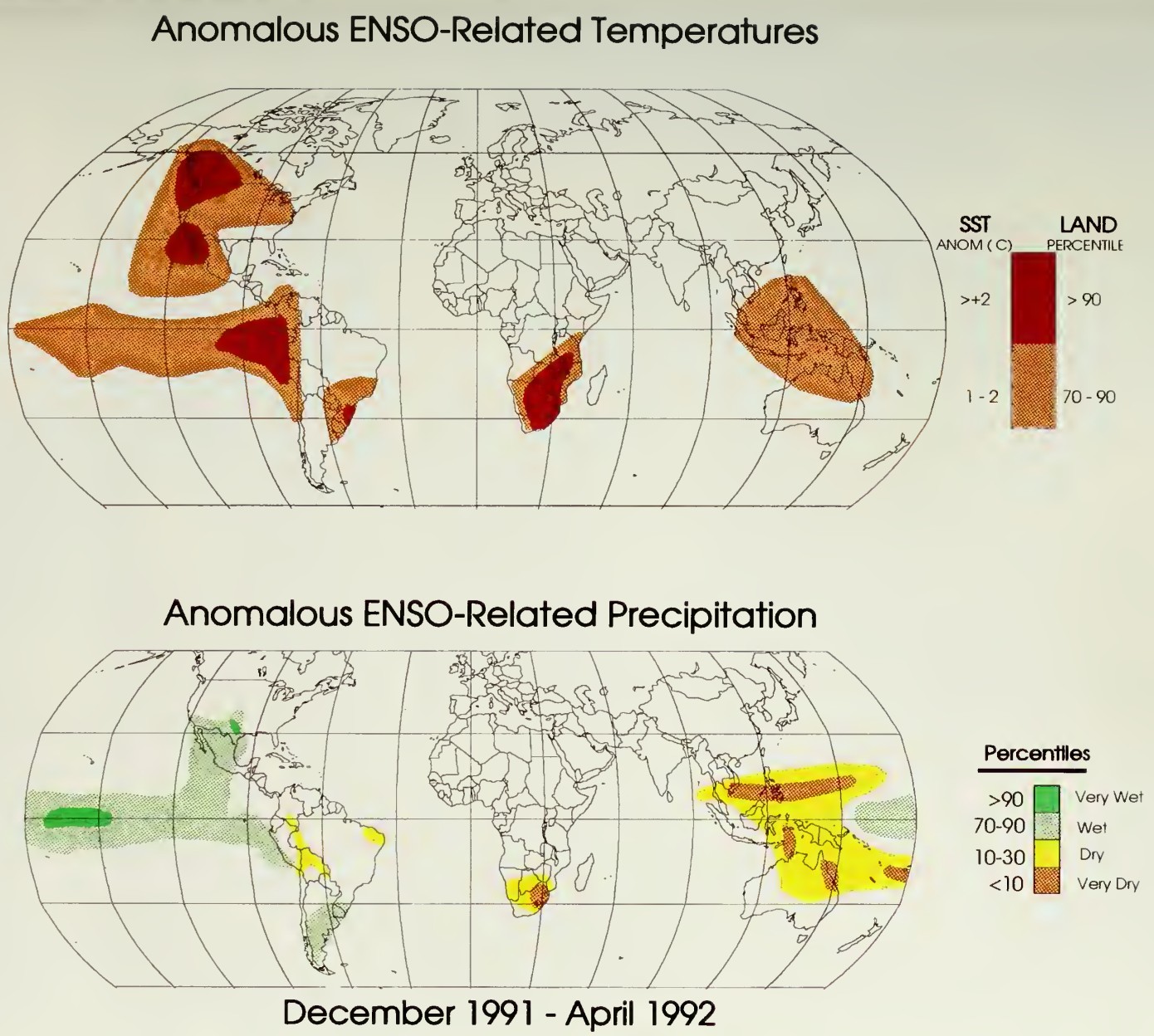

Fig. 6. Schematic depicting regions of anomalous ENSO-related temperatures (top) and anomalous ENSO-related precipitation (bottom) during the December 1991 - April 1992 period.

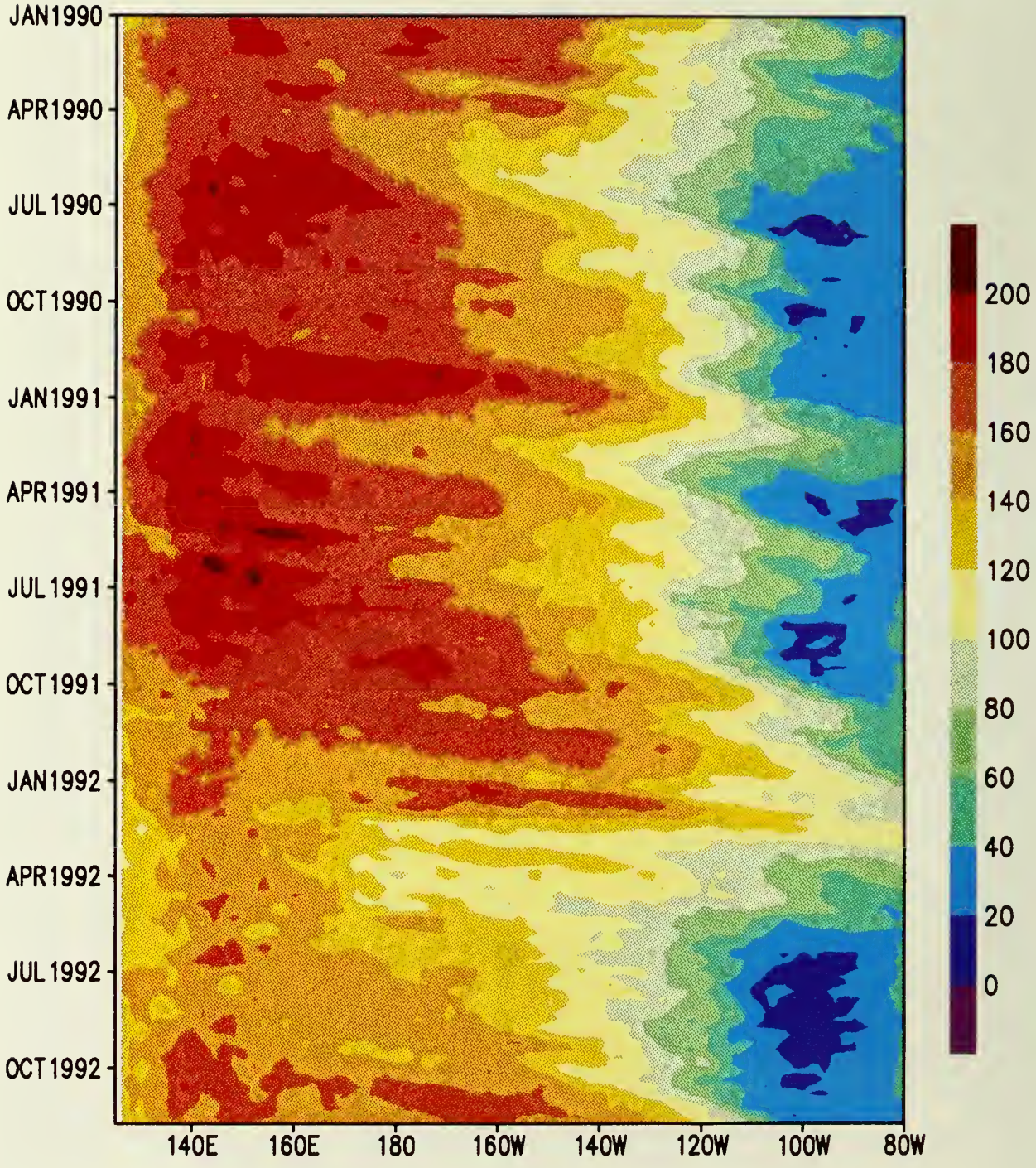

Fig. 7. Time–longitude section of the depth of the 20C isotherm along the equator in the Pacific Ocean. (Data provided by Leetmaa and Ji.)

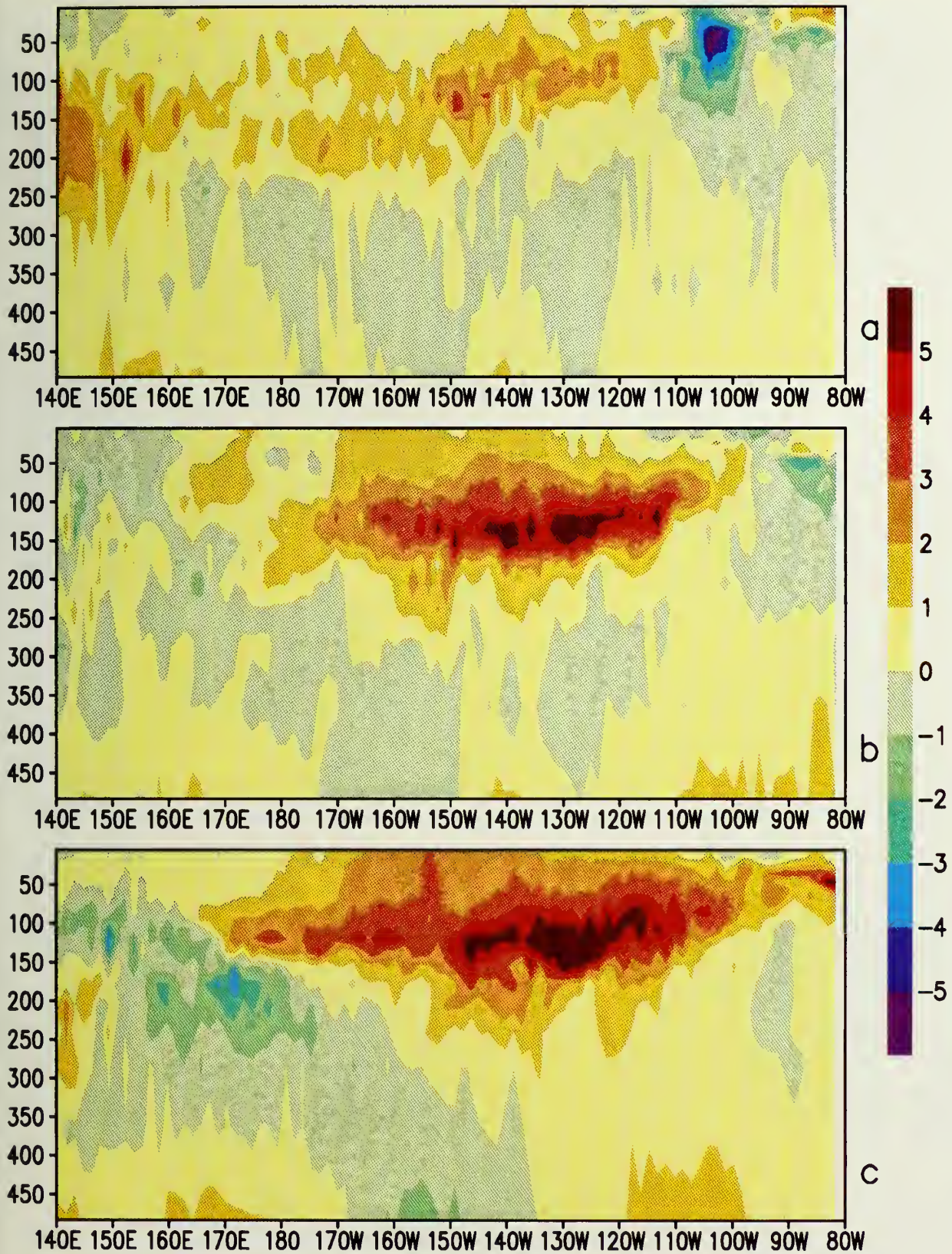

Fig. 8. Depth–longitude section along the equator of anomalous temperature for the weeks centered on a) 14 August 1991, b) 16 October 1991, and c) 18 December 1991. (Data provided by Leetmaa and Ji.)

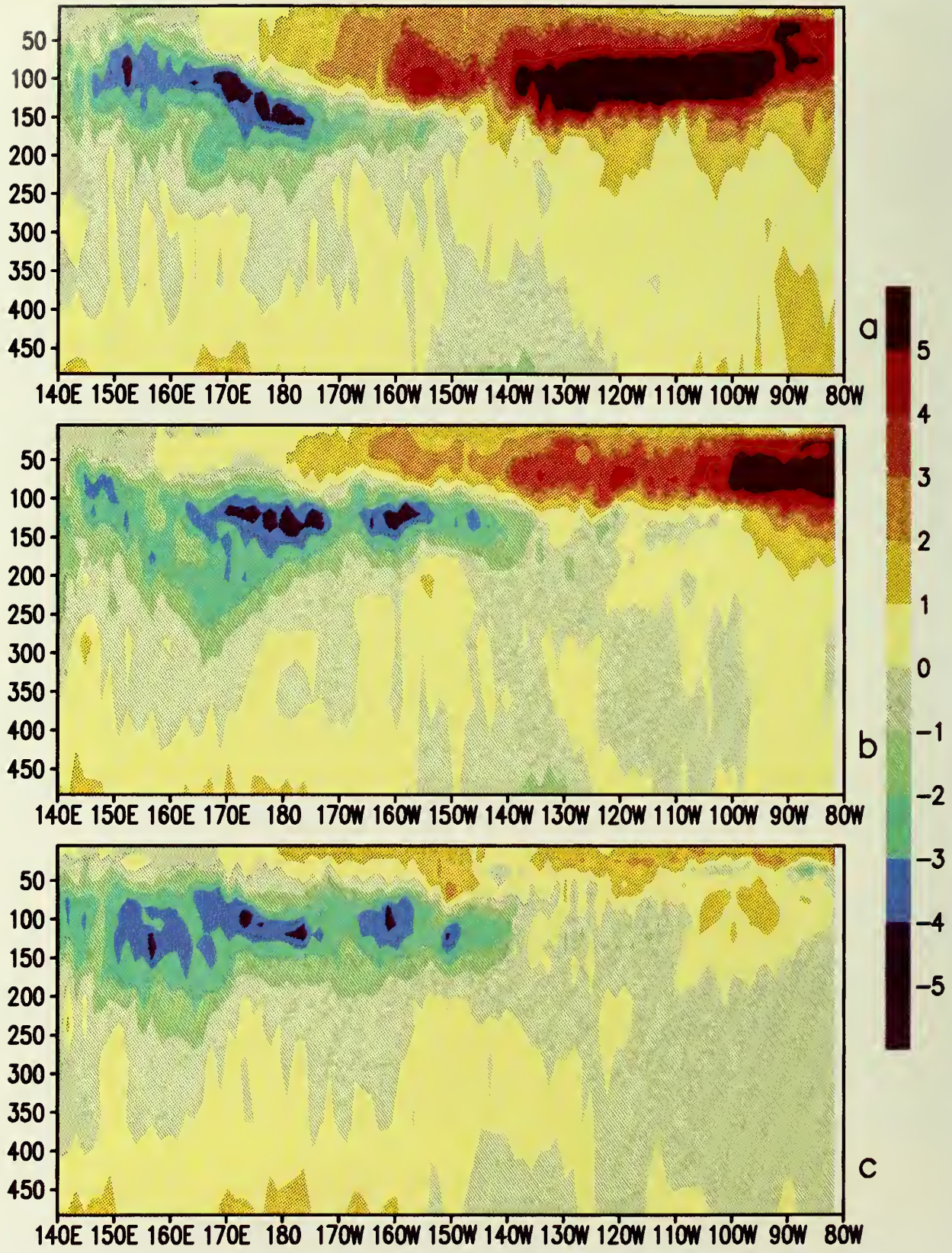

Fig. 9. Depth–longitude section along the equator of anomalous temperature for the weeks centered on a) 19 February 1992, b) 18 March 1992, and c) 20 May 1992. (Data provided by Leetmaa and Ji.)

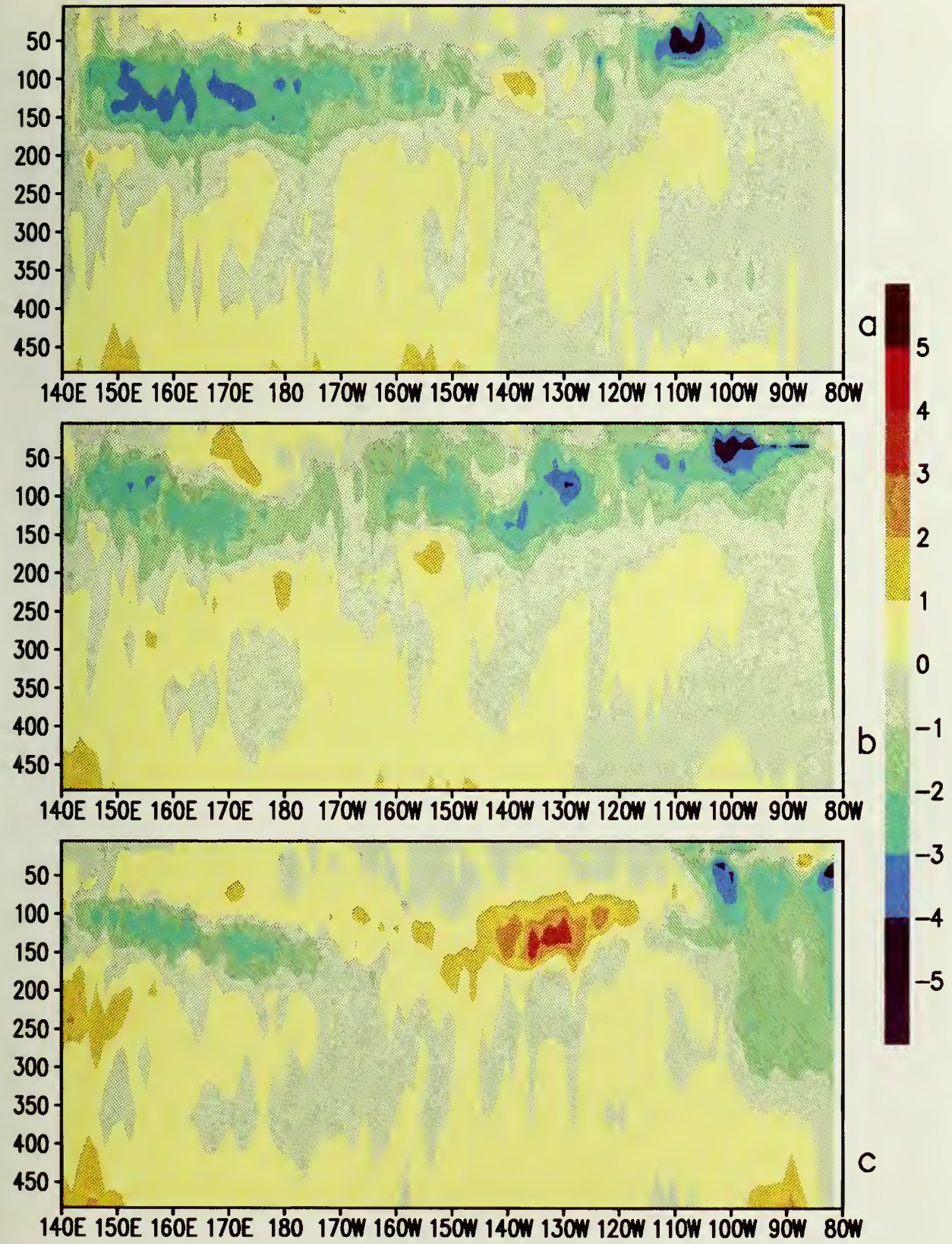

Fig. 10. Depth–longitude section along the equator of anomalous temperature for the weeks centered on a) 15 July 1992, b) 16 September 1992, and c) 16 December 1992. (Data provided by Leetmaa and Ji.)

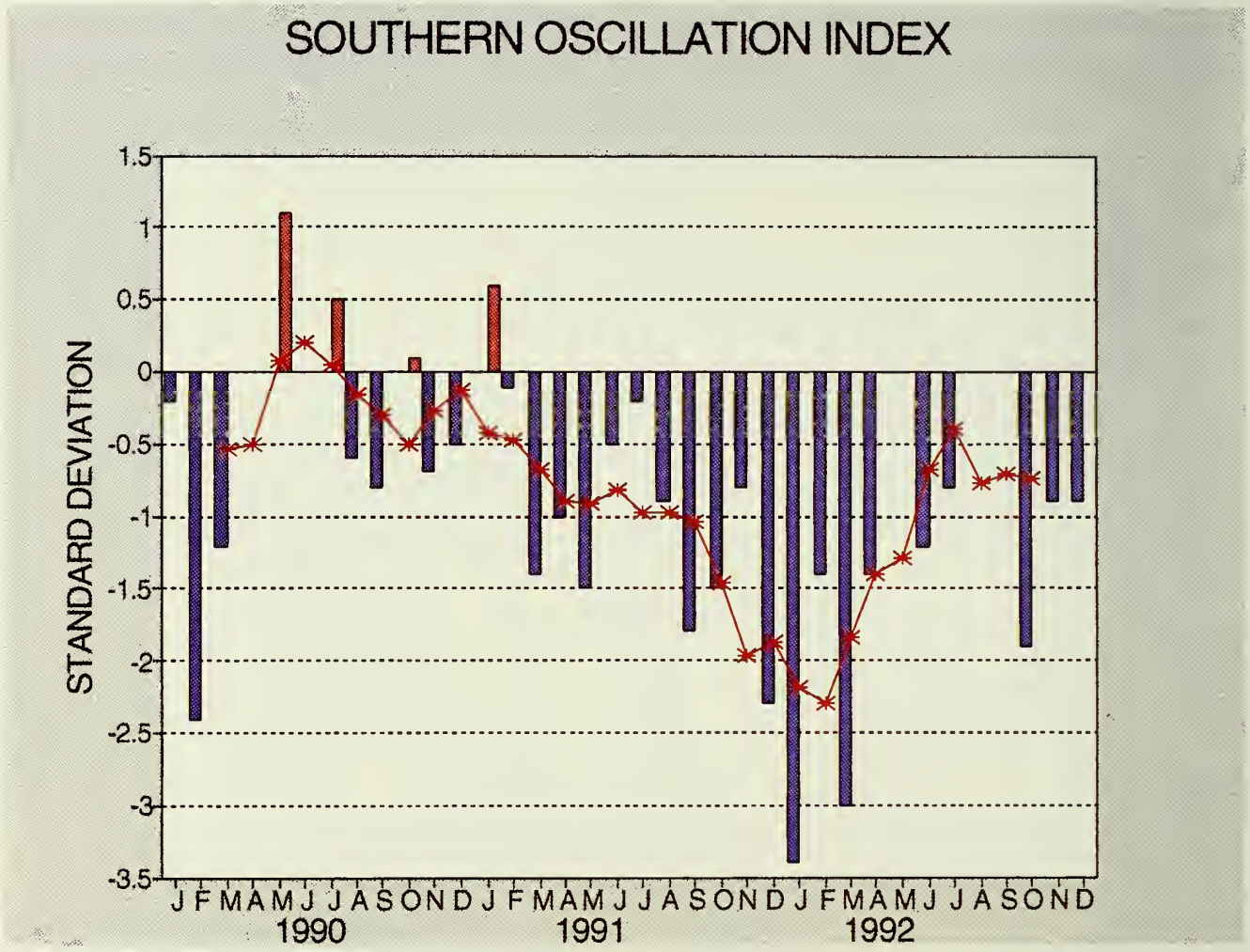

Fig. 11. Standardized Southern Oscillation Index (SOI). Monthly (five month running mean) values are indicated by the bar (line) graph.

2. ATMOSPHERIC CIRCULATION

a. General Circulation

In the tropics, positive zonally-averaged 200 mb height anomalies (**Fig. 12**) were observed between December 1991-April 1992, with negative height anomalies observed thereafter. This height anomaly pattern reflected mature ENSO conditions in the tropical Pacific during the first part 1992, and a weakening of ENSO conditions during May and June. The persistence of negative height anomalies after May also reflected continued above normal temperatures in the tropical lower stratosphere, associated with the eruption of Mt. Pinatubo during July 1991..

Prior to 1992, negative 200 mb height anomalies were observed throughout the tropics during much of 1990, reflecting lingering cold-episode effects that had dominated the tropics since the 1988-1989 Pacific cold event. Positive 200 mb height anomalies then became established in the tropics during January - August 1991, as tropical conditions trended toward the 1991-1992 ENSO event. This transition to positive height anomalies occurred coincident with the development of below normal tropical lower stratospheric temperatures during January 1991. A rapid transition to negative height anomalies then occurred during September 1991, two months following the sharp increase in lower stratospheric temperatures associated with the eruption of Mt. Pinatubo. These negative height anomalies persisted until December 1991, when mature ENSO conditions became established in the tropical Pacific.

In the extratropics, negative 200 mb height anomalies were observed throughout the subtropical and lower mid-latitudes of both hemispheres during much of 1992. Previously, positive height anomalies had generally dominated these latitudes since January 1990. The transition to negative height anomalies occurred during October 1991, in conjunction with increased lower stratospheric temperatures associated with the eruption of Mt. Pinatubo, and with an increased trend toward mature ENSO conditions in the tropical Pacific.

At higher latitudes, positive 200 mb height anomalies were concentrated primarily in the Southern Hemisphere, while negative height anomalies were concentrated in the Northern Hemisphere during 1992. This anomaly pattern in the Southern Hemisphere had persisted since April 1991, and began to dissipate during the second half of 1992. During this period, two prolonged blocking episodes (May-July 1991 and March-June 1992) were observed over the southeastern South Pacific, which contributed to the pronounced maxima in zonally-averaged 200 mb height anomalies near 65°S. The 200 mb height anomaly pattern in both hemispheres during 1992 is also consistent with enhanced sub-tropical westerlies, and weaker than normal mid-latitude westerlies. This wind anomaly pattern is opposite to that observed during much of 1990 and 1991.

Negative height anomalies tended to be concentrated over the polar regions of both hemispheres during 1992. In the Southern Hemisphere, this circulation pattern reflected a particularly enhanced polar vortex throughout much of the year, with maximum anomalous vortex strength observed during the cool season.

Over the Northern Hemisphere, the 500 mb mid-latitude circulation during December 1991-February 1992 was dominated by persistent positive height anomalies over Europe and the western United States and Canada, and by negative height anomalies throughout the eastern North Pacific and central Russia (**Fig. 13a**). During March - May (**Fig. 14a**), negative height anomalies were observed throughout the middle latitudes of the central and eastern North Pacific, while positive height anomalies were observed over the high latitudes of the North Pacific. Farther east, positive height anomalies remained over the eastern North Atlantic and central Europe.

The 500 mb circulation during June-August (**Fig. 15a**) was dominated by positive height anomalies over northwestern North America and by negative height anomalies over central Canada and the north central United States. Weak, but persistent, positive height anomalies remained over Europe. At higher latitudes, negative height anomalies were observed throughout the polar region and Greenland during the entire December 1991-August 1992 period. In contrast, the circulation during September-November (**Fig. 16a**) was dominated by negative height anomalies over Europe and northwestern North America, and by positive height anomalies over the polar region.

Over the Southern Hemisphere, the 500 mb circulation during December 1991- May 1992 was dominated by positive height anomalies over the high latitudes of the eastern South Pacific, and by negative height anomalies over portions of the mid-central and mid-eastern South Pacific (**Figs. 13b, 14b**). This height anomaly pattern then weakened during June-August (**Fig. 15b**), and completely dissipated during September-November (**Fig. 16b**). Farther west, negative height anomalies were observed over the high latitudes of the central Indian Ocean throughout the entire December 1991-August 1992 period. This overall anomalous circulation pattern was associated with enhanced westerlies over the mid-central Indian Ocean, and with reduced westerlies and a strong spilt-flow/ blocking configuration over the high latitudes of the central and eastern South Pacific.

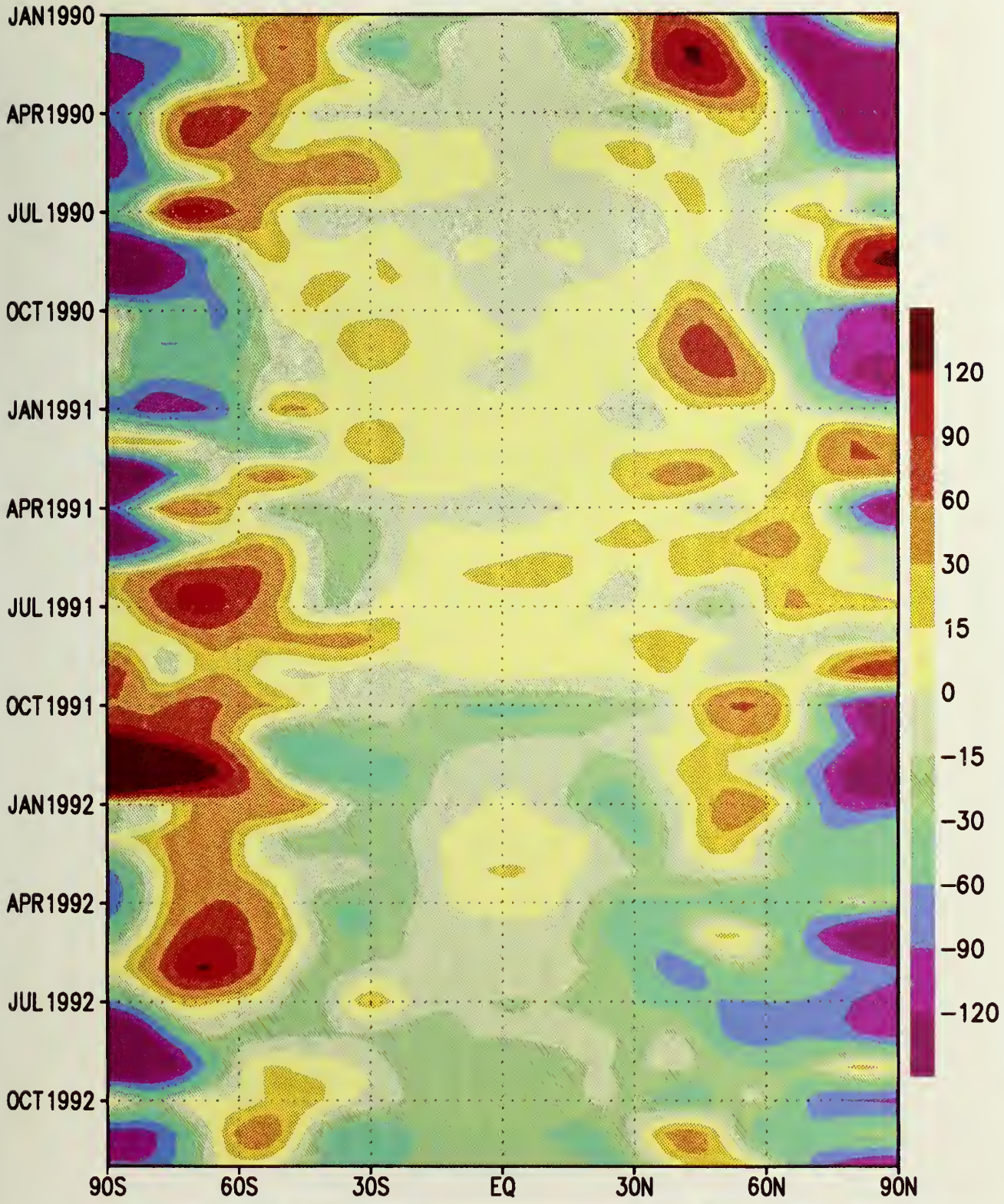

Fig. 12. Time–latitude section of zonally averaged monthly mean 200 mb height anomalies (m). Anomalies are departures from the 1979–1988 base period. (Source: CAC)

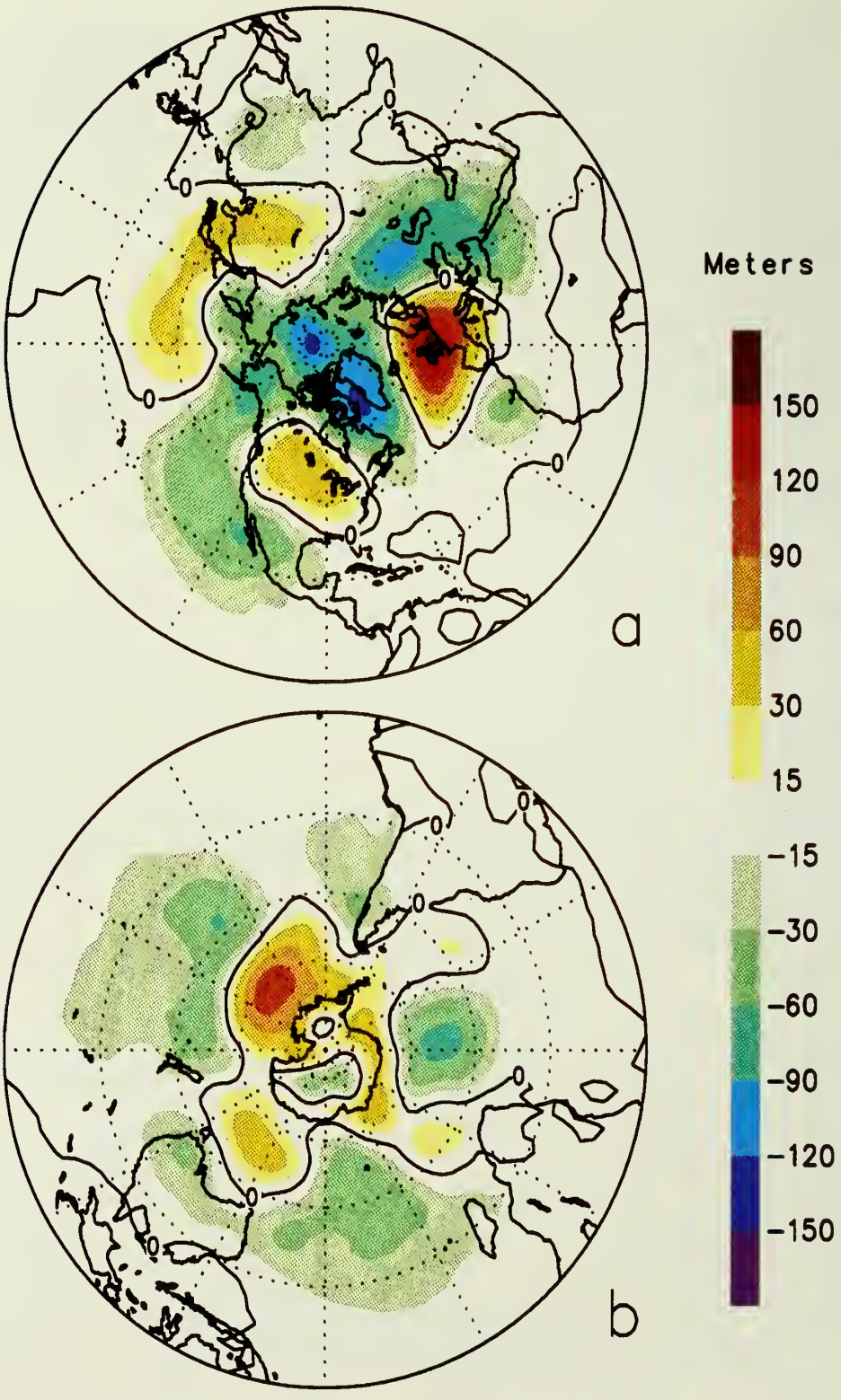

Fig. 13. 500 mb height anomalies for December 1991 – February 1992 for the a) Northern Hemisphere and the b) Southern Hemisphere. Anomalies are computed from the 1979–88 base period.

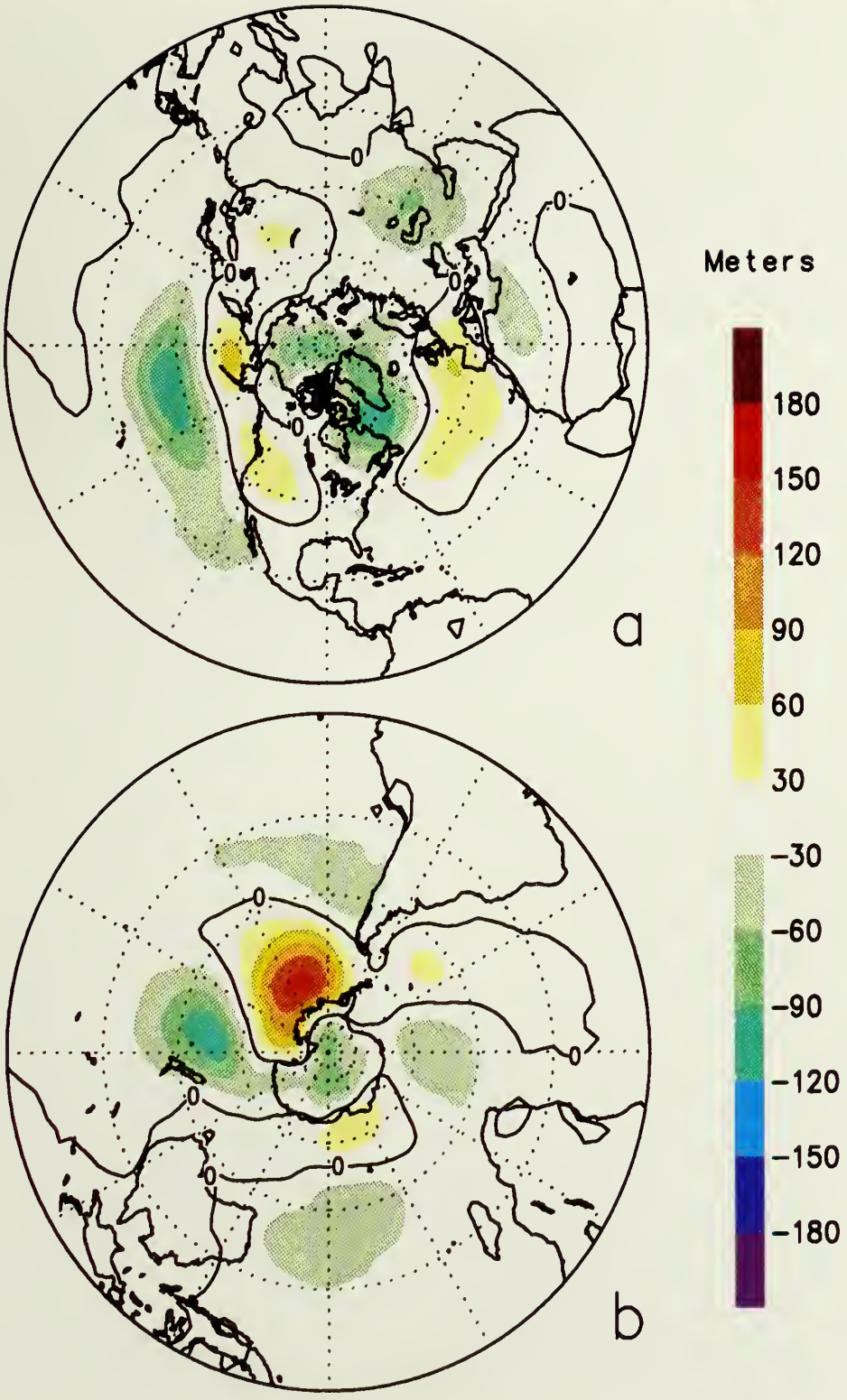

Fig. 14. 500 mb height anomalies for March – May 1992 for the a) Northern Hemisphere and the b) Southern Hemisphere. Anomalies are computed from the 1979–88 base period.

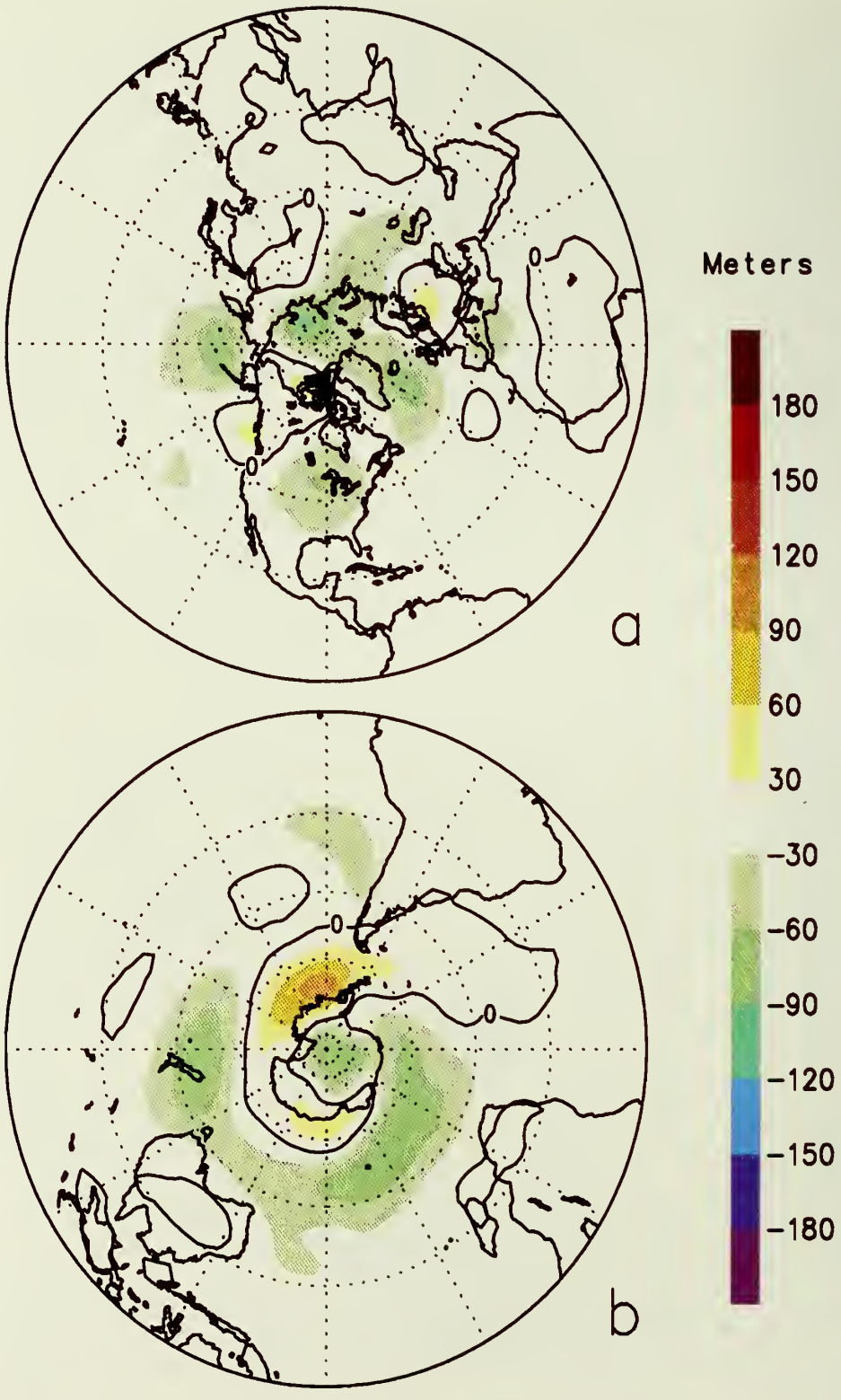

Fig. 15. 500 mb height anomalies for June – August 1992 for the a) Northern Hemisphere and the b) Southern Hemisphere. Anomalies are computed from the 1979–88 base period.

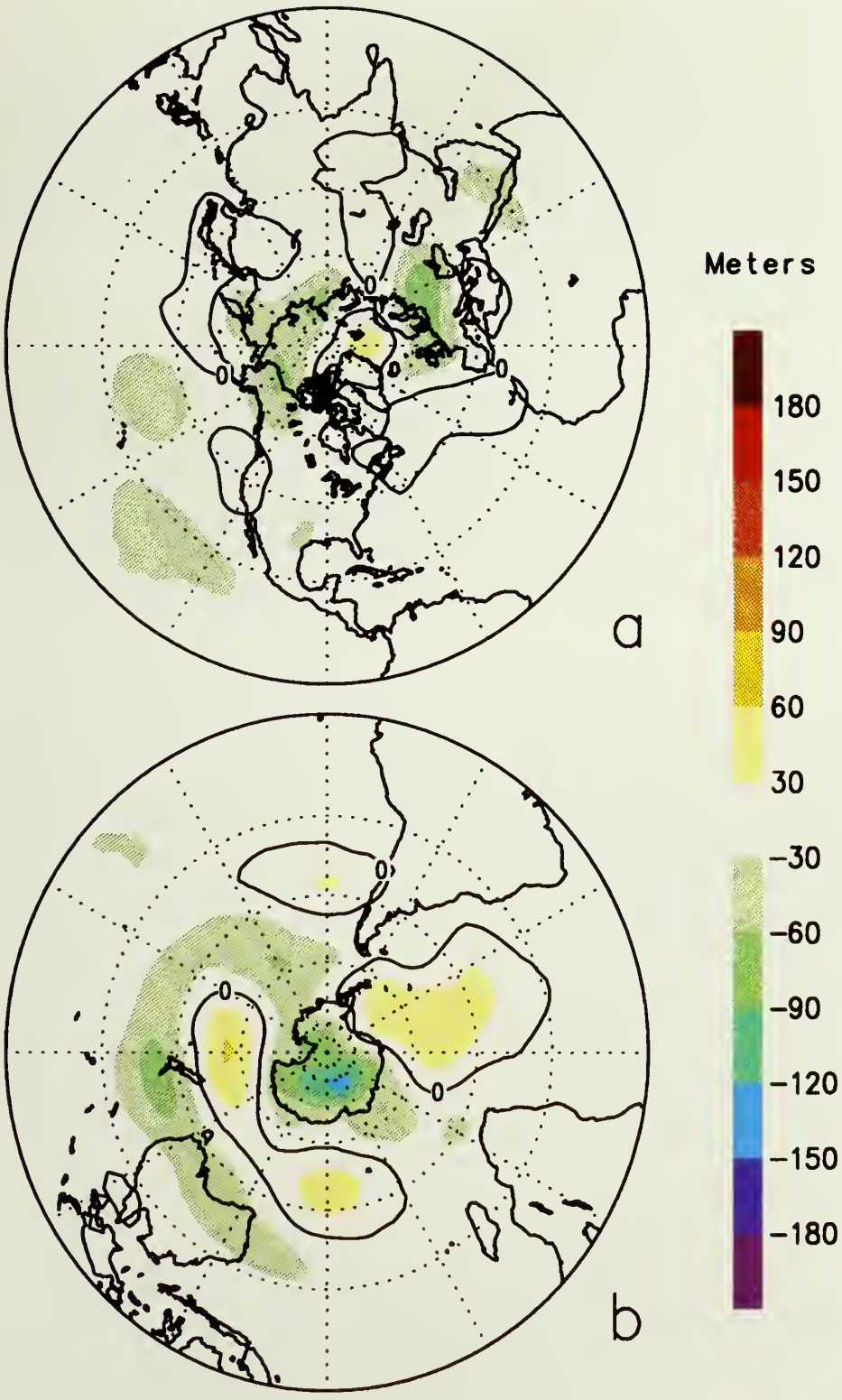

Fig. 16. 500 mb height anomalies for September – November 1992 for the a) Northern Hemisphere and the b) Southern Hemisphere. Anomalies are computed from the 1979–88 base period.

b. Specific Circulation Events

The mid-latitude circulation during two periods in which height anomalies were particularly persistent over both North America and Europe (December 1991 - February 1992 and March-August 1992) are described below. Each of these episodes was associated with highly anomalous surface temperature and precipitation patterns, and with a well-defined pattern of lower stratospheric temperature anomalies.

December-February (DJF) 1991-1992

The Northern Hemisphere flow pattern during DJF was dominated by extremely persistent and long-lived circulation anomalies throughout much of the middle latitudes (**Figs. 13a, 17, 18**). Persistent positive height anomalies were observed primarily throughout both the northern United States and western Europe. Persistent negative height anomalies were observed throughout the polar region and Greenland, over virtually the entire eastern North Pacific, and throughout the eastern Mediterranean Sea and Caspian Sea sectors. The positive height anomalies throughout Europe were associated with strong negative lower stratospheric temperature anomalies (**Fig. 19a**).

The anomalous circulation over North America was dominated by a pronounced split-flow pattern over the western United States, and by a strongly enhanced subtropical jet, extending eastward from the eastern North Pacific to the southeastern United States. This enhanced jet, in association with mature ENSO conditions in the tropical Pacific, produced above normal precipitation totals over much of the southwestern and southern United States (see Sec. 6). Farther north, anomalous southwesterly flow was observed throughout the Pacific Northwest, the northern Great Plains and Canada, and over large portions of southern Alaska. These regions experienced well above normal surface temperatures during the period (see Sec. 3).

The circulation over the North Atlantic and Europe during DJF was dominated by an anomalous wave pattern extending southeastward from Greenland to western Russia, and by a major blocking anticyclone over Europe. This wave pattern was associated with well-above normal surface temperatures throughout Europe, and with much below normal surface temperatures throughout the eastern Mediterranean and Middle East (see Sec. 3).

May-August 1992

The Northern Hemisphere flow pattern during May-August was dominated by persistent negative height anomalies throughout the eastern United States and eastern Canada, over the polar region and Greenland, and throughout the eastern Mediterranean Sea sector (**Figs. 14a, 15a, 20, 21**). Persistent positive height anomalies were observed primarily over the eastern Gulf of Alaska and over central Europe. Each of these regions experienced above normal surface temperatures during the period. The overall height anomaly pattern (**Fig. 15a**) is also strongly negatively correlated with the pattern of lower stratospheric temperature anomalies (**Fig. 19b**).

Over North America, the highly amplified wave pattern was associated with anomalous northwesterly flow throughout central and eastern Canada and the Great Lakes region. Individual

low-pass filtered height analyses indicate that the northwesterly flow originating over eastern Siberia and the Arctic Ocean region dominated the entire period between May and mid-August (**Figs. 22, 23a**), resulting in a continuous influx of arctic air into central and eastern Canada. The southern extent of this anomalously cold air then reached well into the central United States, in association with the persistent negative height anomalies over the region. The anomalous wave pattern began to dissipate during early August, and had completely disappeared by late August (**Fig. 23b**). This major circulation transition was associated with the flow being directed from the eastern North Pacific (instead of the Arctic) to central Canada, and with a return to near-normal surface temperatures throughout central and eastern Canada and the United States.

Analogs to the above persistent circulation over North America, along with the corresponding pattern of well-below normal surface temperatures, can be found in 1950, 1951, 1958, 1967, 1972, 1982 and 1985. Clearly, this circulation pattern is not necessarily associated with volcanic eruptions such as Mt. Pinatubo. In contrast, the opposite phase of this circulation pattern, characterized by negative height anomalies over the Gulf of Alaska and by positive height anomalies over the eastern United States and eastern Canada, is associated with well-above normal surface temperatures throughout the central and eastern United States and Canada. Analogs to this opposite flow pattern can be found during the summers of 1952-1955, 1959, 1980, 1983, 1987, 1988 and 1991.

Over the European sector, the highly-amplified wave pattern was associated with anomalous southwesterly flow over much of Europe and southern Scandinavia, and with anomalous northwesterly flow over the eastern Mediterranean sector. This wave pattern was also associated with a major blocking anticyclone over Europe (10°W-25°E) between mid-May and mid-June, and with a well-defined trough amplification farther downstream (**Fig. 21**). This downstream trough amplification was associated primarily with well below normal surface temperatures over central Russia, and with a reinforcement of the negative height anomalies and below normal surface temperatures over the eastern Mediterranean sector during the period.

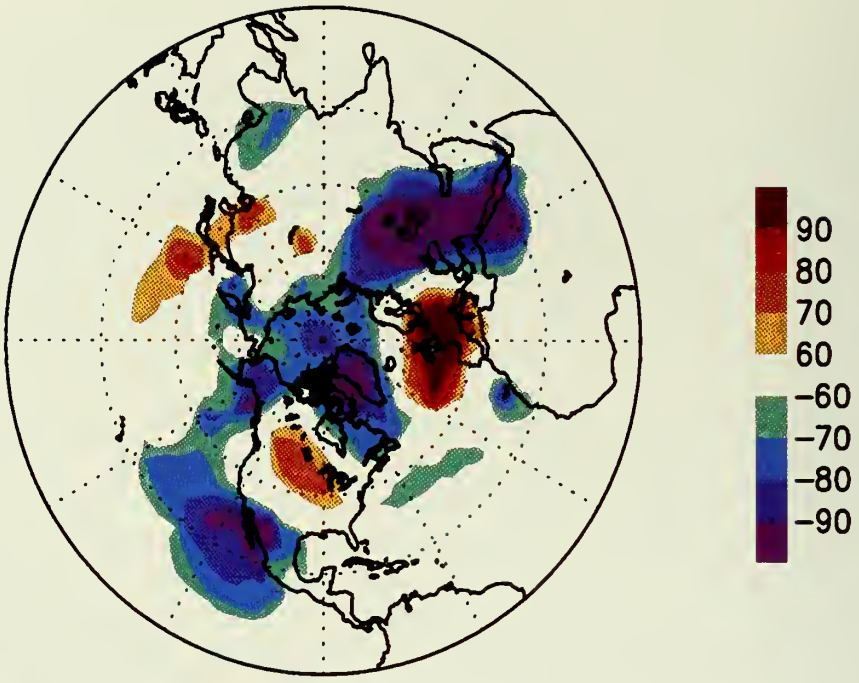

Fig. 17. Percentage of days during December 1991–February 1992 in which daily low-pass fltered 500 mb height anomalies greater than 15 m and less than −15 m were observed. Cutoff period of low pass filter is 30 days. Anomalies are computed from the 1979–1988 base period.

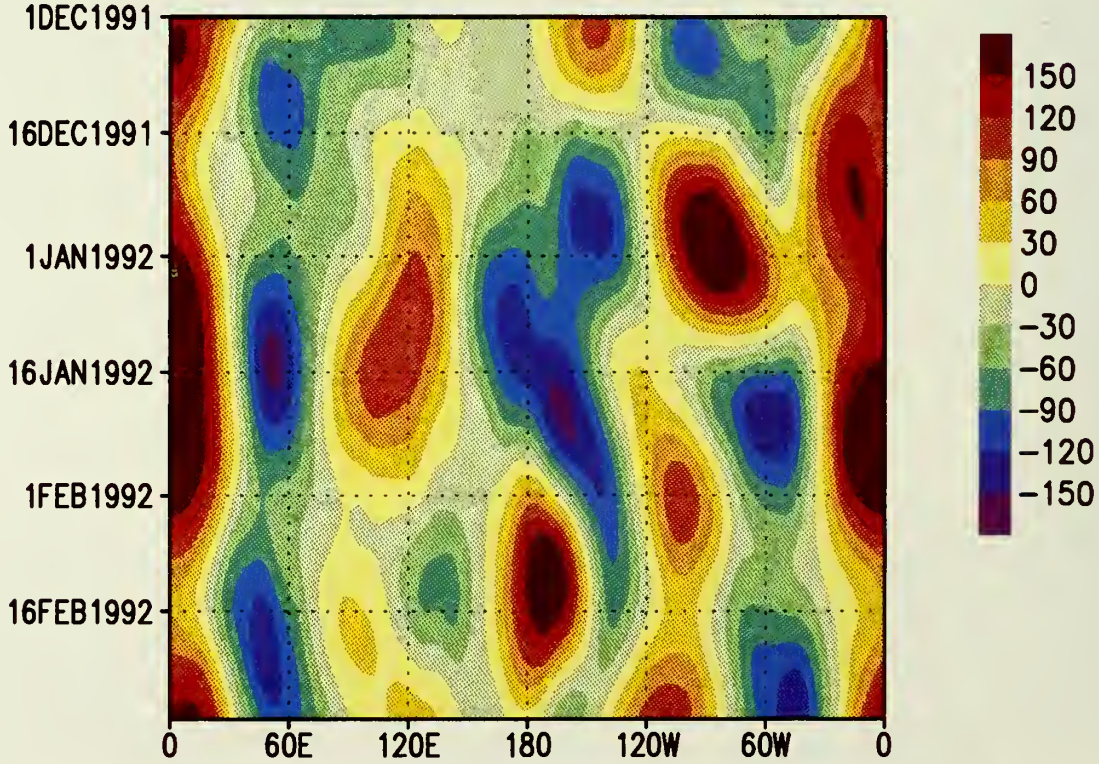

Fig. 18. Daily low-pass filtered 500 mb height anomalies (m) from December 1991–February 1992 averaged over the 10 deg latitude band centered on 50 deg. N. Cutoff period for filter is 30 days.

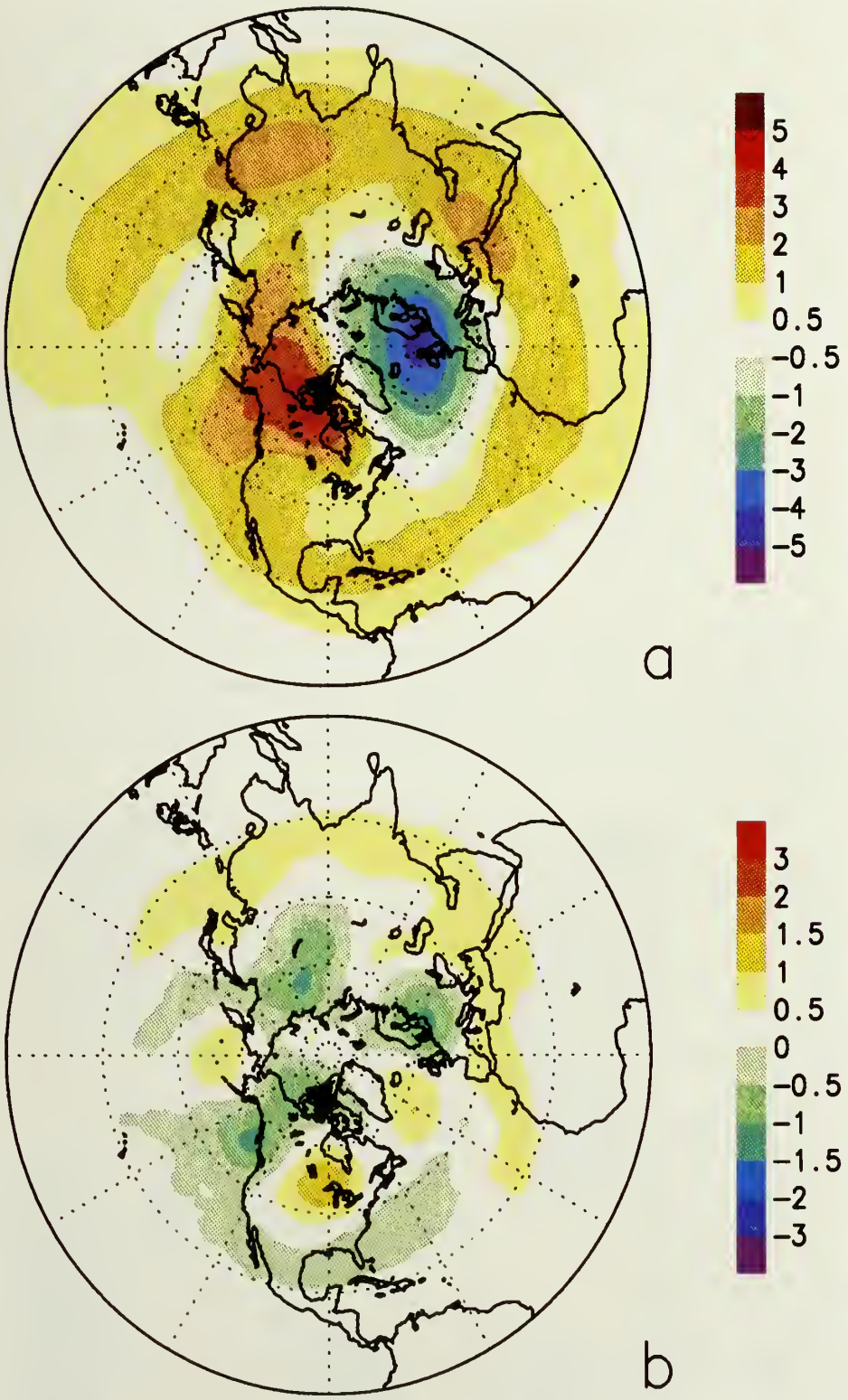

Fig. 19. Lower stratospheric temperature anomalies (deg. C) derived from satellite Microwave Sounding Unit (MSU) observations for a) December 1991 – February 1992 and b) June – August 1992. Anomalies are computed relative to the 1982–1991 base period. (Data provided by Spencer and Christy)

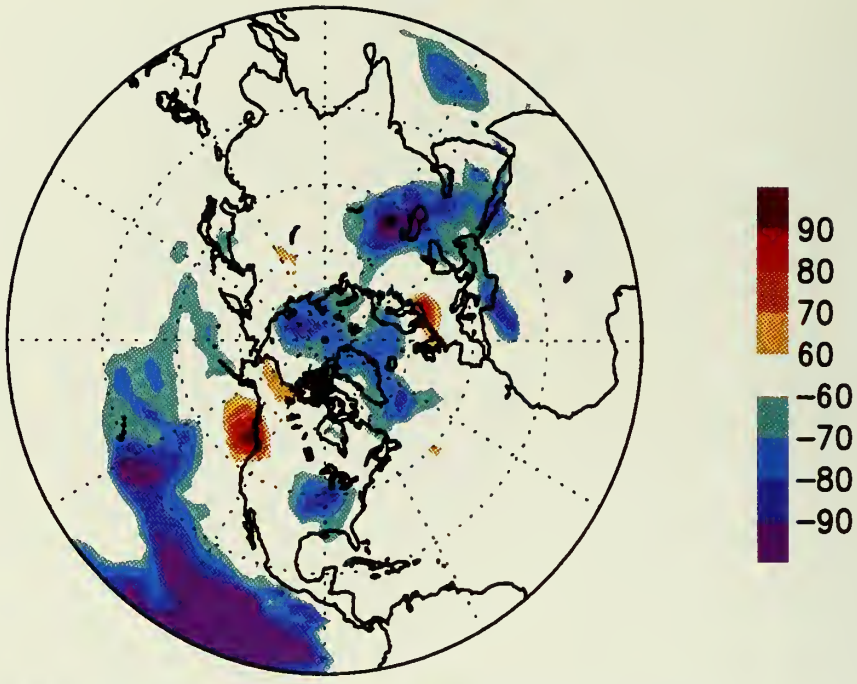

Fig. 20. Percentage of days during May – August 1992 in which daily low-pass filtered 500 mb height anomalies greater than 15 m and less than −15 m were observed. Cutoff period of low pass filter is 30 days. Anomalies are computed from the 1979–1988 base period.

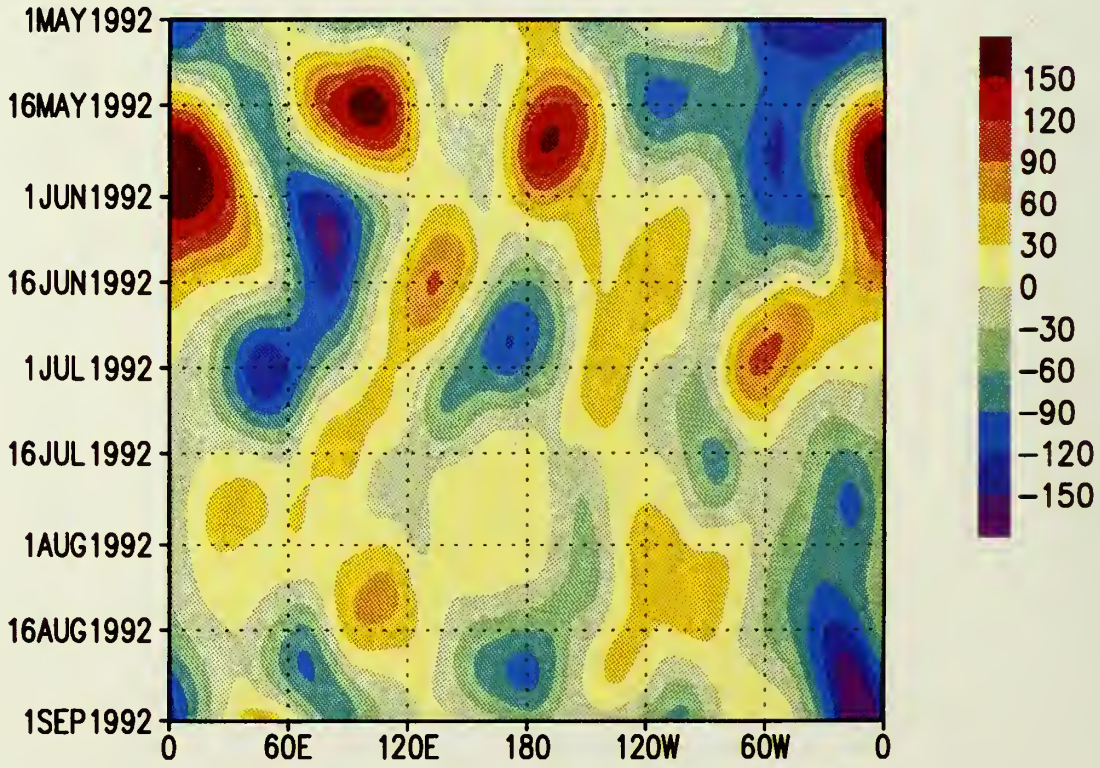

Fig. 21. Daily low-pass filtered 500 mb height anomalies (m) from May – August 1992 averaged over the 10 deg latitude band centered on 60 deg. N. Cutoff period for filter is 30 days.

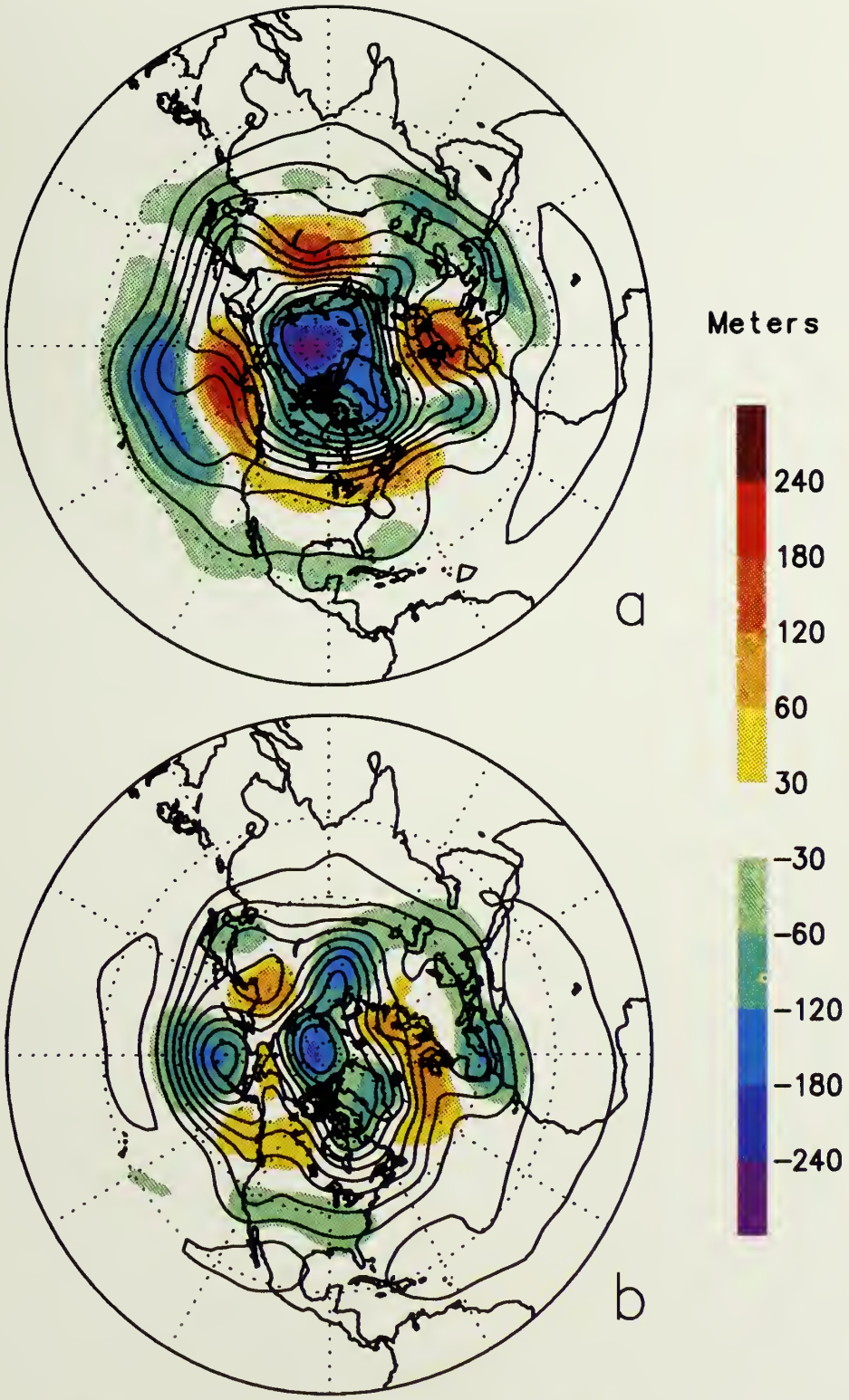

Fig. 22. Low-pass filtered 500 mb height anomalies (shaded) and low pass 500 mb mean heights (contours) valid: a) 17 May 1992 and (b) 14 June 1992. Cutoff period of low pass filter is 30 days.

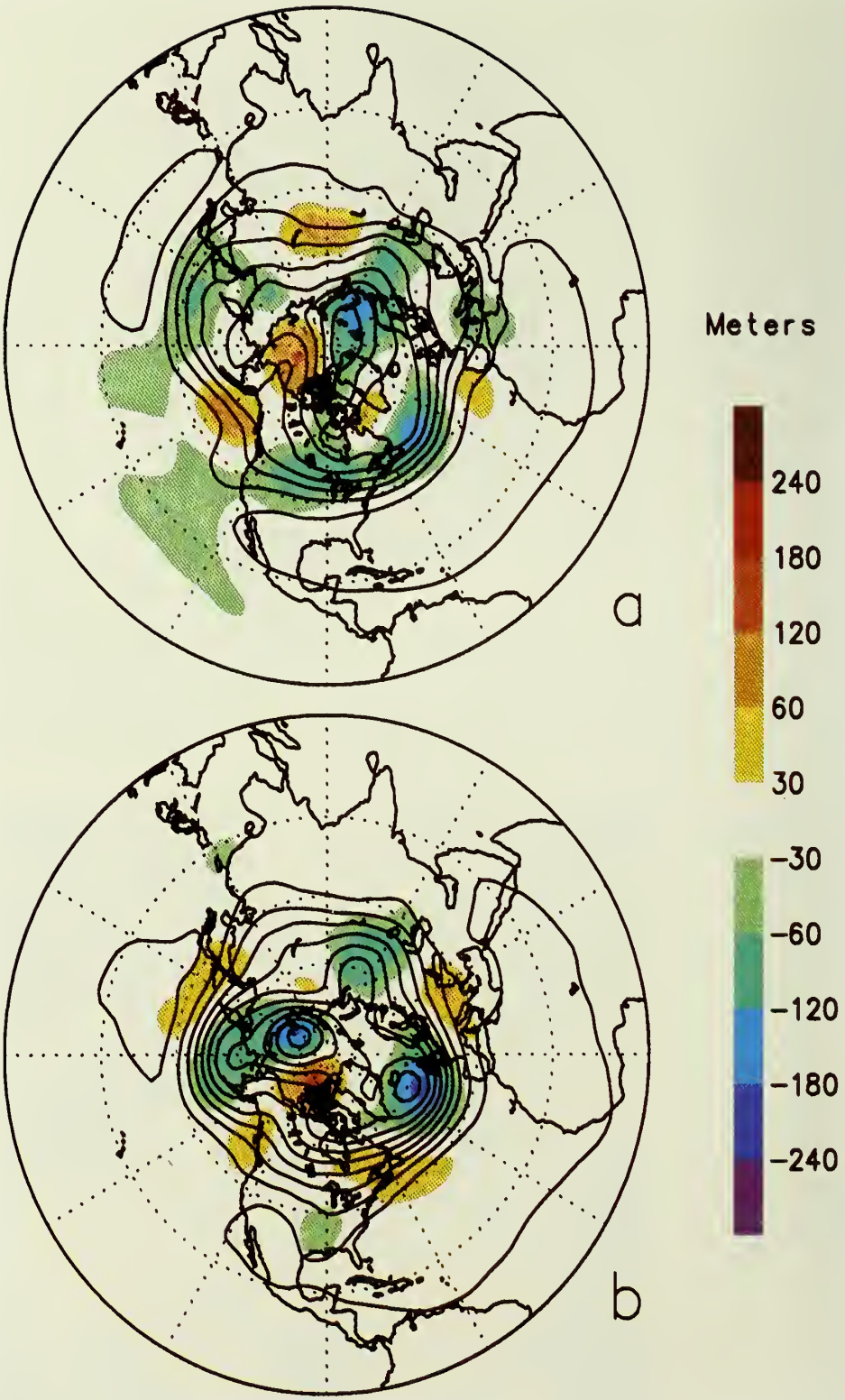

Fig. 23. Low-pass filtered 500 mb height anomalies (shaded) and low pass 500 mb mean heights (contours) valid: a) 10 July 1992 and (b) 22 August 1992. Cutoff period of low pass filter is 30 days.

3. TEMPERATURE

a. Surface

Global surface temperature anomalies exhibited two distinct patterns during 1992. The pattern during the first three months of the year (**Fig. 24a**) was strikingly different from the observed temperature anomalies during the last nine months (**Fig. 24b**). Large positive temperature anomalies (> 4.0°C) covered most of Asia, western Canada and the United States early in the year, while large negative anomalies were observed over Greenland and the Middle East. The positive temperature anomalies over North America during this period were associated with the 1991-92 ENSO, as were the positive SST anomalies in the tropical Pacific and along the west coast of South America. Positive temperature anomalies also engulfed much of the southern half of Africa during this period. Since April, however, the observed pattern of temperature anomalies has been significantly different, with negative anomalies dominating most of North America and northern Asia. Smaller positive anomalies remained over only the west coast of North America , central Europe, and to a lesser extent, east-central Eurasia.

During the year as a whole (**Fig. 25**), the largest negative surface temperature anomalies were observed across northeastern Canada and Greenland and over the Middle East. The negative anomalies across Greenland were reminiscent of the pattern which occurred during the decade of the 1980s (*Halpert and Ropelewski, 1991*). Positive temperature anomalies were observed across western North America, Eastern Asia and most of Europe. The positive anomalies across western North America and Siberia have also occurred frequently during the past 10 years. Positive SST anomalies were also observed across the tropical Pacific ocean in conjunction with the long-lived ENSO episode. Across the Southern Hemisphere, most of the temperature anomalies over land were small, except for the positive anomalies across the drought-stricken regions of southern Africa.

The estimated global surface temperature anomaly over land for 1992 (0.2°C) indicates that the past year is the 8th warmest year since 1951, but the second coolest of the past six years (**Fig. 26a**). A longer time series of estimated global surface temperature anomalies, this time over land and marine areas (**Fig. 26b**), shows that the past year was the coolest year since 1986. Both time series show the predominance of positive anomalies during the past 20 years. The longer time series should be viewed with some caution as values early in the record are less reliable than later anomalies. The temperature trends were similar in both the Northern (**Fig. 27**, top) and Southern Hemispheres (**Fig. 27**, bottom), although the cooling in the Southern Hemisphere was less pronounced. Much of the global warmth over land during 1992, as detailed above, occurred in the first three months of year. Global and Northern Hemispheric temperature anomalies averaged about 0.8°C above normal during the January through March period. However, temperatures fell to below normal levels throughout much of the Northern Hemisphere by July and remained below normal for much of the rest of the year. This continues a tendency in recent years for a warm first half of the year and a cooler second half of the year (**Fig. 28**). The early warmth during 1992 can be at least partially attributed to the ENSO episode (**Fig. 6**) and the later cooling to the volcanic shading effects of Mount Pinatubo. These cooling effects are strongest in the summer, as wintertime temperatures are effected more by circulation. However, whether the recent sequence of years with warm first halves and cooler second halves

is related to any long-term changes or is simply an unusual sequence of events remains to be determined.

A time series of estimated monthly global surface temperature anomalies over land (**Fig. 29**) shows that the return to normal global mean temperatures was accompanied by a return to normal median temperature anomalies as well. January through March temperature anomalies were similar to the past years (see *Halpert and Ropelewski, 1992*), with about 70% of the land areas having positive temperature anomalies. However, as noted above, the spatial distribution of negative and positive anomalies was much different from April through December, with approximately half of the land areas experiencing below normal temperatures.

Seasonal temperature anomalies changed quite dramatically throughout 1992 (**Figs. 30-31**). The temperature pattern during the December 1991 through February 1992 period (**Fig. 30a**), was quite similar to the January - March period discussed previously. The pattern of positive anomalies weakened during the March - May period (**Fig. 30b**), and by the June - August period (**Fig. 31a**), negative anomalies dominated North America and western Asia. Significant positive anomalies were only found over Europe during this season. Finally, most of the Northern Hemisphere experienced normal to below normal temperatures during the September - November season (**Fig. 31b**). Across the Southern Hemisphere, positive anomalies were observed across southern Africa during all seasons except for the June - August period. Temperature anomalies over Australia were quite variable during the year, with positive anomalies dominating the country during March - May, and negative anomalies occurring over the southern half of Australia during the September - November season. Also evident in this sequence of maps is the slow decay of the positive SST anomalies across the equatorial Pacific associated with the ENSO episode.

Temperature anomalies across North America mirrored those that occurred around the rest of the Northern Hemisphere during 1992. The first three months of the year were dominated by temperature anomalies which were more than 6°C above normal in an area across the northern Great Plains extending into western Canada (**Fig. 32a**). The rest of the year was strikingly different, with negative anomalies dominating the eastern two-thirds of the United States and Canada (**Fig. 32b**). Temperatures across the Far West, however, remained well above normal throughout the entire year. Averaged temperature anomalies across the United States was estimated to be the 21st warmest year in the 98 year record, but the second coolest of the last seven years (**Fig. 33**). The variability in temperature anomalies across the United States was quite pronounced, with more than 50% of the nation experiencing much above normal temperatures during February, while more than half of the country had much below normal temperatures during July and August (**Fig. 34**).

Surface temperature estimates are always held suspect because temperature anomalies may result from a variety of sources, e.g. urban heat island, instrument location changes. Estimates of the monthly average surface temperature anomalies for the U.S. can also be obtained by a statistical technique known as *specification*, which calculates the expected temperature anomalies based on monthly mean 700 mb height anomalies (Klein, 1983). The coefficients developed for this technique incorporate information about the relationship between U.S. surface air temperature and quasi-hemispheric 700 mb height field determined from a training data set for the 1948-81

period. In a given year, it is likely that observed and specified temperatures will differ from one another, since other processes not accounted for in the training data set can influence the observed anomalies. Extended periods of differences of one sign may indicate the influence of a single process, or a set of processes which produce the same bias, that did not occur during the training period.

During 1990-91, the difference between observed and specified temperatures (Tobs - Tsp) was positive (0.3-0.4°C) (**Fig. 35**). This may indicate that the surface temperatures from which the coefficients for the specification equations were developed were cooler for the same upper air height anomaly pattern during the training period than they are now. During 1992, observed U.S. surface temperature anomalies were almost 0.5°C warmer than those specified from the concurrent 700 mb height. While the positive bias in 1990-91 might have been attributed to the unprecedented high temperature during those years, it is noteworthy that the same results occurred in the much cooler year of 1992. In fact, given the 700 mb height, the specified U.S. surface air temperature was slightly below the 1951-80 average, while the observed temperature was 0.45°C above average. However, this recent warm bias in U.S. annual average surface air temperature has not lasted long enough to be statistically significant, nor can its cause be determined from the current analysis.

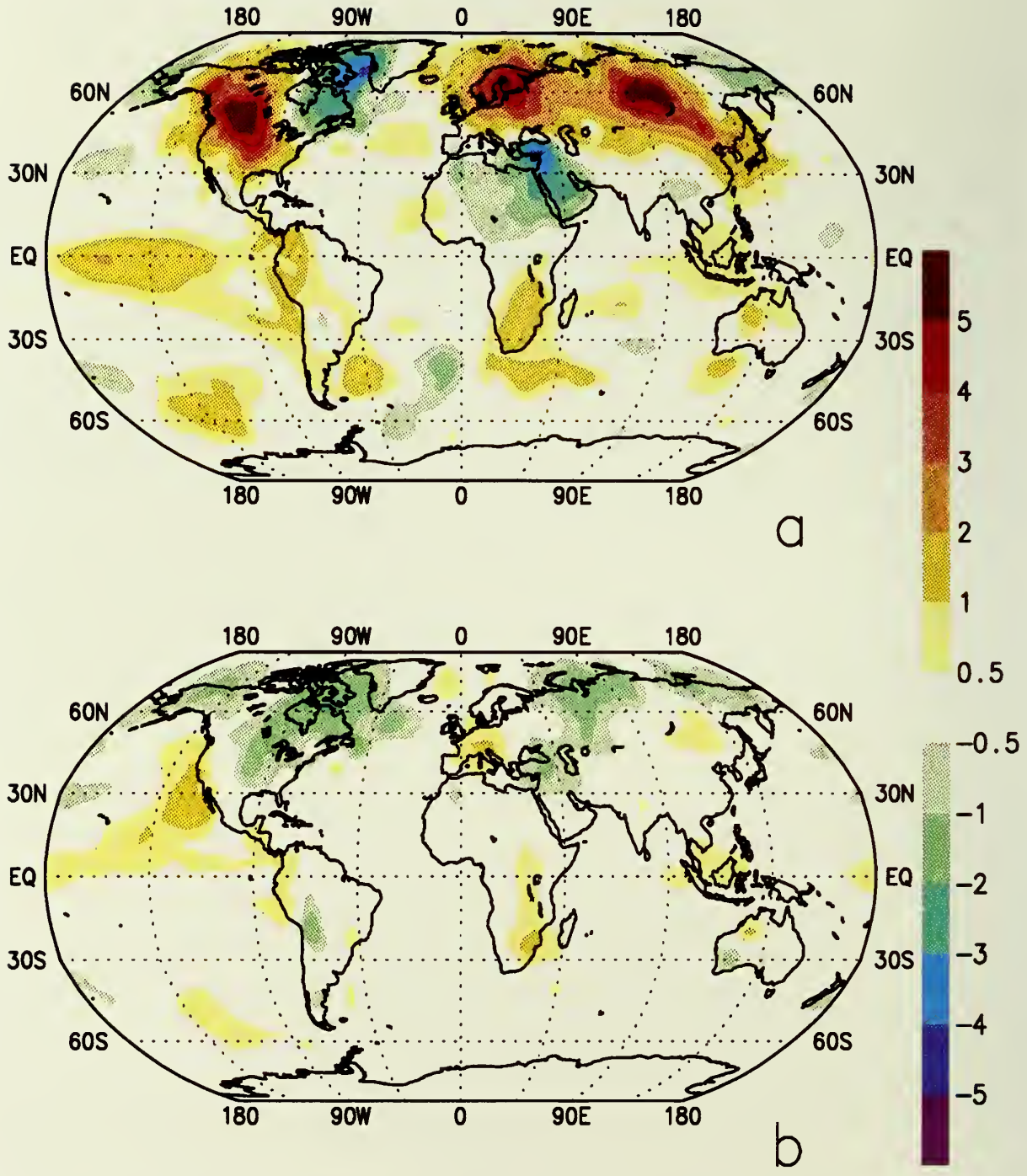

Fig. 24. Surface temperature anomalies (Deg. C) for a) January – March 1992 and b) April – December 1992. Analysis based on station data over land and sea surface temperature (SST) over the water. Anomalies for station data are from the 1961–1990 base period, while SST anomalies are computed as departures from the COADS/ICE climatology. (Source: CAC)

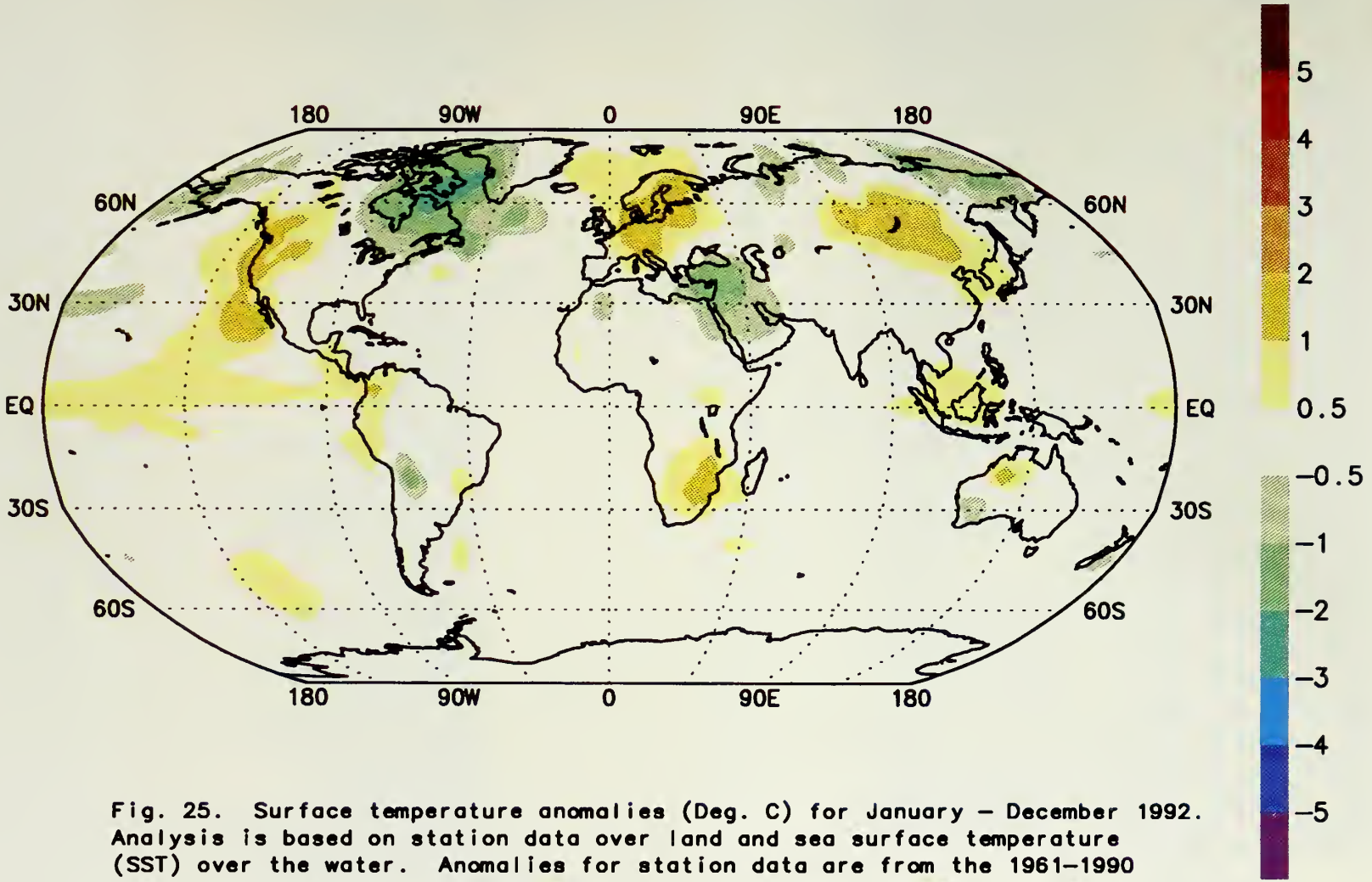

Fig. 25. Surface temperature anomalies (Deg. C) for January – December 1992. Analysis is based on station data over land and sea surface temperature (SST) over the water. Anomalies for station data are from the 1961–1990 base period, while SST anomalies are computed as departures from the COADS/ICE climatology (Source: CAC).

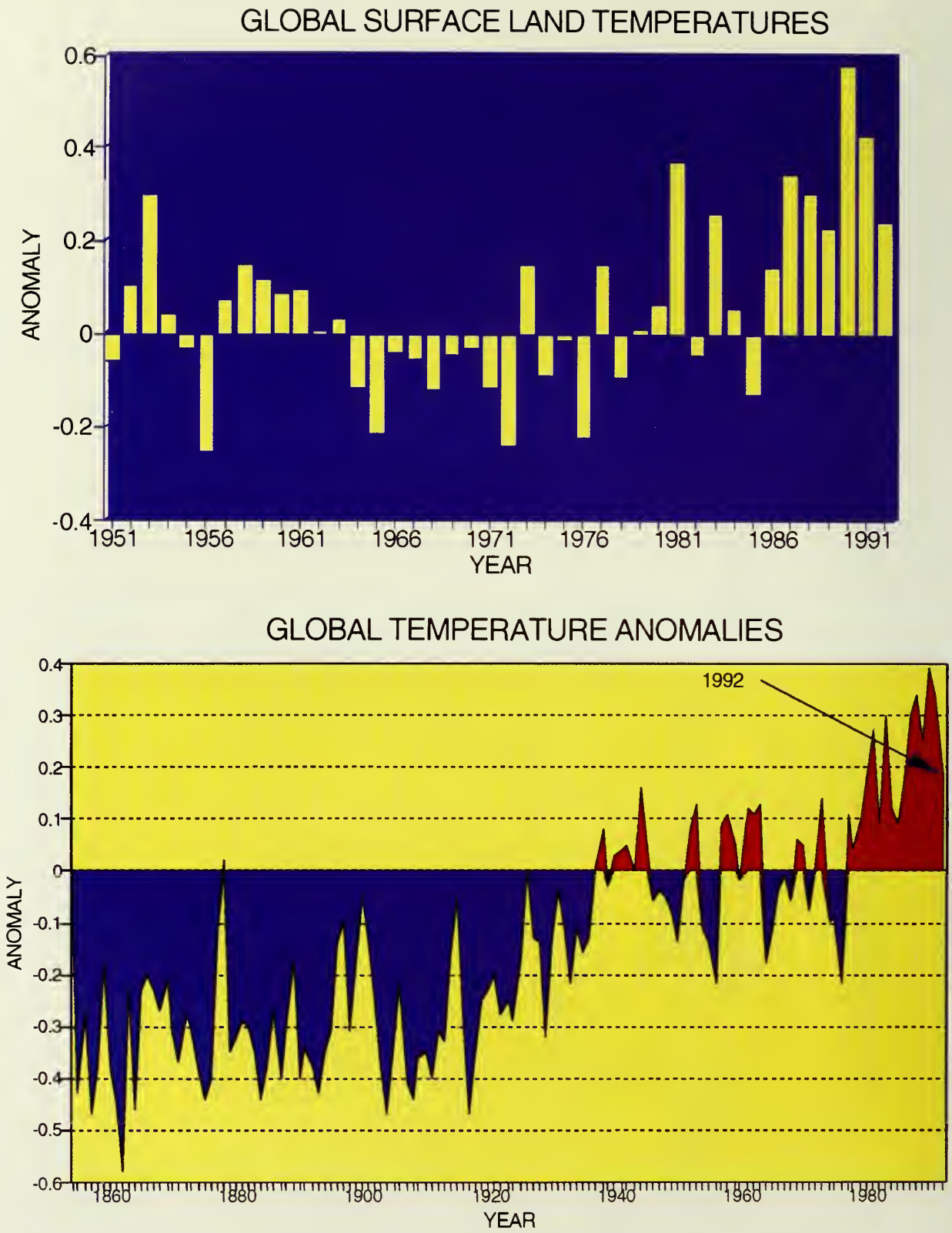

Fig. 26. Annual estimated global (land only) surface temperature (°C) anomalies computed from the 1951-1980 base period (top) (Source: CAC), and annual estimated global temperature anomalies (°C) for the land and marine regions (bottom). (Data provided by P. Jones and D. Parker.). Land and marine anomalies are computed as departures from the 1950-1979 base period.

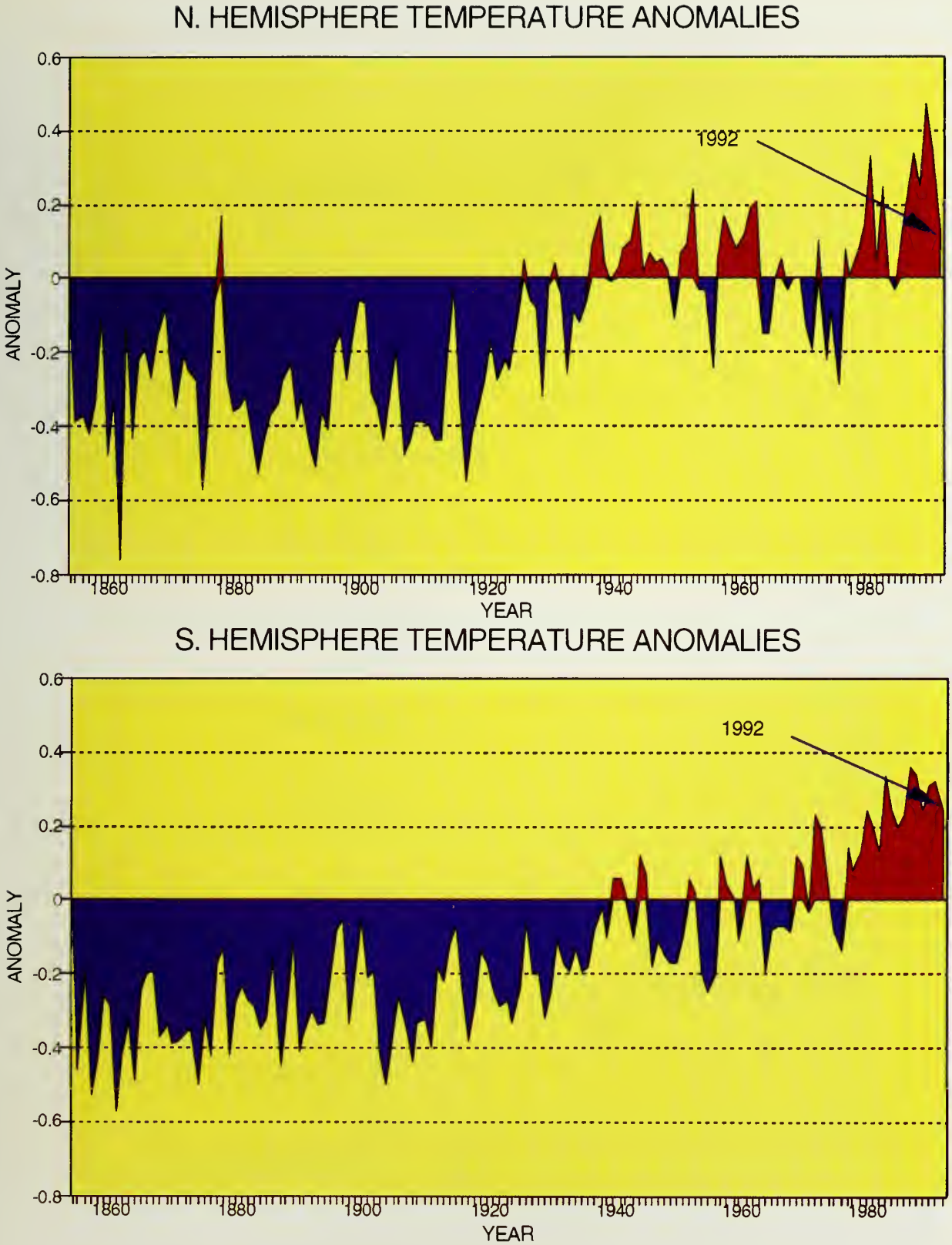

Fig. 27. Annual estimated temperature anomalies for the land and marine regions of the Northern Hemisphere (top) and the Southern Hemisphere (bottom). Anomalies are computed as departures from the 1950-1979 base period. (Data provided by P. Jones and D. Parker.)

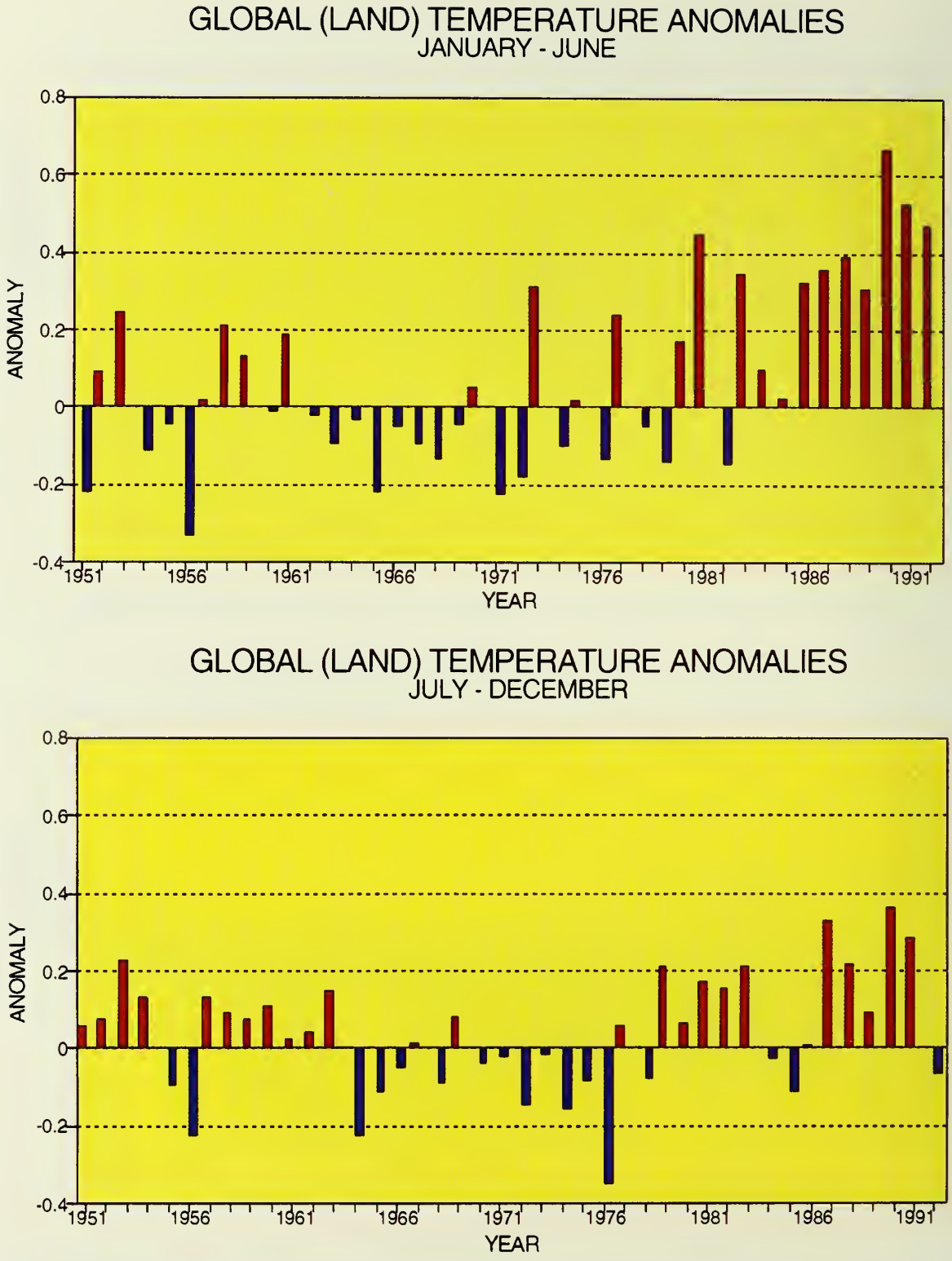

Fig. 28. Estimated Northern Hemisphere temperature anomalies (°C) over land for the January - June period (top) and the July - December period (bottom). Anomalies are computed as departures from the 1951-1980 base period. (Source: CAC)

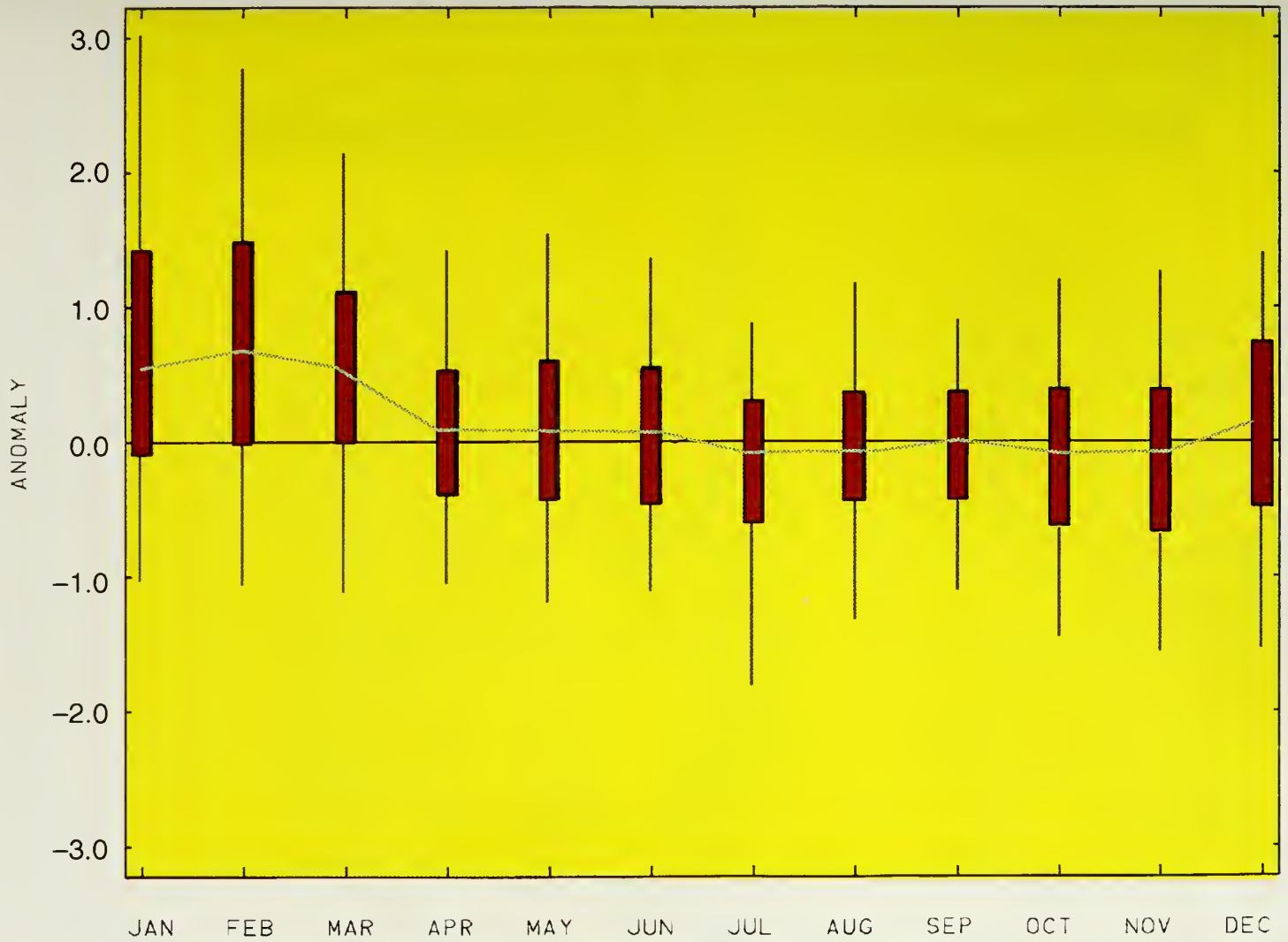

Fig. 29. Global monthly surface temperature index based on the average temperature anomalies in 2° latitude by 2° longitude areas over land for 1992. The solid line represents the median value. Thus, 50% of the land areas experienced temperature anomalies at least as large as the median for a given month. Each "box", or rectangle, delineates the anomaly at the 70th and 30th percentile while the vertical lines delineate the 90th and the 10th percentile values. The anomalies are computed as departures from the 1951-1980 base period. (Source: CAC)

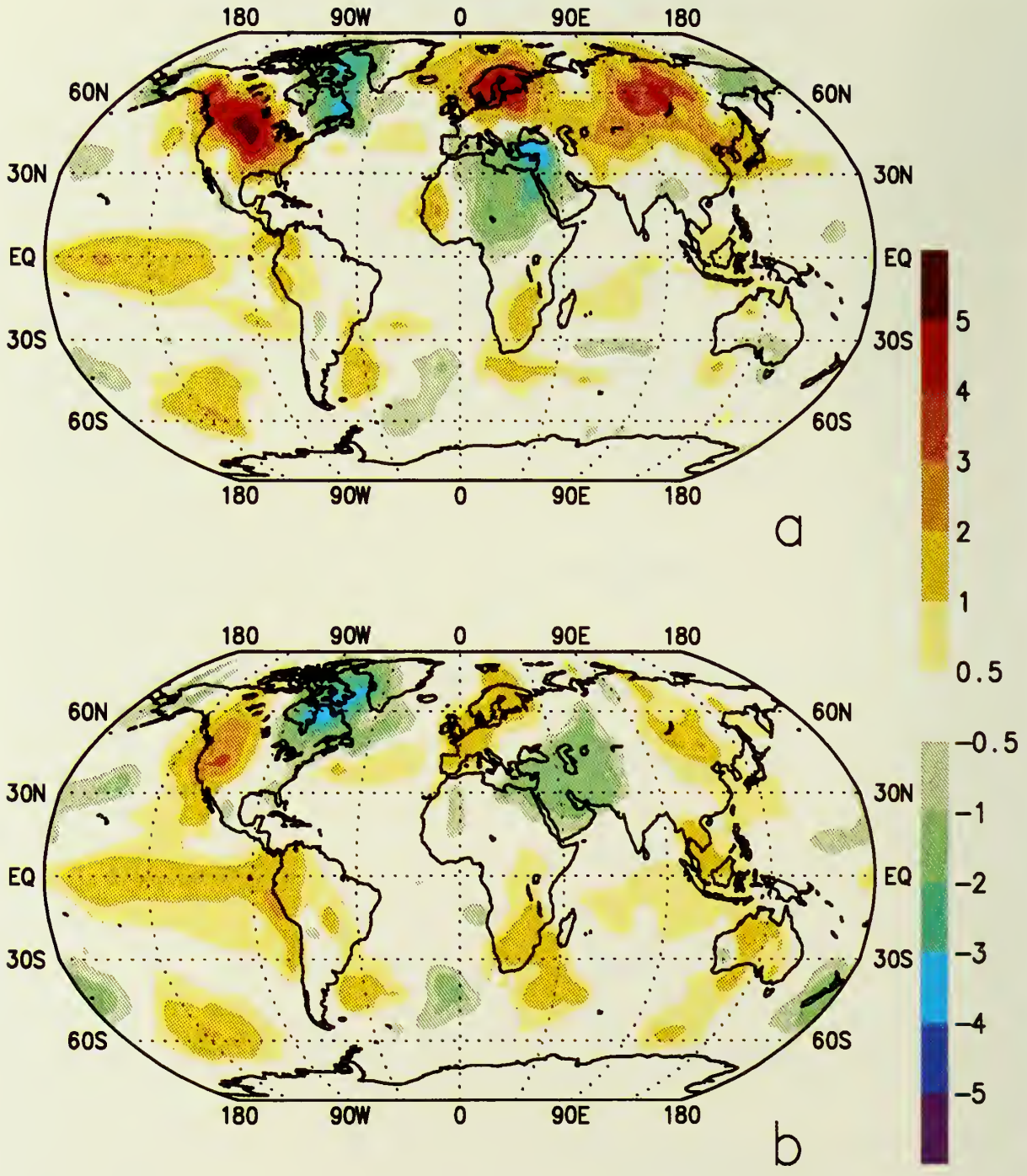

Fig. 30. Surface temperature anomalies (Deg. C) for a) December 1991–February 1992 and b) March – May 1992. Analysis based on station data over land and sea surface temperature (SST) over the water. Anomalies for station data are from the 1961–1990 base period, while SST anomalies are computed as departures from the COADS/ICE climatology. (Source: CAC)

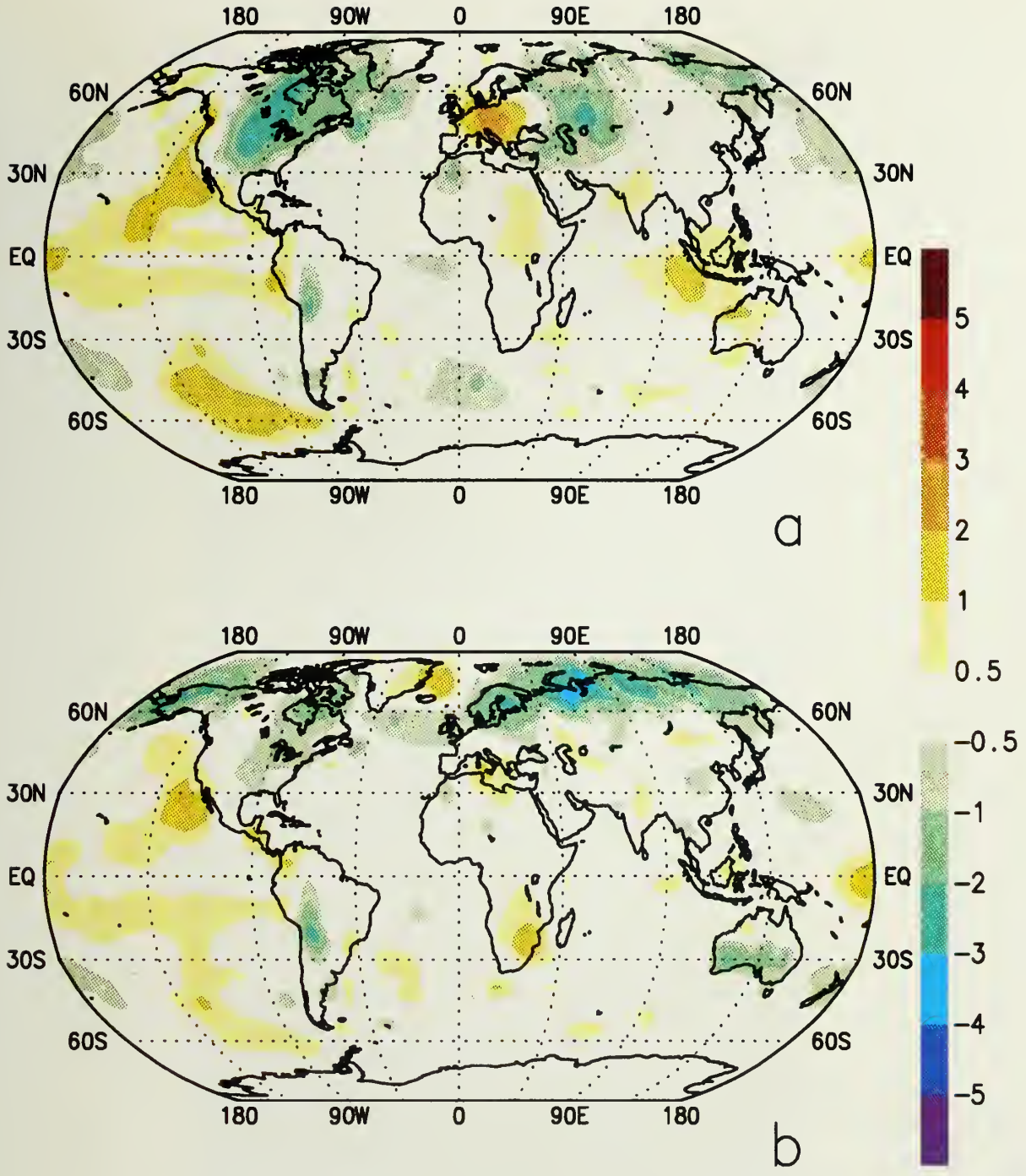

Fig. 31. Surface temperature anomalies (Deg. C) for a) June – August 1992 and b) September – November 1992. Analysis based on station data over land and sea surface temperature (SST) over the water. Anomalies for station data are from the 1961–1990 base period, while SST anomalies are computed as departures from the COADS/ICE climatology. (Source: CAC)

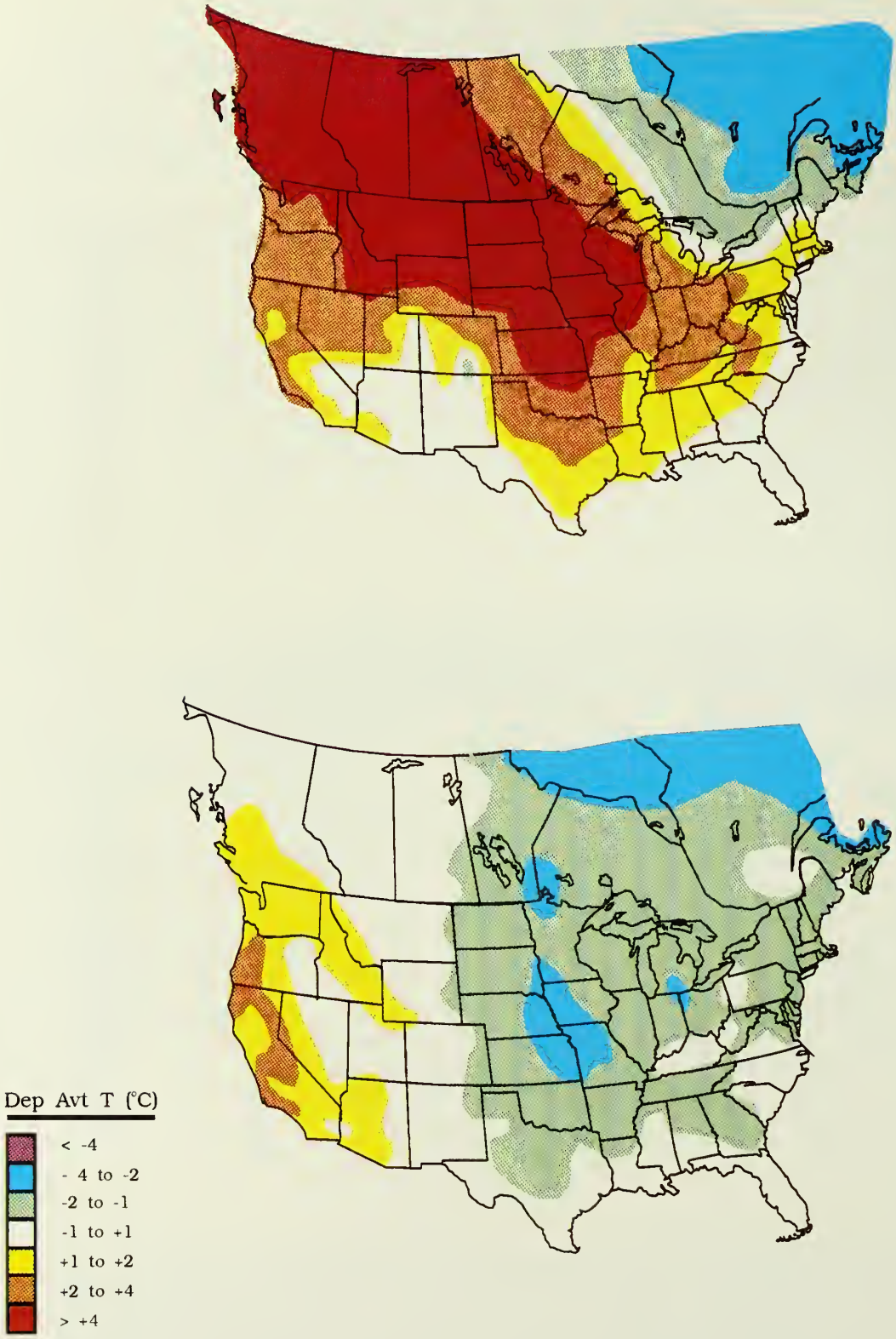

Fig. 32. Surface temperature anomalies for January - March 1992 (top) and for April - November 1992 (bottom). Anomalies are computed as departures from the 1951-1980 base period.

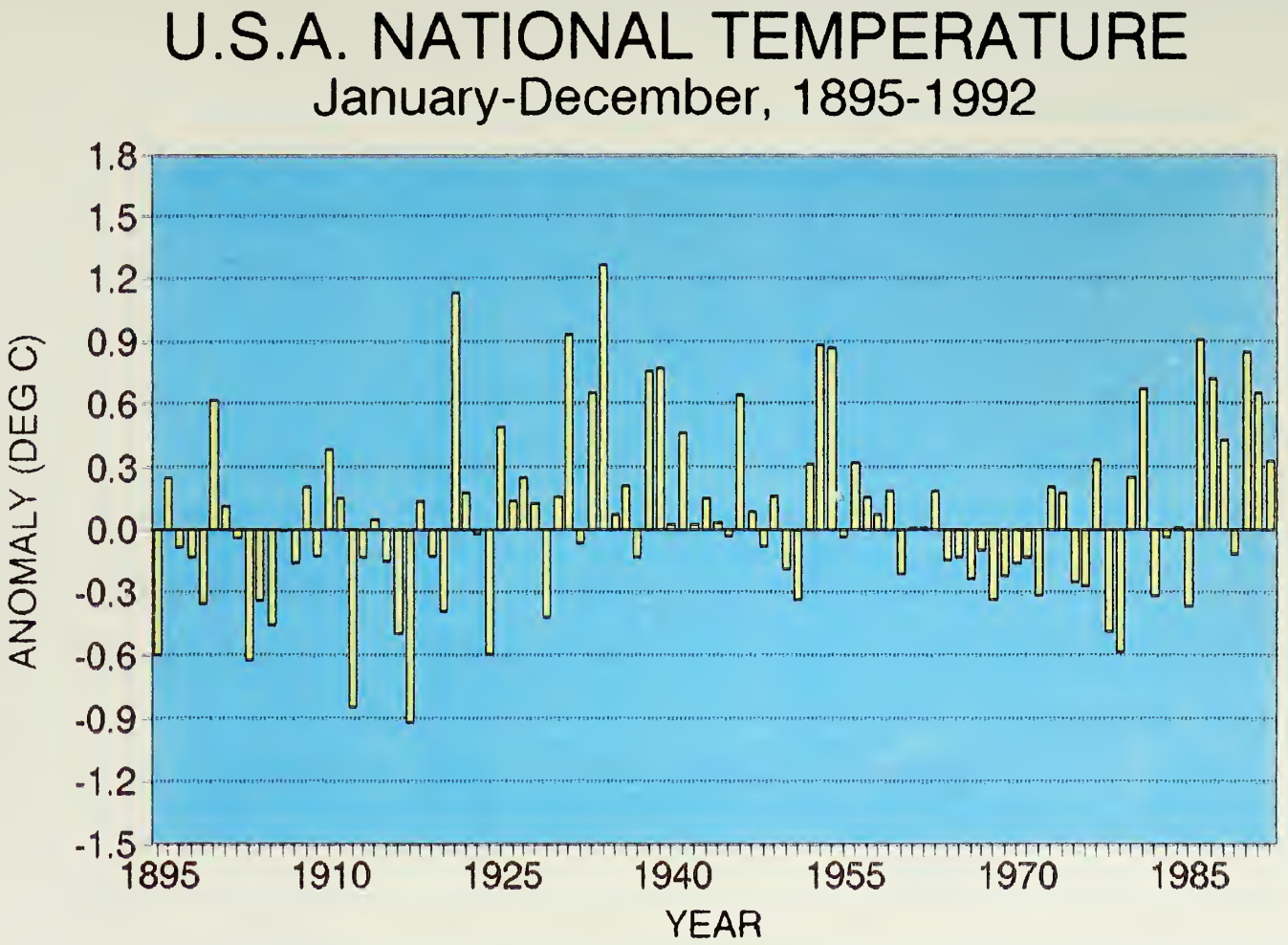

Fig. 33. Annual estimated temperature anomalies for the contiguous United States. Anomalies are computed as departures from the 1951-1980 base period. (Source: NCDC)

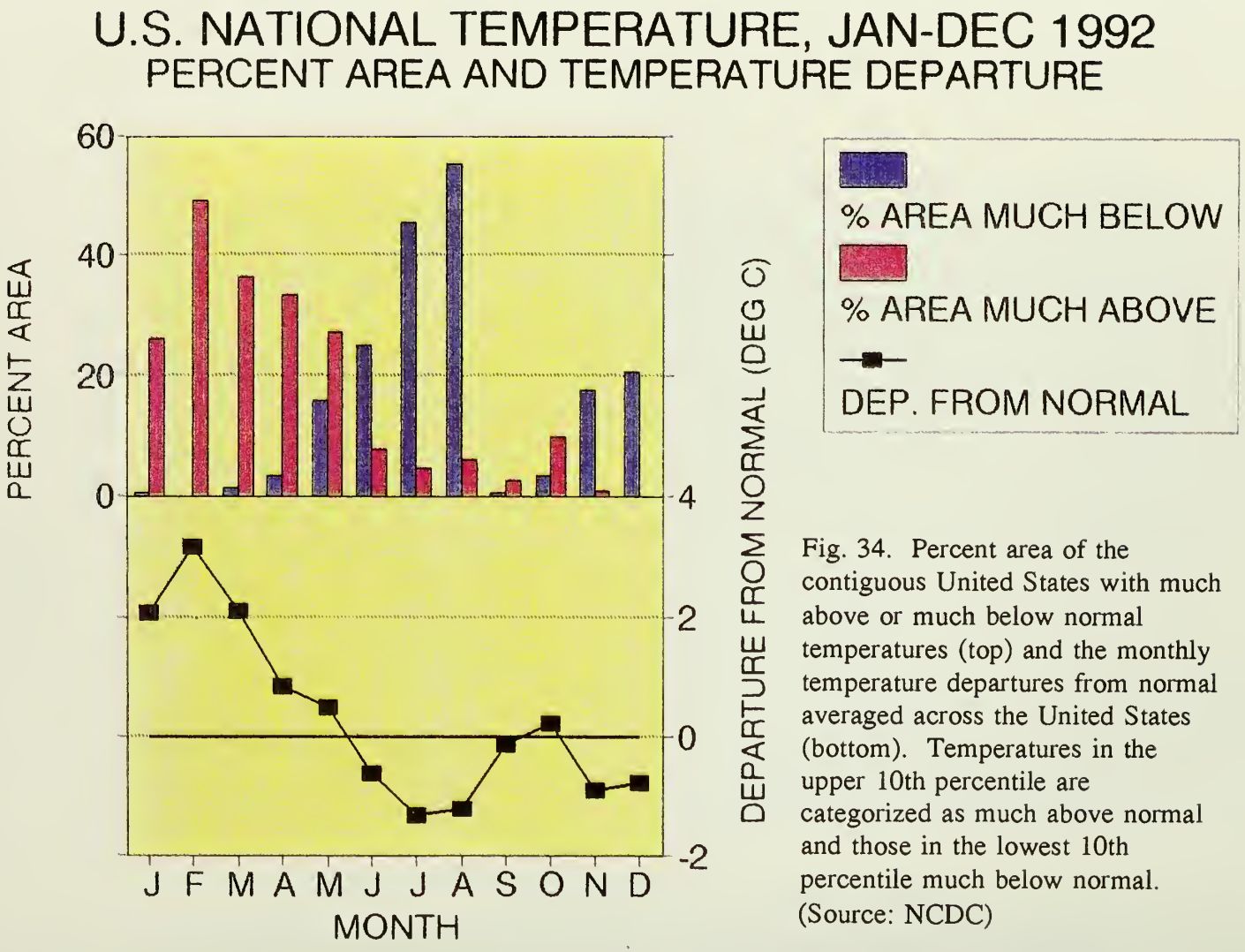

Fig. 34. Percent area of the contiguous United States with much above or much below normal temperatures (top) and the monthly temperature departures from normal averaged across the United States (bottom). Temperatures in the upper 10th percentile are categorized as much above normal and those in the lowest 10th percentile much below normal. (Source: NCDC)

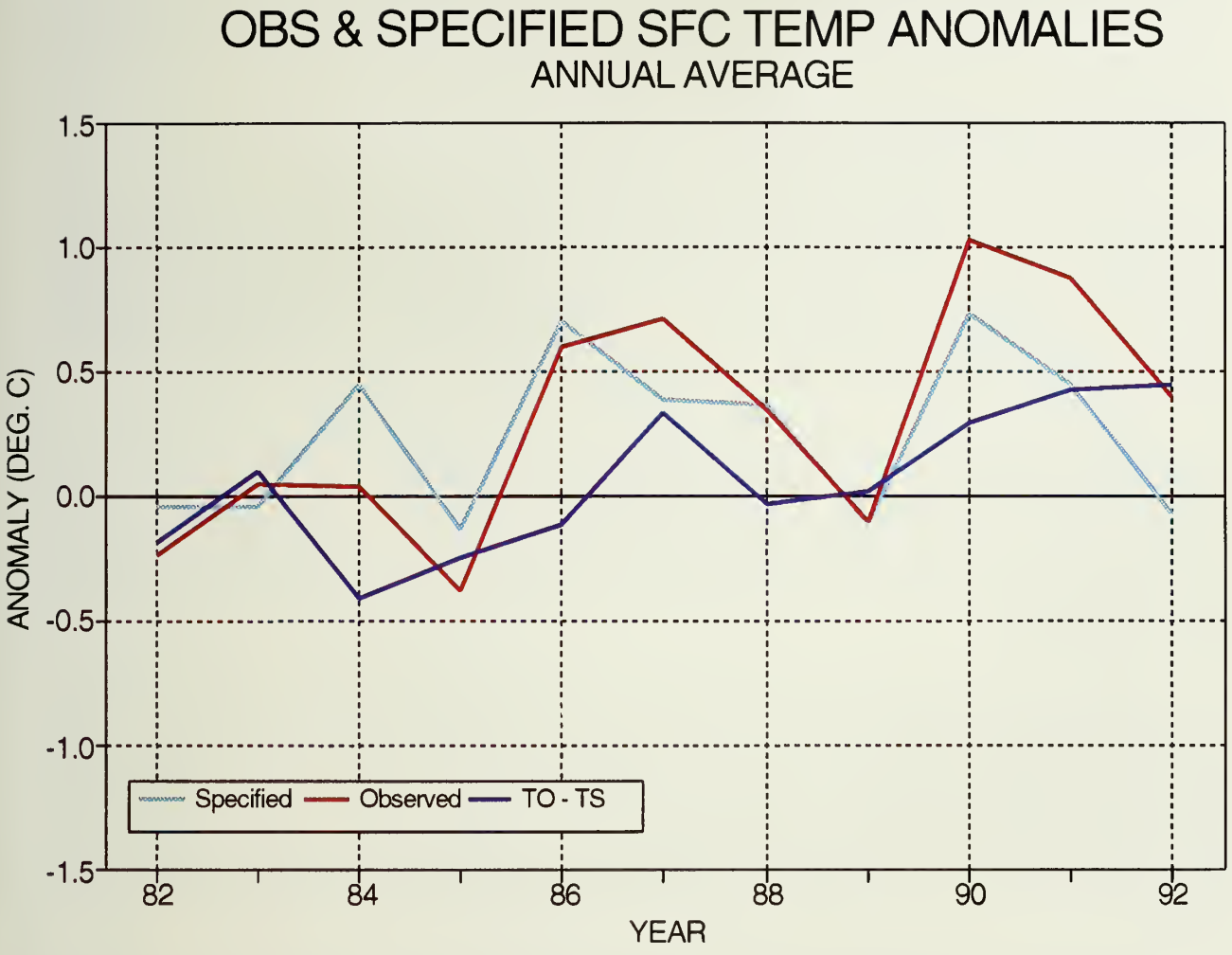

Fig. 35. Annual average United States observed surface temperature anomalies (yellow), specified anomalies from observed quasi-hemispheric 700 mb heights (light blue) and the difference between the observed and the specified anomalies (dark blue). (Source: CAC)

b. Troposphere/Stratosphere

Below normal temperatures were observed during 1992 in the troposphere as measured by radiosonde balloon-borne instruments (**Fig. 36**) and by satellite-derived measurements (**Fig. 37**). The temperature anomaly for 1992 (-.19°C) is the lowest since 1976 (**Fig. 36**, top) and is a decrease of more than 0.5°C from what was observed during 1991. This sharp decrease in mean tropospheric temperature is thought to primarily be due to the shading effects of the aerosols from the Mt. Pinatubo eruption.

The effects of the 1992 ENSO event on tropospheric temperature anomalies can be estimated by linear regression (*Angell, 1990*). If these estimates are used to adjust the tropospheric temperature record (**Fig. 36**, bottom), 1992 temperatures equal the previous coldest year in the record (1964), which followed the Agung eruption. The adjusted temperature decrease between 1991 and 1992 becomes an even more impressive 0.75°C. This shows the probable effect of volcanic eruptions overwhelming the influence of global warming.

Lower stratospheric and mean tropospheric temperature anomalies are provided respectively by channel 4 and channel 2 of the Microwave Sounding Unit (MSU) (*Spencer and Christy, 1992*). A time series of these temperatures shows that aerosols ejected by major volcanic eruptions (El Chichon, 1982 and Mt. Pinatubo, June 1991) are associated with large lower stratospheric temperature increases (**Fig. 37**), and large mean tropospheric temperature decreases (**Fig. 38**).

In the lower stratosphere, temperatures in the tropical belt increased within the first two weeks following the eruption of Mt. Pinatubo (**Fig. 37a**), peaking during August 1991. Lower stratospheric temperatures also increased in the middle and high latitudes of both hemispheres following the eruption (**Fig. 37b, c**), although a distinct warming trend in these regions, possibly associated with the change in sign of the quasi-biennial oscillation (QBO), appears to have begun prior to the eruption. By mid-1992, temperatures in all three zonal bands began returning toward normal.

Following the eruption, lower stratospheric temperatures remained above normal throughout the subtropical latitudes in the Northern Hemisphere until June 1992 and until September in the Southern Hemisphere (**Fig. 39**). In contrast, large positive temperature anomalies persisted over the equatorial region for only four months following the eruption, before weakening as mature ENSO conditions developed in the tropical Pacific. Although positive anomalies increased early in 1992, these larger anomalies only lasted until April. As expected, this pattern of anomalies in the tropics and subtropics was strongly anti-correlated with the pattern of 200 mb height anomalies (**Fig. 12**). In the extratropics, the largest positive lower stratospheric temperature anomalies were observed over the South Pole during the Austral Spring in both 1991 and 1992, when the polar vortex climatologically weakens, and volcanic aerosols may have been advected into the region.

In the troposphere, global mean temperatures did not show a distinct decline until nearly two months following the eruption (**Fig. 38a**). Temperatures in both hemispheres then decreased at approximately the same rate (**Fig. 38b, c**). In the Southern Hemisphere, the decline in mean

tropospheric temperatures ended during the Austral spring (September - November) of 1991, although temperatures remained consistently below normal through the end of 1992. In the Northern Hemisphere, mean tropospheric temperatures decreased until about June 1992, after which temperatures rose rapidly for the remainder of the year, although remaining below the long-term mean. Consequently, the global mean temperature variability during 1992 is dominated by the large temperature variations in the Northern Hemisphere.

Following the eruption of Mt. Pinatubo, the mean tropospheric temperatures decreased in the tropical and subtropical latitudes of both hemispheres (**Fig. 40**). This is well correlated with the 200 mb height anomalies (**Fig. 12**), and anti-correlated with the lower stratospheric temperature anomalies (**Fig. 39**). However, mean tropospheric temperatures in the tropical belt rose to above normal between November 1991 and June 1992, a period during which mature ENSO conditions dominated the tropical Pacific. Negative temperature anomalies subsequently returned to the tropical belt following the weakening of the ENSO episode.

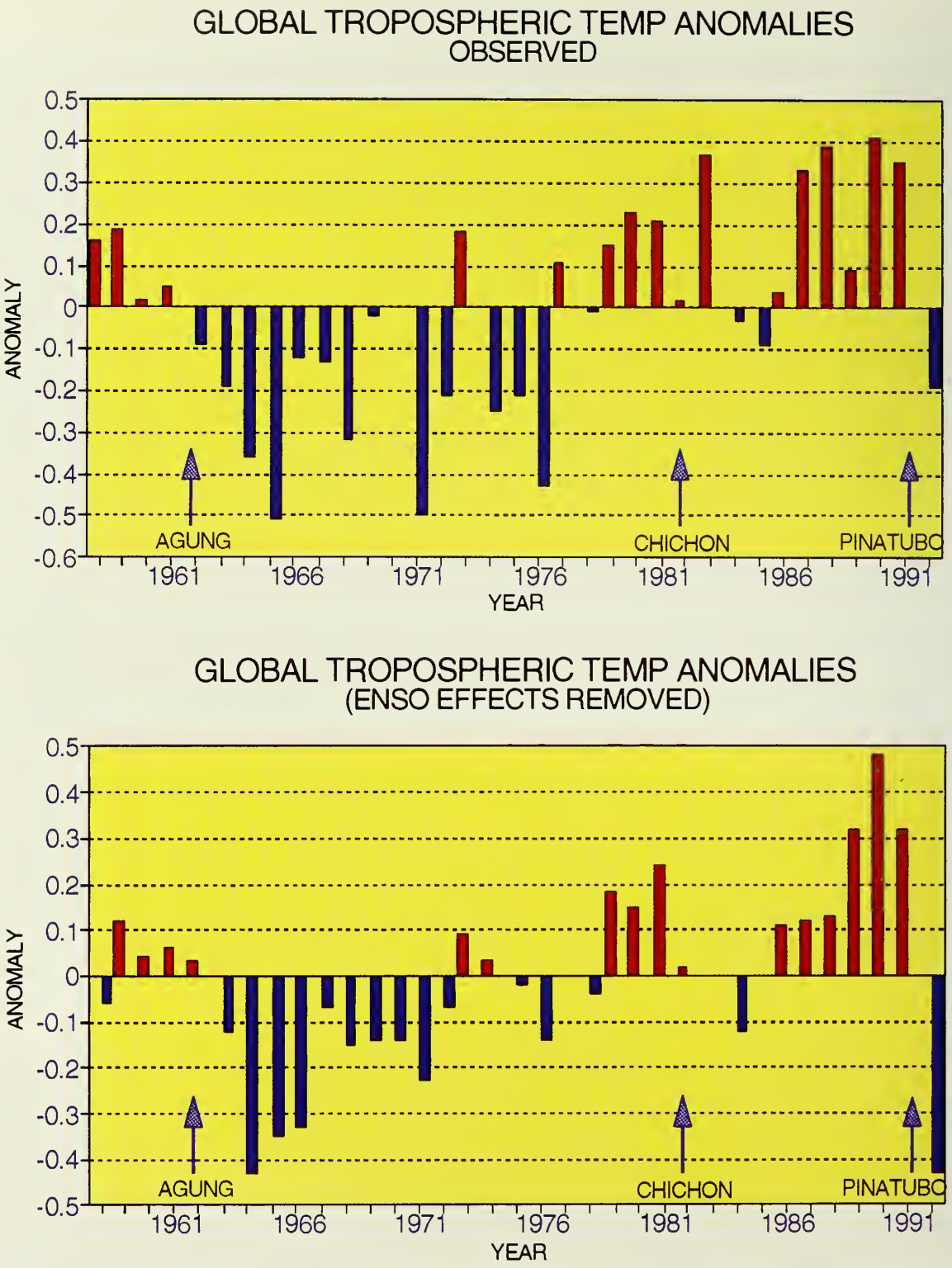

Fig. 36. Annual global tropospheric (850 - 300 mb) temperature anomalies derived from radiosonde data (top) and anomalies derived from radisonde data with the influence of ENSO statistically filtered out (bottom). Annual values of global tropospheric temperature anomalies are based on a 63 station radiosonde network and computed from the 1958-1991 base period. (Data provided by J. Angell.)

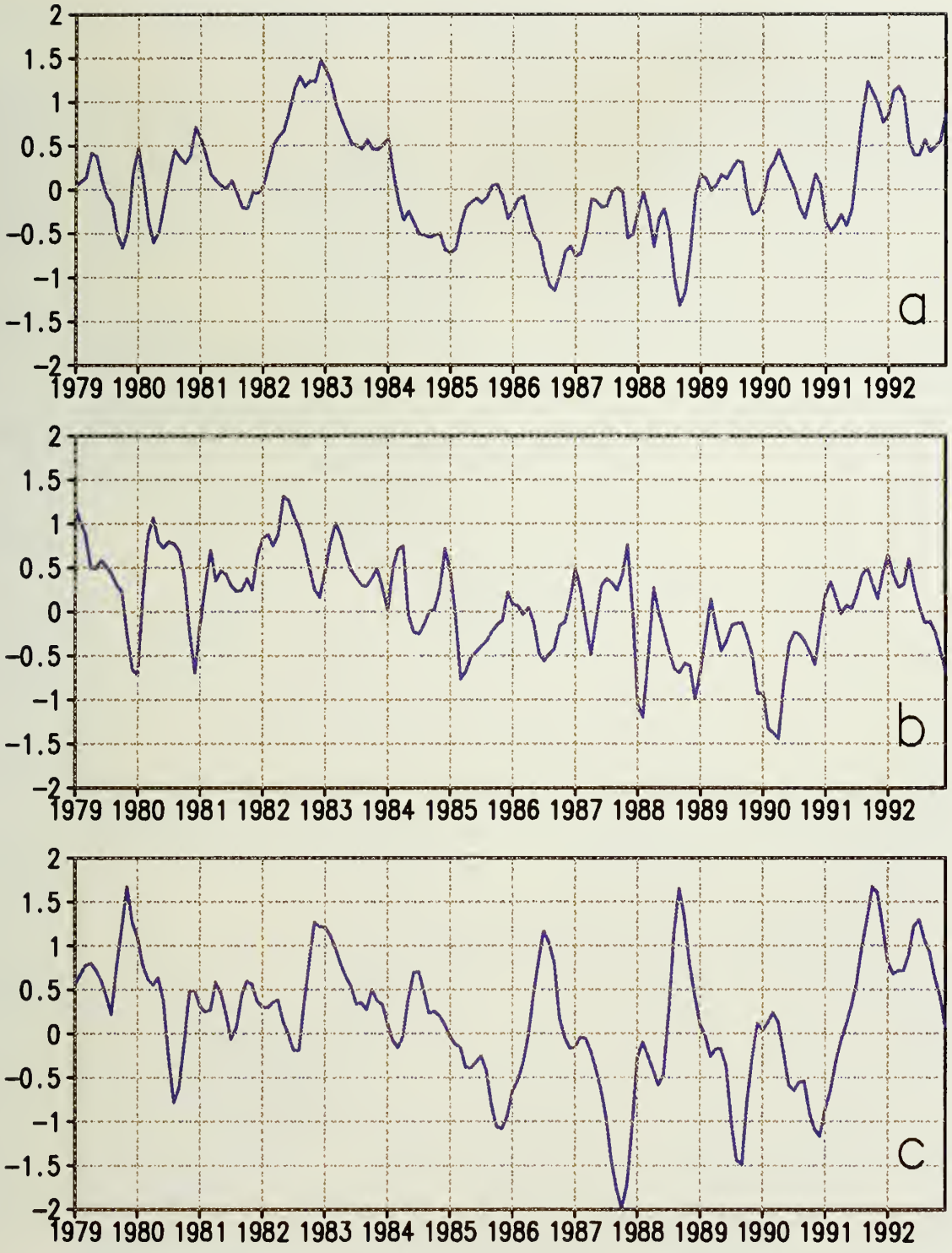

Fig. 37. Lower stratospheric temperature anomalies from the Microwave Sounding Unit (MSU) channel 4 for the a) tropical belt (30S – 30N), b) northern extratropics (30N – 85N) and c) southern extratropics (30S – 85S). Anomalies are computed from the 1982–91 base period. (Data provided by Spencer and Christy.)

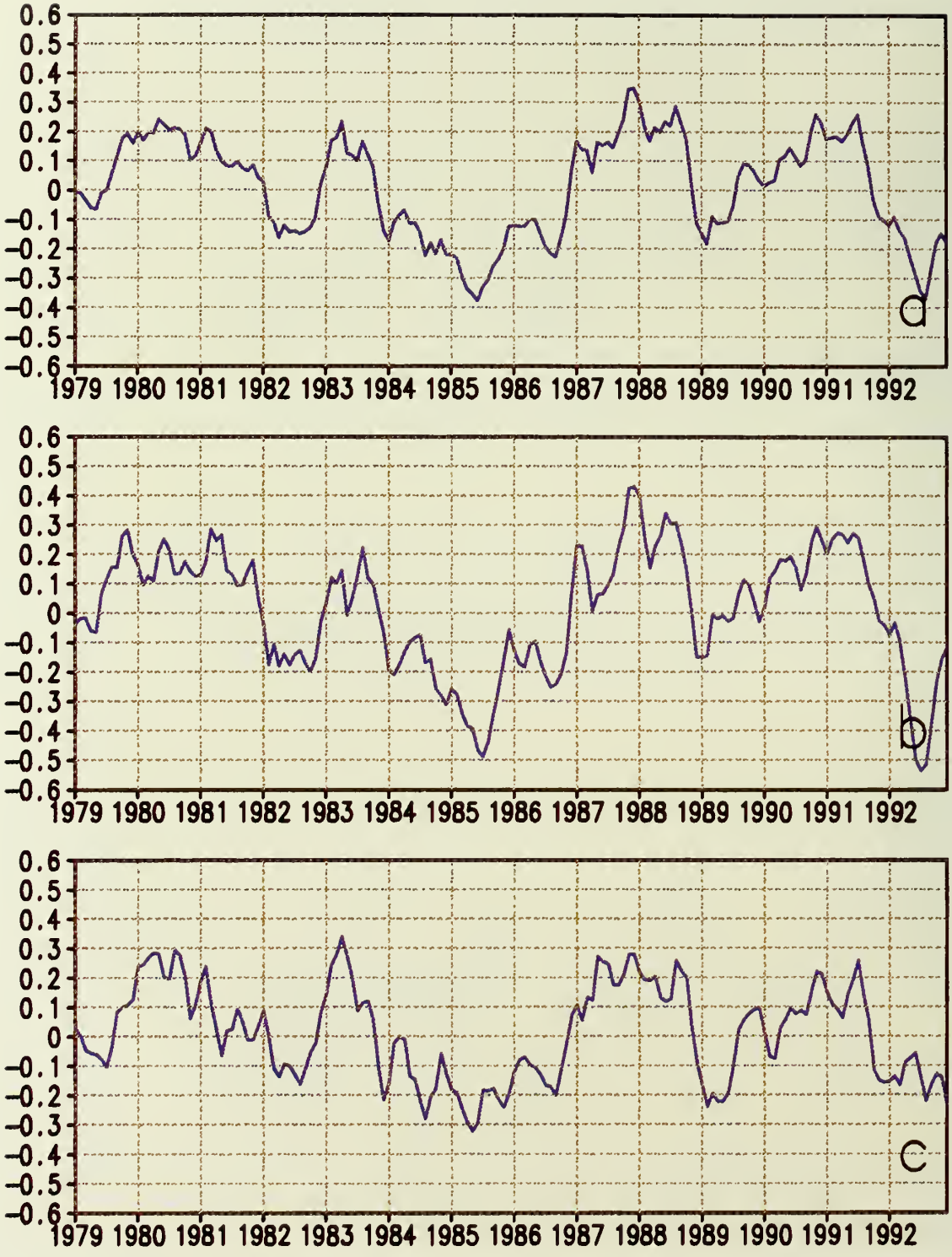

Fig. 38. Mean tropospheric temperature anomalies from the Microwave Sounding Unit (MSU) channel 2 for the a) globe (85S – 85N), b) Northern Hemisphere (0N – 85N) and c) Southern Hemisphere (0S – 85S). Anomalies are computed from the 1982–91 base period. (Data provided by Spencer and Christy.)

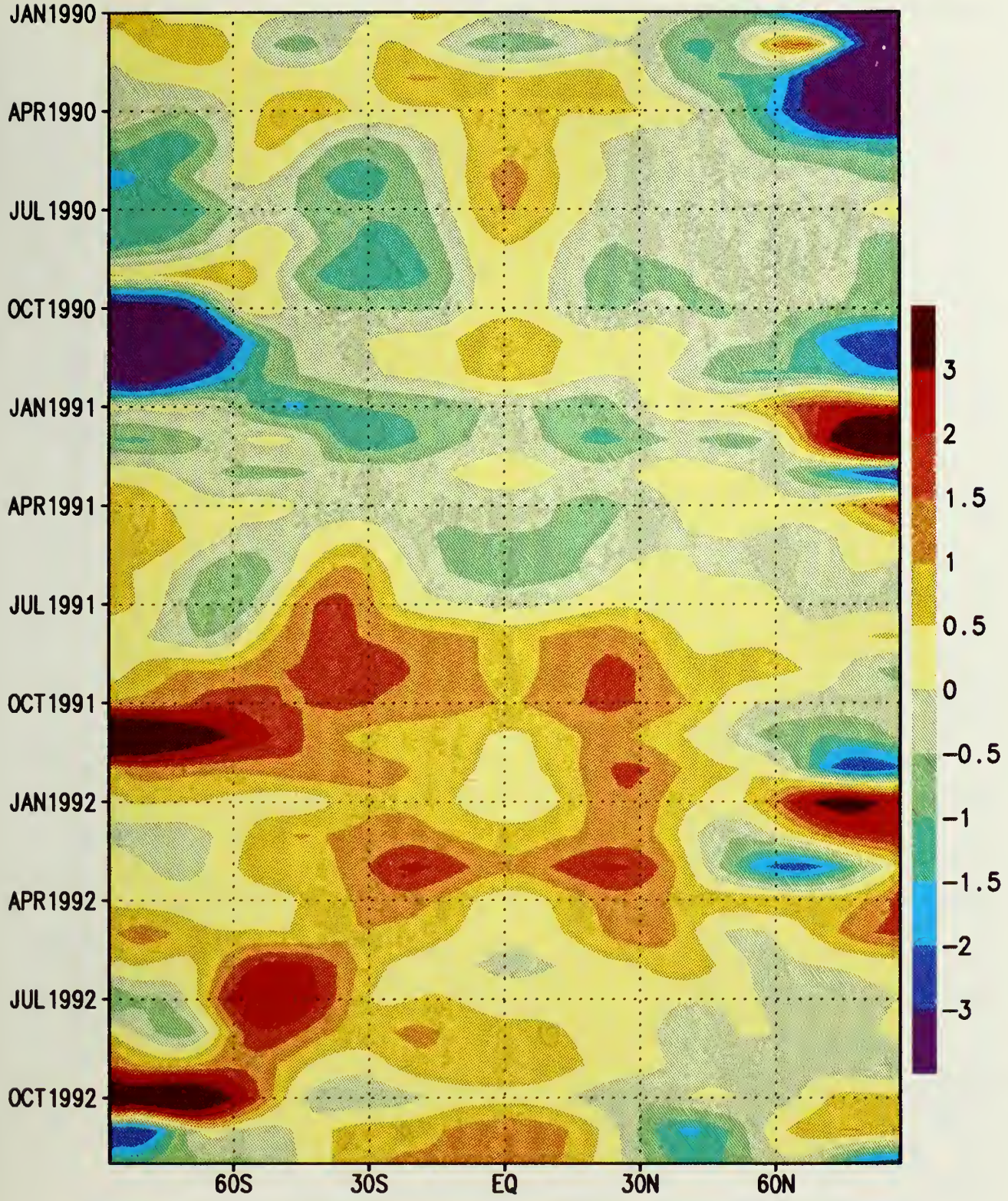

Fig. 39. Time–latitude cross section of zonally averaged lower stratospheric temperature anomalies (Deg. C) from the Microwave Sounding Unit (MSU) channel 4. Anomalies are computed from the 1982–1991 base period. (Data provided by Spencer and Christy.)

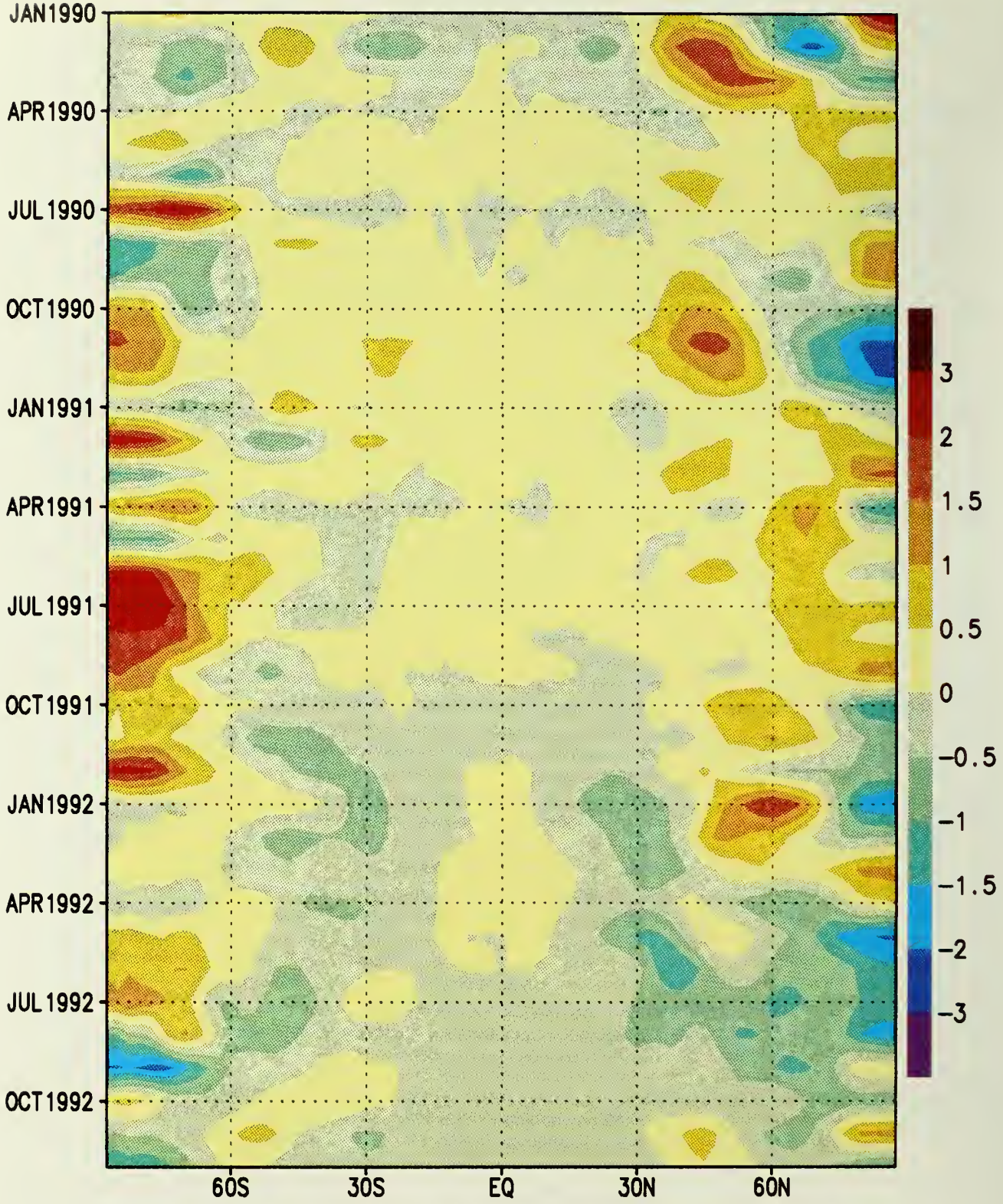

Fig. 40. Time–latitude cross section of zonally averaged mean tropospheric temperature anomalies (Deg. C) from the Microwave Sounding Unit (MSU) channel 2. Anomalies are computed from the 1982–1991 base period. (Data provided by Spencer and Christy.)

4. AEROSOLS

Mt. Pinatubo in the Philippines erupted many times in June of 1991, the major event occurring on the 15th. Sulfur dioxide gas injected into the stratosphere combined with water vapor in the first few months to form sulfuric acid particles, which increase the amount of sunlight reflected back to space. The greater the concentration of particles in the atmosphere, the greater the reflectivity, and the larger the aerosol optical thickness, (AOT). Typical values of AOT are less than 0.1 except where wind-blown dust, smoke from bio-mass burning, or haze from industrialized regions are present in the troposphere. However, since the eruption of Mt. Pinatubo, AOT values have exceeded 0.1 over most of the Earth's surface.

On the average, every increase in AOT of 0.1 corresponds to an increase in the Earth's albedo of 1%. Since the average albedo of the earth is about 30%, an increase in AOT of 0.1 corresponds to a 3.3% increase in the amount of energy reflected back to space. As a result, volcanic dust in the stratosphere has a cooling effect on the Earth's climate.

The weekly zonal averages of AOT values (**Fig. 41**) shows the increase in AOT in the tropics starting in week 24, 1991, associated with the major eruption of Mt. Pinatubo that same week. The AOT peaked in weeks 33-36, gradually diminishing to the end of 1992. Beginning around week 32 of 1992 (mid-August), AOT values increased south of 40°S, as a result of the transport of Mt. Pinatubo aerosols from the tropics and from particles produced by the smaller (1/10th of Mt. Pinatubo) eruption of Mt. Hudson in Chile in mid-August 1991. The AOT values reached a maximum in week 48, and then diminished to the end of the year. The increase in AOT northward of 30°N from week 50 of 1991 to week 18 of 1992 (mid-April), was associated with the northward transport of the Mt. Pinatubo aerosol, as well as from wind-blown dust from the Asian continent. By the end of 1992, diffusion and fall out of aerosols with time have returned the AOT observation in the tropics to approximately pre-eruption conditions.

The difference between monthly mean AOT values after the eruption of Mt. Pinatubo and monthly mean values observed for two years prior to the eruption for three different latitude bands (tropical, mid-northern, and mid-southern) is an estimate of the concentration of volcanic particles in the stratosphere (**Fig. 42**). Only in the 40°S-60°S band does AOT not appear to be gradually decreasing in particle concentration from the time of maximum: August 1991 for the tropics, November 1991 for the mid-Southern Hemisphere, and April 1992 for the mid-Northern Hemisphere. By the end of 1992, stratospheric particle concentrations had dropped to well below half of their peak in the tropics (15% of peak) and in the mid-Northern Hemisphere (40% of peak), but remained relatively high in the mid-Southern Hemisphere (60% of peak). Barring any future volcanic eruptions, predictions based on these observed decreases in stratospheric particle concentration indicate that the volcanic particle cloud should dissipate (AOT departures will be near zero) by the end of 1993.

The regional evolution of the volcanic cloud during 1992 is shown in **Figs. 43 and 44**. In January, 1992, particles from Mt. Pinatubo first begin to be present in high concentrations over large areas north of 30°N. By April 1992, they had clearly made their way to the high northern latitudes. At the same time, AOT anomalies in the tropical band had been diminishing in concentration until, by December 1992, much of the tropics returned to near pre-eruption

concentrations. Interestingly, AOT in the mid-latitude Southern Hemisphere band, which appeared to be diminishing in March of 1992 (cf. **Figure 42**; AOT values cannot be derived over high latitudes in winter), remained well above normal by December 1992. This suggests that particles from the tropics have been transported to these higher southern latitudes by the winter/spring circulation patterns of the Southern Hemisphere, consistent with the observed decline of AOT in the tropics during 1992.

Another measure of atmospheric aerosols is the "apparent" transmission, or transmission ratio (*Ellis and Pueschel, 1971*), which is derived from broadband (0.3 to 2.8μm) direct solar irradiance observations at Manua Loa Observatory, Hawaii (**Fig. 45**). The relative effect of three major volcanic events over Manua Loa can be seen in 1963, 1982, and 1992. Of particular interest is the smaller maximum but longer sustained effect of Pinatubo relative to El Chichon (in 1982). This is indicative of the larger overall global presence of aerosols injected into the atmosphere by Pinatubo and the greater potential for global climate effects such as suggested by the AOT (**Fig. 41**) and the time series of global and hemispheric lower tropospheric temperature anomalies (**Fig. 37**).

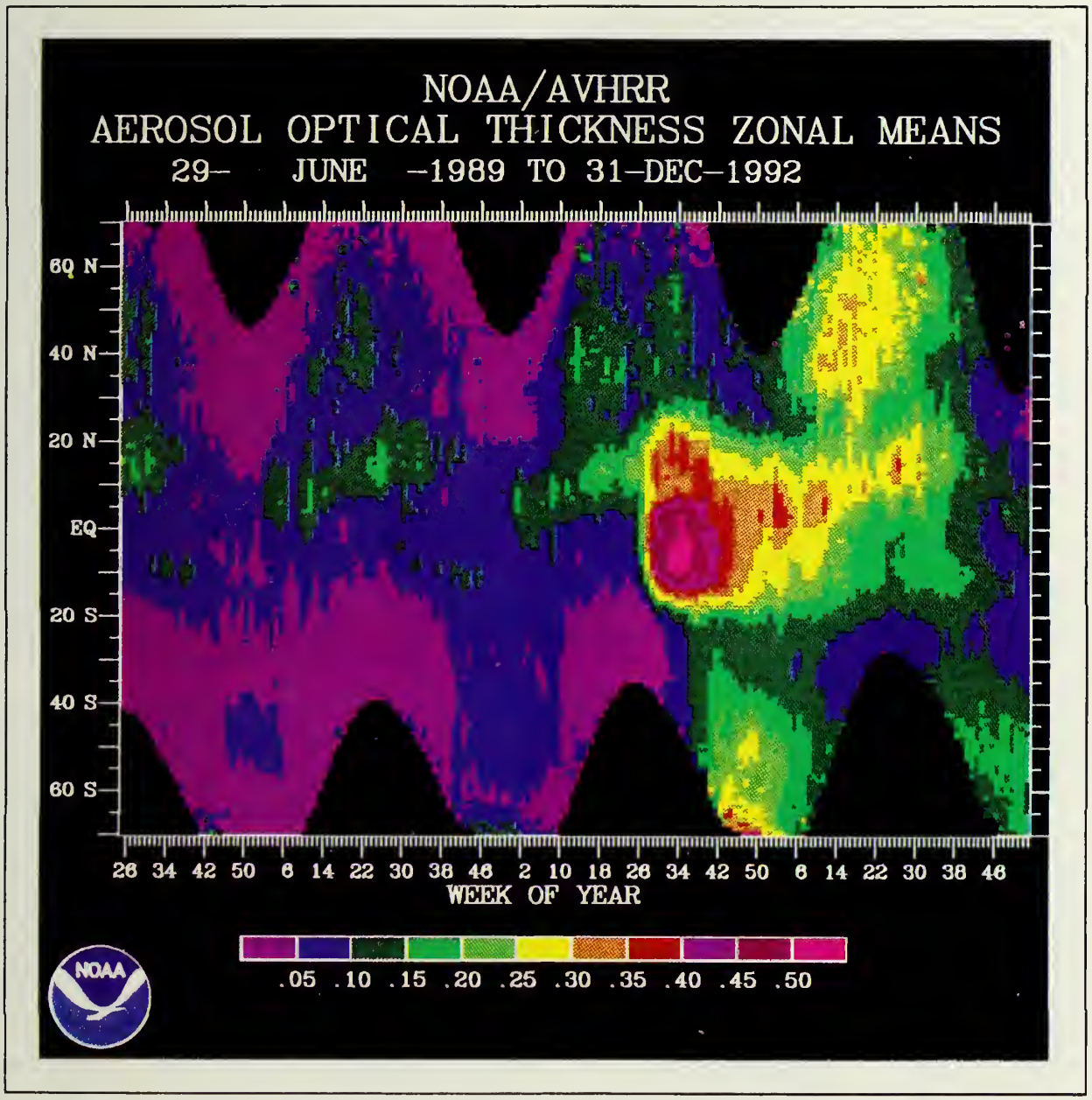

Fig. 41. Weekly zonal averages of the aerosol optical thickness (AOT) from 70°S to 70°N for the period June 29, 1989 through December 31, 1992. (Data provided by L. Stowe.)

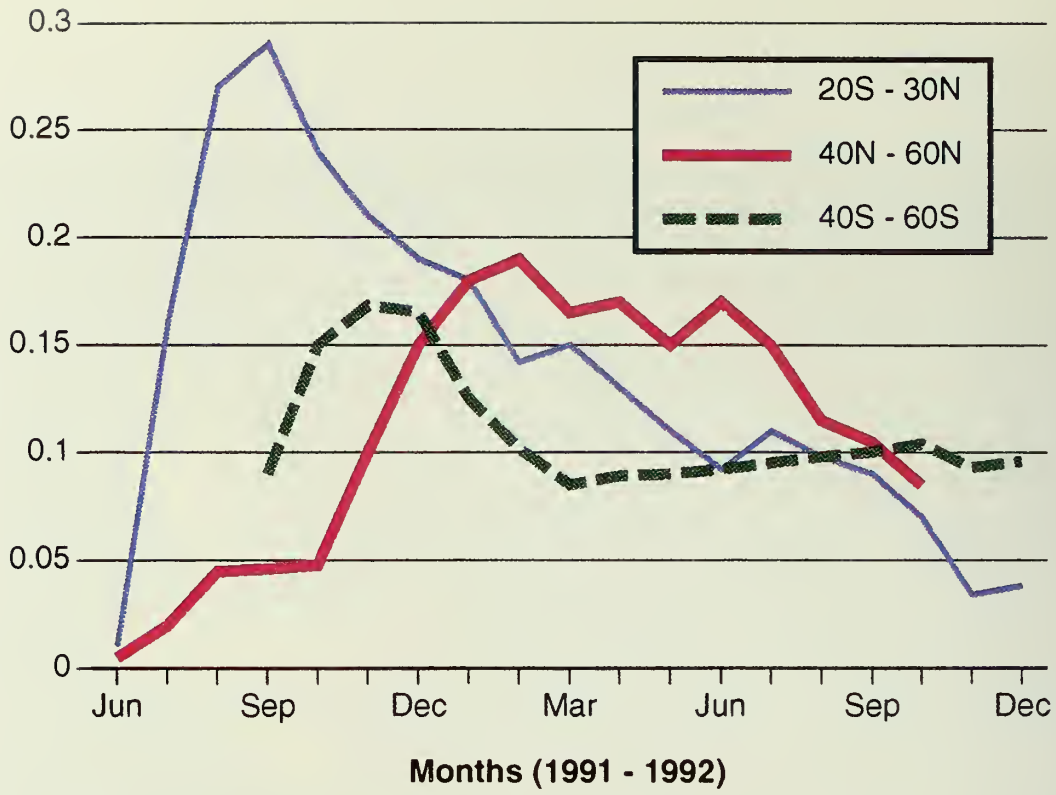

Fig. 42. Departure of aerosol optical thickness (AOT) from two-year (July 1989 through June 1991) mean zonal values for the tropics, the Northern Hemisphere mid-latitudes and the Southern Hemisphere mid-latitudes. (Data provided by L. Stowe.)

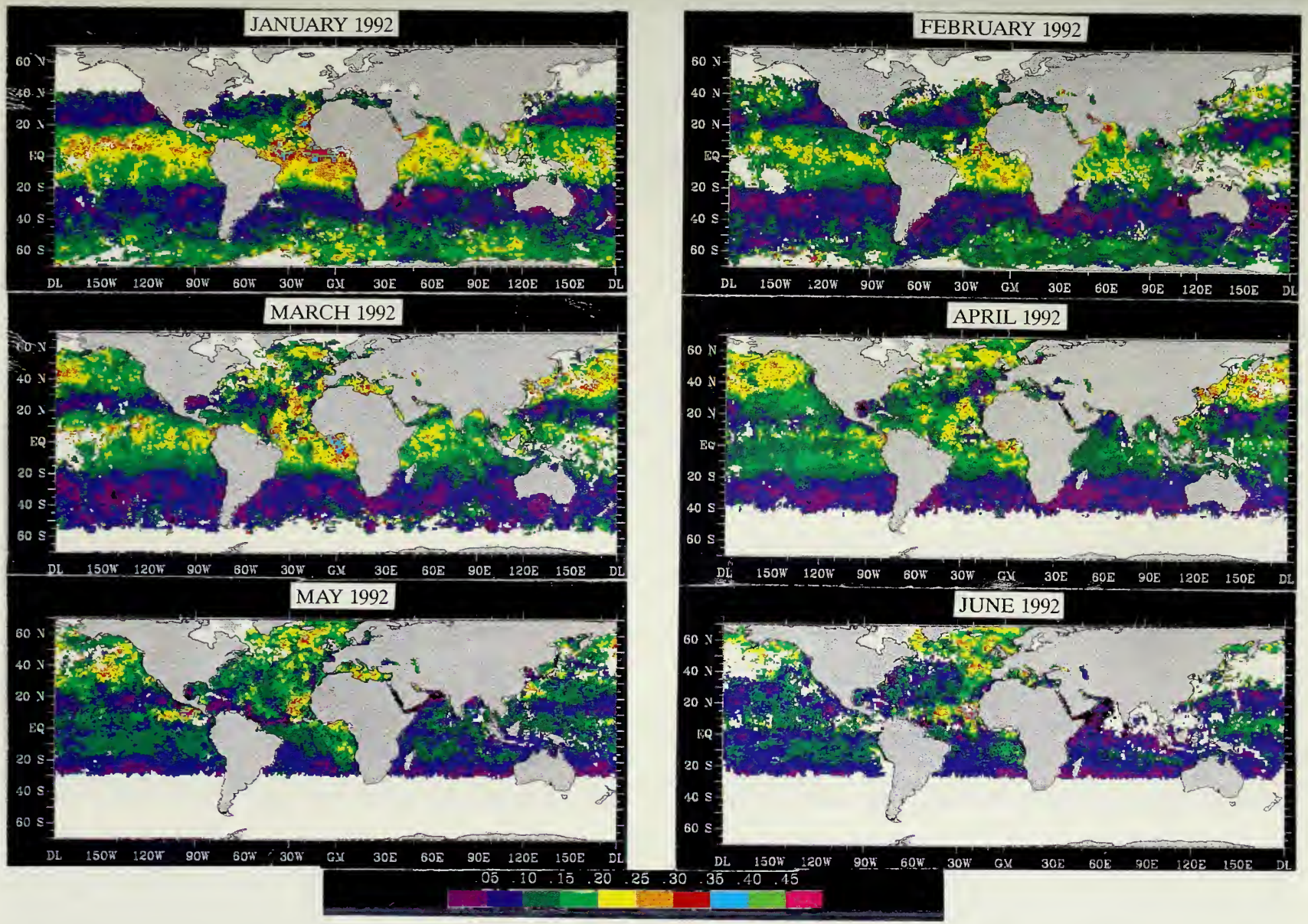

Fig. 43. Monthly aerosol optical thickness departures from the July 1989 - June 1991 normal for the first half of 1992. Colors (see color bar) represent increases in stratospheric particle concentration from 70°S to 70°N. (Data provided by L. Stowe.)

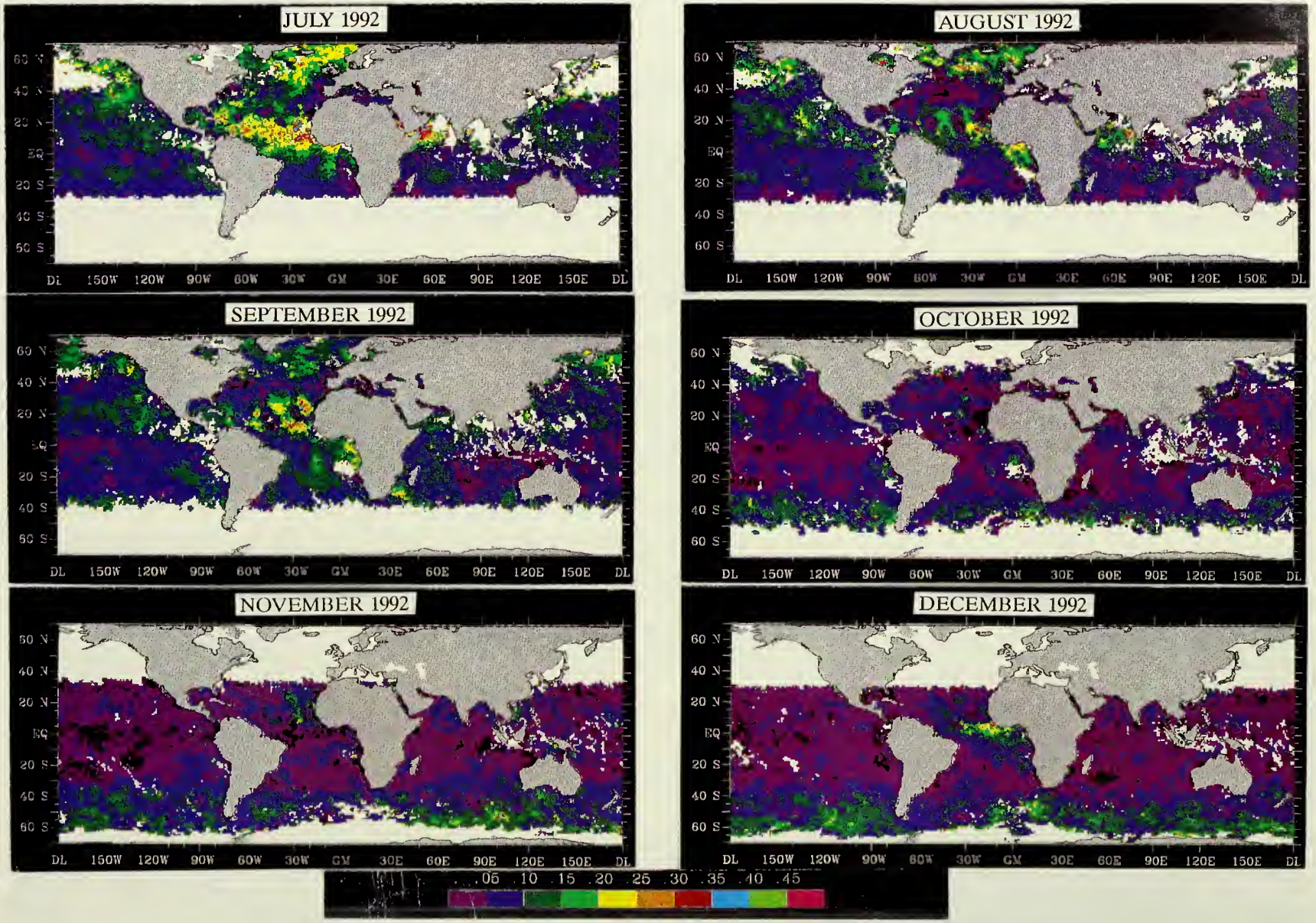

Fig. 44. Monthly aerosol optical thickness departures from the July 1989 - June 1991 normal for the second half of 1992. Colors (see color bar) represent increases in stratospheric particle concentration from 70°S to 70°N. (Data provided by L. Stowe.)

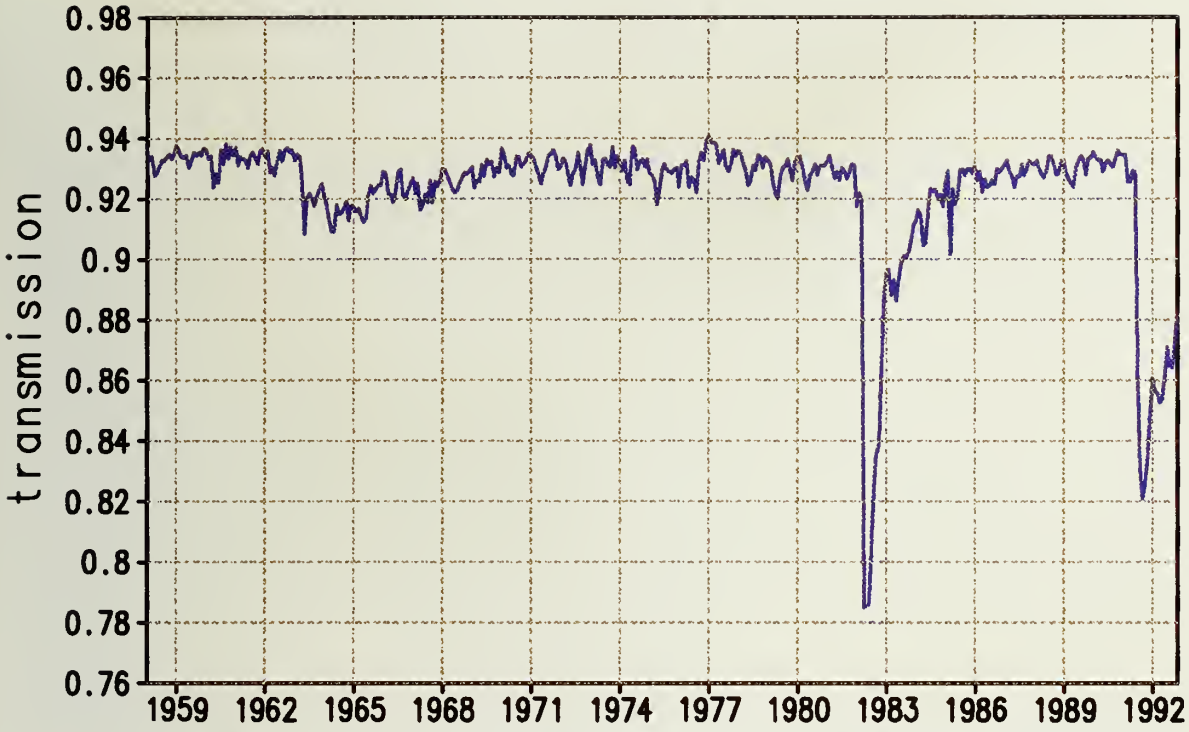

Fig. 45. "Apparent" atmospheric solar transmission at Manua Loa Observatory, Hawaii as determined from direct solar radiation measurements. (Data provided by E. Dutton at NOAA/CMDL.)

5. TRACE GASES

a. Ozone

Observations indicating that the Antarctic region undergoes a major depletion of column ozone during the Southern Hemisphere spring season has led to major international efforts to regularly observe and to explain this phenomenon. Enhanced ozone depletion is now recognized to be due to chemical reactions associated with polar lower-stratospheric clouds in the very cold winter.

Ozone over Antarctica reached record levels of depletion during September and October 1992. The rapid decrease of total ozone from late August through late October as observed from the NOAA-11 TIROS Operational Vertical Sounder (TOVS) is shown in **Fig. 46**. The evolution of the ozone hole is illustrated first on August 31, when a small area of low ozone developed over the Antarctic Peninsula. The continued development of the area of low ozone over the polar region is apparent by September 7. By October 5, an area of severely low ozone values extended over the tip of South America. The area of low ozone continued to expand, covering almost the whole Antarctic continent by October 11, with extremely low values near the South Pole. On October 22, the area of low ozone was displaced off the Pole toward the Indian Ocean, with an area of relatively high ozone encroaching toward the polar region, on the Pacific side of the Antarctic continent. By December 6, the area of low ozone had diminished considerably.

Monthly averages of total ozone values over the polar region, 70°S to the South Pole (**Fig. 47**), show the decline in ozone amounts over the south polar region in 1992 and in recent years since 1979. The monthly average minimum values in the Austral Spring (September- October) has decreased from about 275 Dobson Units (DU) in 1979 to under 200 DU in recent years. The maximum monthly average values for the high-latitude Southern Hemisphere also show substantial decreases from 1979 to 1992, indicating that the ozone decreases have not been limited to the winter and spring seasons.

The daily extent of the ozone depleted area, defined here by the percent of the area of the Southern Hemisphere where TOVS data indicate values below 212 DU (**Fig. 48**), shows the magnitude of ozone depletion over the Antarctic region. Ozone values below 212 DU of total ozone are not generally observed outside the polar regions, and were not observed in the polar regions before the early 1980's. It therefore represents a convenient threshold value for depicting the "ozone hole". An area of strongly depleted ozone was seen by the beginning of September 1992, about 10 days sooner than any previous year. In late September to early October 1992, the area of the ozone hole was at its largest extent, and was almost 50 percent larger than the maximum value previously registered in 1991 and 1987.

The vertical extent of the fully depleted region over the South Pole in 1992 also increased, extending over the 14 to 18 km region. Some of this enhanced ozone depletion may be associated with increased ozone destruction in the presence of aerosols from the Pinatubo volcanic eruption. The low stratospheric temperatures during August 1992, and other factors attendant with the increasing westerly phase of the QBO, may also have been contributing factors in the enhanced ozone destruction. These factors add to the depletion due to reactions of chlorine

species on polar stratospheric clouds. As chlorine and bromine abundances continue to increase in the stratosphere, further gradual decline of ozone is anticipated.

b. Carbon Dioxide

Carbon dioxide is the most important gas associated with global warming other than water vapor. It has been measured continuously at Manua Loa Observatory, Hawaii, since the late 1950's. Monthly mean values for the period are shown in **Fig. 49**. The data through 1973 are from *Keeling et al. (1982)*, while data since 1973 are from the NOAA program (*Thoning et al., 1989*). The record constitutes the longest carbon dioxide measurement series in the world and clearly shows steadily increasing concentrations with time.

Manua Loa Observatory, located at an elevation of 11,000 feet on the flank of Manua Loa volcano, is an ideal site for carbon dioxide measurements. There is no nearby vegetation and the prevailing nighttime downslope winds give a representative sampling of mid-tropospheric air from the middle of the North Pacific Ocean. As such, the record is a reliable indicator of large spatial scale long-term carbon dioxide growth. As an example of the recent trend, the average concentration increase at Manua Loa between 1986 and 1991 was 1.6 ppm per year. While data for all of 1992 have not yet been fully processed, it appears that the growth rate for 1992 will be something less than 1.0 ppm per year. The reasons for this relatively small increase have not yet been determined, but a possible contributing factor is the coincident ENSO episode, which is thought to provide the major variability associated with trends in atmospheric carbon dioxide.

c. Methane

Methane, the third most important greenhouse gas, is measured in air samples collected approximately weekly from various sites in the NOAA/CMDL cooperative air sampling network. Air sampling sites are distributed over a wide range in latitude: 90°S to 82°N. The average increase in the globally averaged methane mixing ratio over the period 1983-1991 is about 11.4 ppb per year or approximately 0.7% per year when referenced to the middle of the sampling record (**Fig. 50**). The long-term growth in methane has decreased from about 13.5 ppb per year in 1983 to about 9.3 ppb per year in 1991 (see *Steele et al., 1992*).

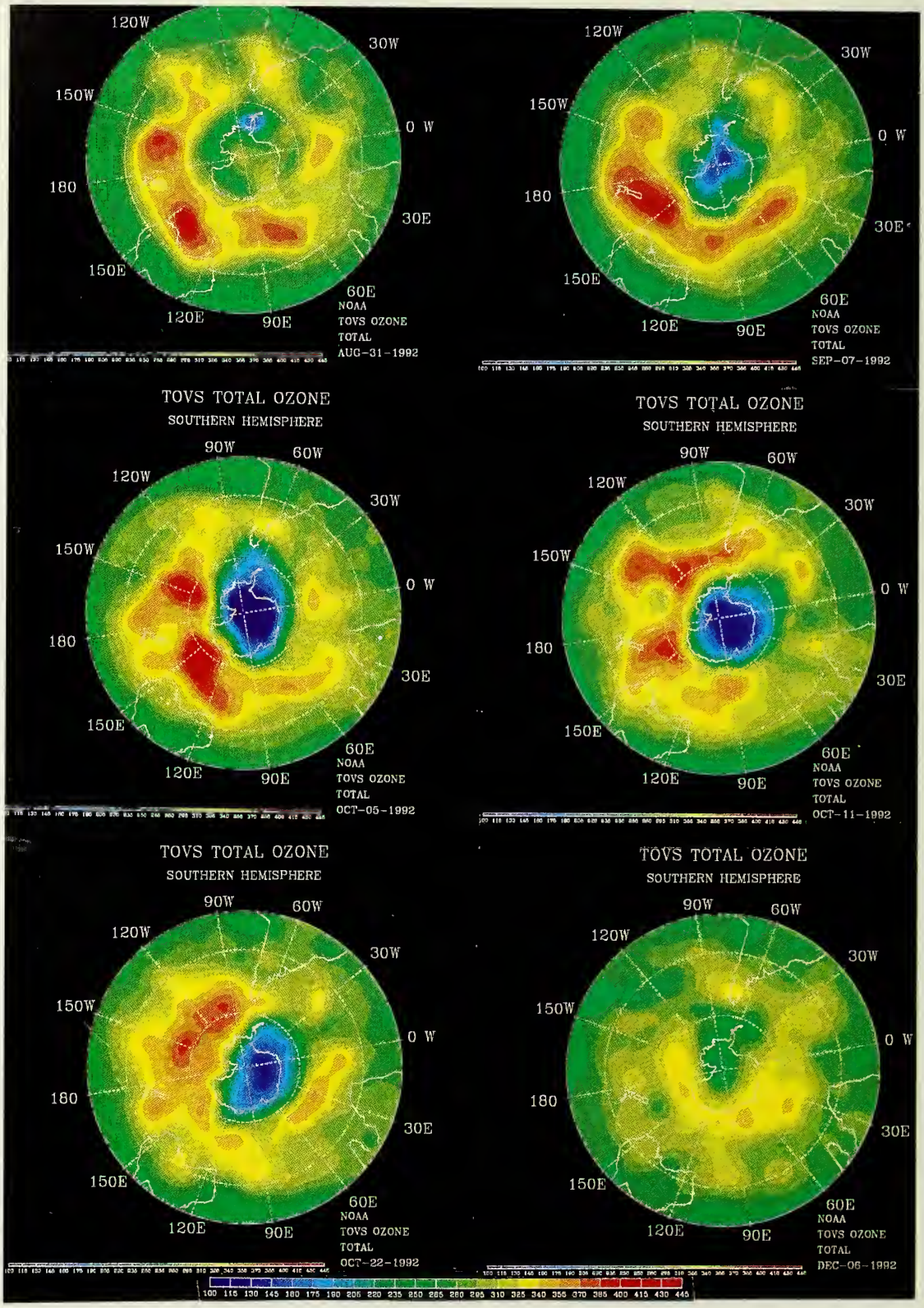

Fig. 46. Total ozone from NOAA 11 TOVS for August 31, September 7, October 5, October 11, October 22, and December 6, 1992. The color scale shows areas of lowest ozone in dark blue and highest ozone in red. (Source: CAC)

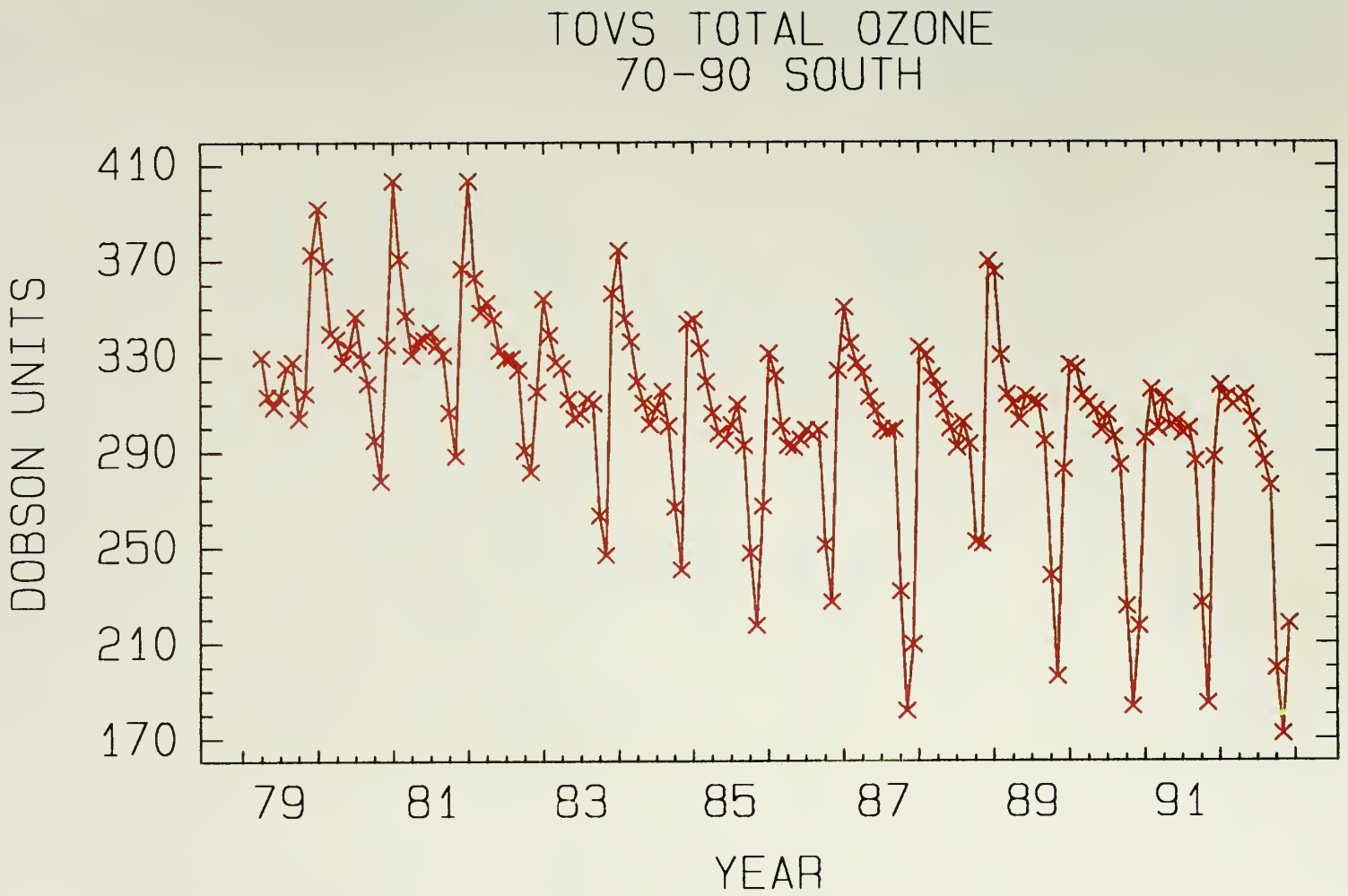

Fig. 47. Time series of monthly average TOVS total ozone values (Dobson Units) over the region 70°S to the South Pole for the period 1979 to 1992.

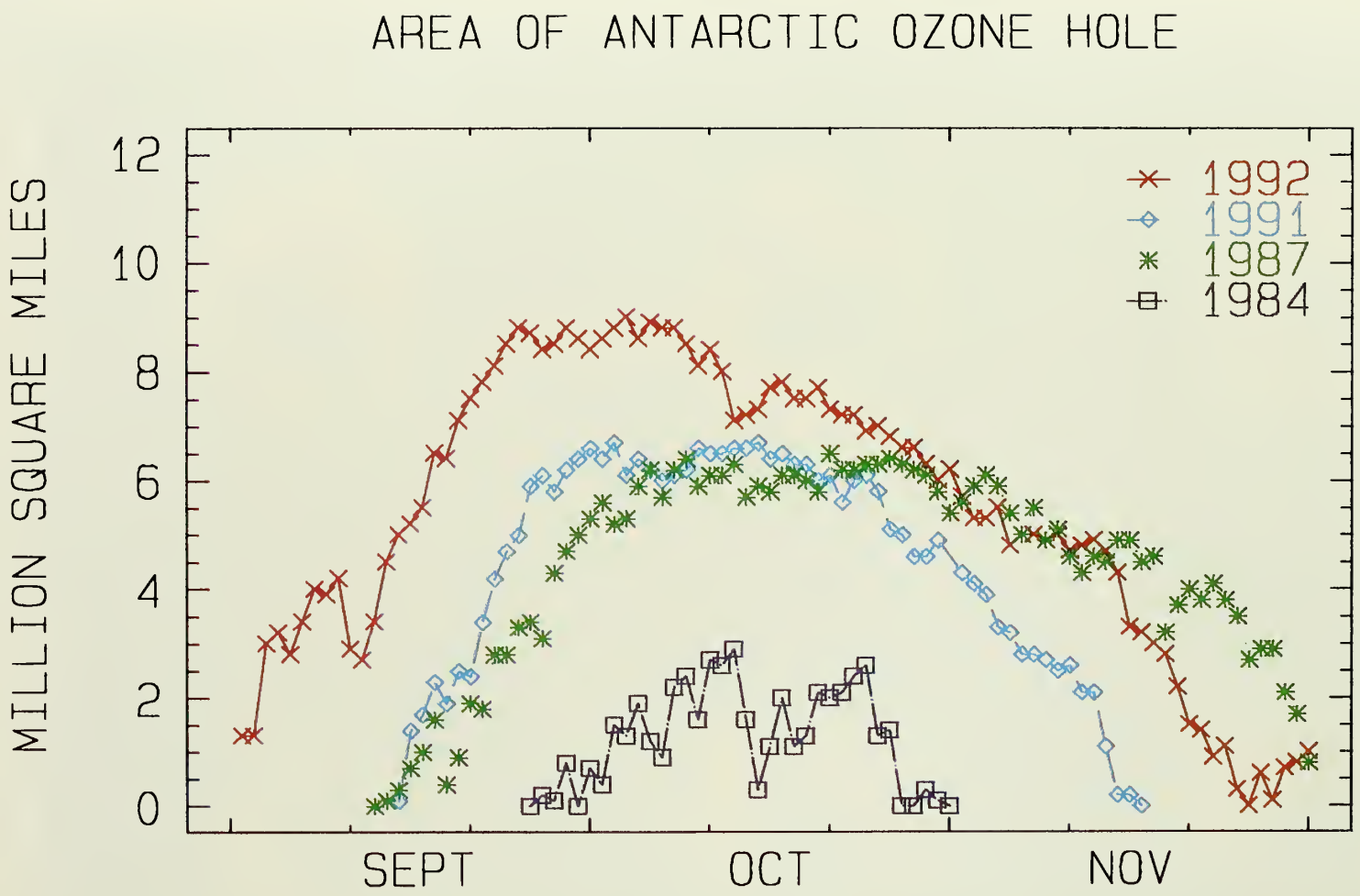

Fig. 48. Time series of the area (million square miles) over which TOVS total ozone was measured to be less than 212 Dobson Units for the September - December period for 1984, 1987, 1991, and 1992.

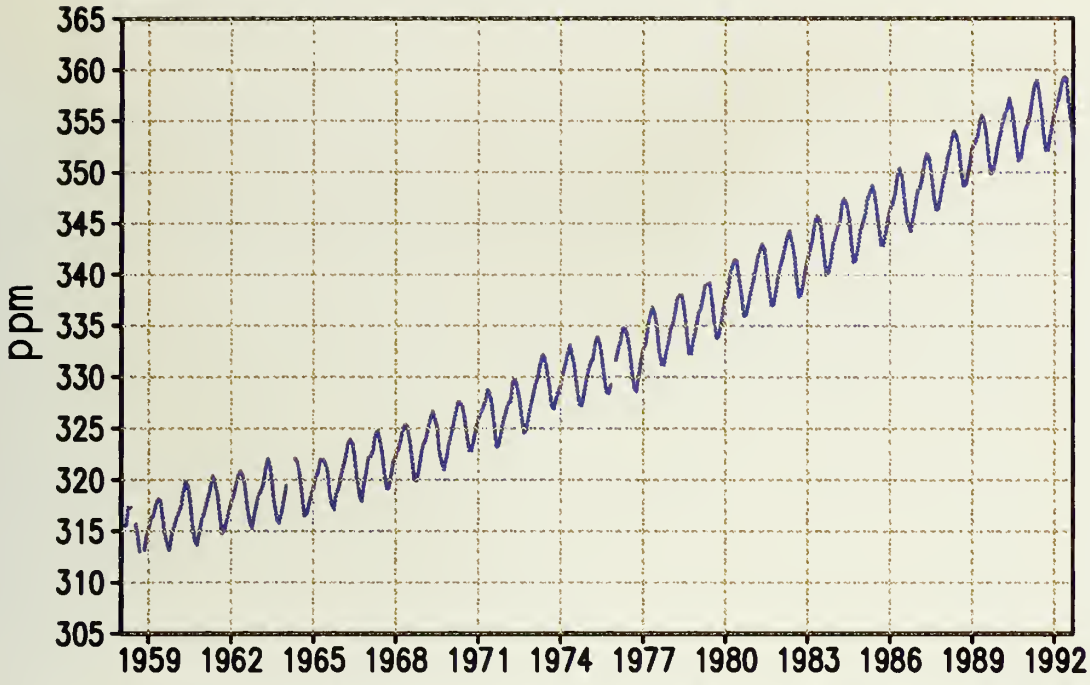

Fig. 49. Monthly mean carbon dioxide concentrations (ppm) measured at Manua Loa, Hawaii, 1957–1992. The data through 1973 are from C. D. Keeling at Scripps Institute of Ocean. (Data provided by NOAA/CMDL.)

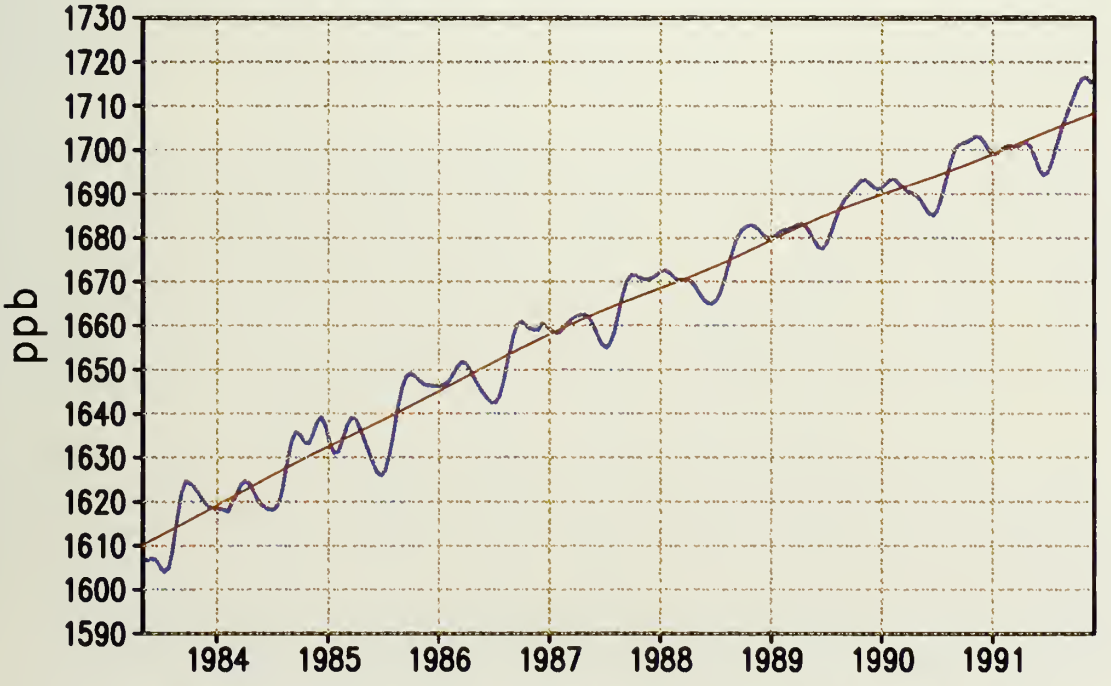

Fig. 50. Globally averaged, biweekly methane mixing ratios in parts per billion by volume determined from the NOAA/CMDL Carbon Cycle Group cooperative air sampling network. Solid line (red) shows growth with seasonal cycle removed.

6. PRECIPITATION

a. Global

While a significant part of the 1992 temperature structure and evolution can be associated with the climatic influences of the aerosols associated with the Mt Pinatubo eruption, there are no widely accepted hypotheses relating volcanic aerosols to global and regional precipitation patterns. However, many of the precipitation patterns observed during 1992 can be interpreted in terms of typical patterns associated with the ENSO phenomenon. Several of the ENSO-related precipitation anomalies are discussed below.

In the southwestern U.S., extremely wet conditions characterized much of the period between December 1991 and May 1992 (**Fig. 51**). Persistent ENSO conditions also helped to provide above normal rainfall in the southeastern U.S. starting in the fall (**Fig. 52**, bottom) and continuing through the end of the year. In southern Florida and Louisiana, these rains added to the precipitation totals associated with hurricane Andrew, one of the strongest hurricanes to hit the United States.

Elsewhere in the U.S., the ENSO-precipitation relationships are not as consistent from episode to episode. Nonetheless, the ENSO-related circulation patterns helped to keep the northwestern U.S. dry during its normal rainy season (December 1991 through May 1992, **Fig. 51**), continuing a multi-year pattern of drought. However, much heavier than normal precipitation along the west coast of the United States during the early winter of 1992/93 may significantly ease the impact of the long term drought.

Both the summer monsoons in India (June through August 1992, **Fig. 53**, bottom) and Australia (December 1991 to March 1992, **Fig. 54**, bottom) had below normal rainfall, as can be expected during ENSO conditions. The ENSO-related precipitation deficits persisted through virtually the entire Australian monsoon season. Likewise, extremely dry conditions also characterized many of the western Pacific Islands during 1992. However, the precipitation deficits were not as extreme during the Indian summer monsoon, perhaps reflecting the weakening of ENSO conditions during most of the Northern Hemisphere summer season.

The ENSO-related precipitation deficits in southern Africa for the November 1991 through May 1992, exacerbated long-term drought conditions (**Figs. 51**, **54**, top). South Africa, in particular, suffered its 5th driest June through July yearly totals in 70 years. These extremely dry conditions were comparable to those associated with the great 1982/83 ENSO event. Fortunately, the 1992-93 rainy season got off to a relatively good start, with widespread moderate to heavy rains falling on much of this region during late October through December.

In South America, heavier than normal ENSO-related precipitation was evident in southern Brazil and Uruguay (**Fig. 51**). Heavy rainfall continued to occur well past the seasons that are statistically related to ENSO (November to March), causing local flooding and mud slides over large areas in the region.

Not all of the precipitation anomalies experienced during 1992 can be related to the current ENSO episode. In particular, much of Western Europe experienced a much drier than normal winter and spring, but wetter than normal conditions in the summer and fall (**Figs. 51, 52**). Further to the east, in Central Europe, precipitation anomalies showed a contrast between summer drought and fall precipitation excess (**Fig. 52**).

In northern Africa, drought not directly related to ENSO was experienced in the Sahel (**Fig. 53**, top), continuing a multi-decade shift to dryer conditions in that part of the world. This long term shift is making it difficult to characterize the contemporaneous rainy seasons in a meaningful way. Thus, while the 1992 rains were clearly below normal, the same can be said for 24 of the past 30 Sahelian rainy seasons. It is perhaps more significant that early estimates place the 1992 Sahel rainy season as the 3rd consecutive season to be dry with respect to the mean rainfall during the past three dry decades.

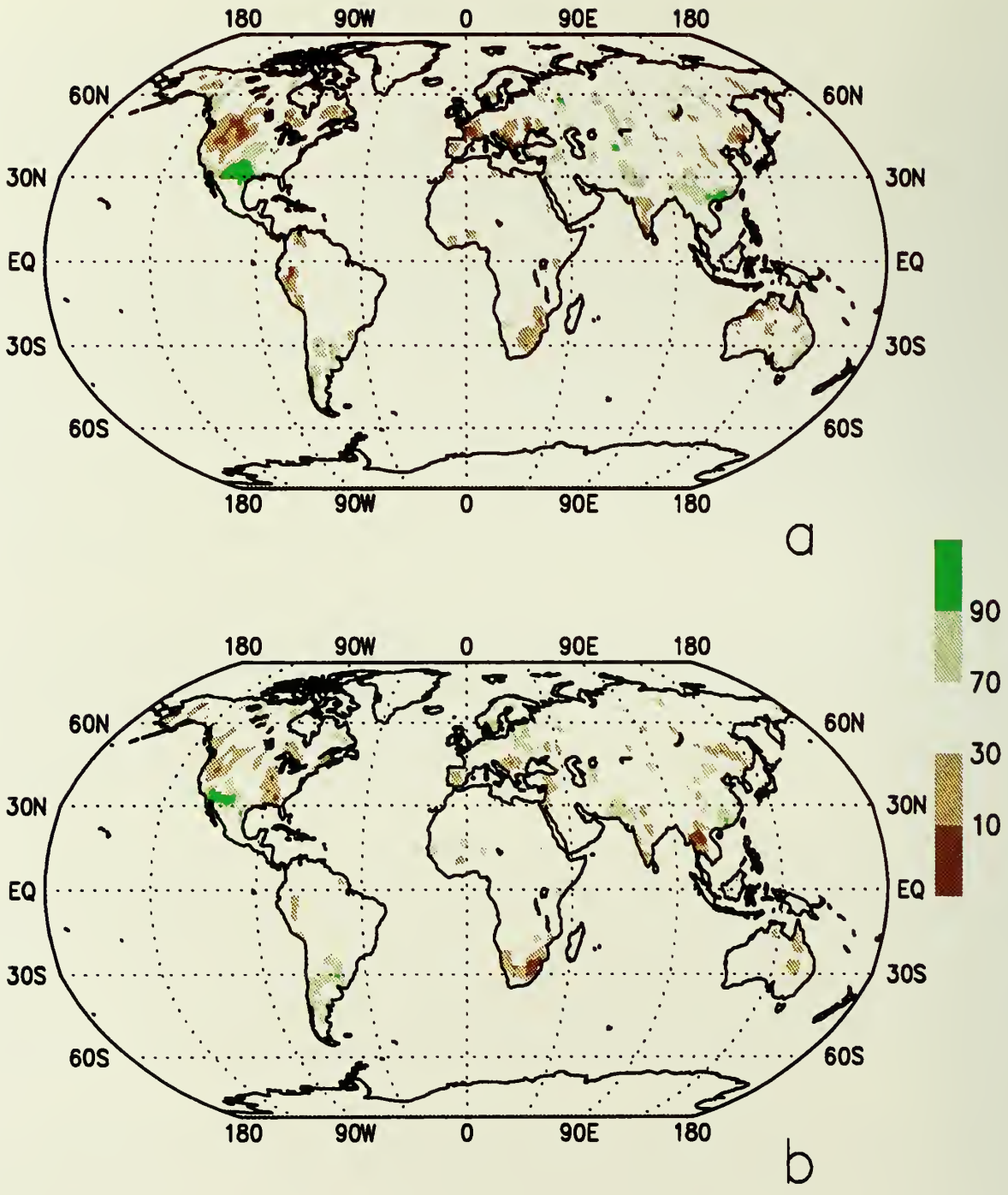

Fig. 51. Precipitation percentiles for a) December 1991–February 1992 and b) March – May 1992 based on a gamma distribution fit to the 1961–1990 base period. Analysis not done in areas with insufficient data.

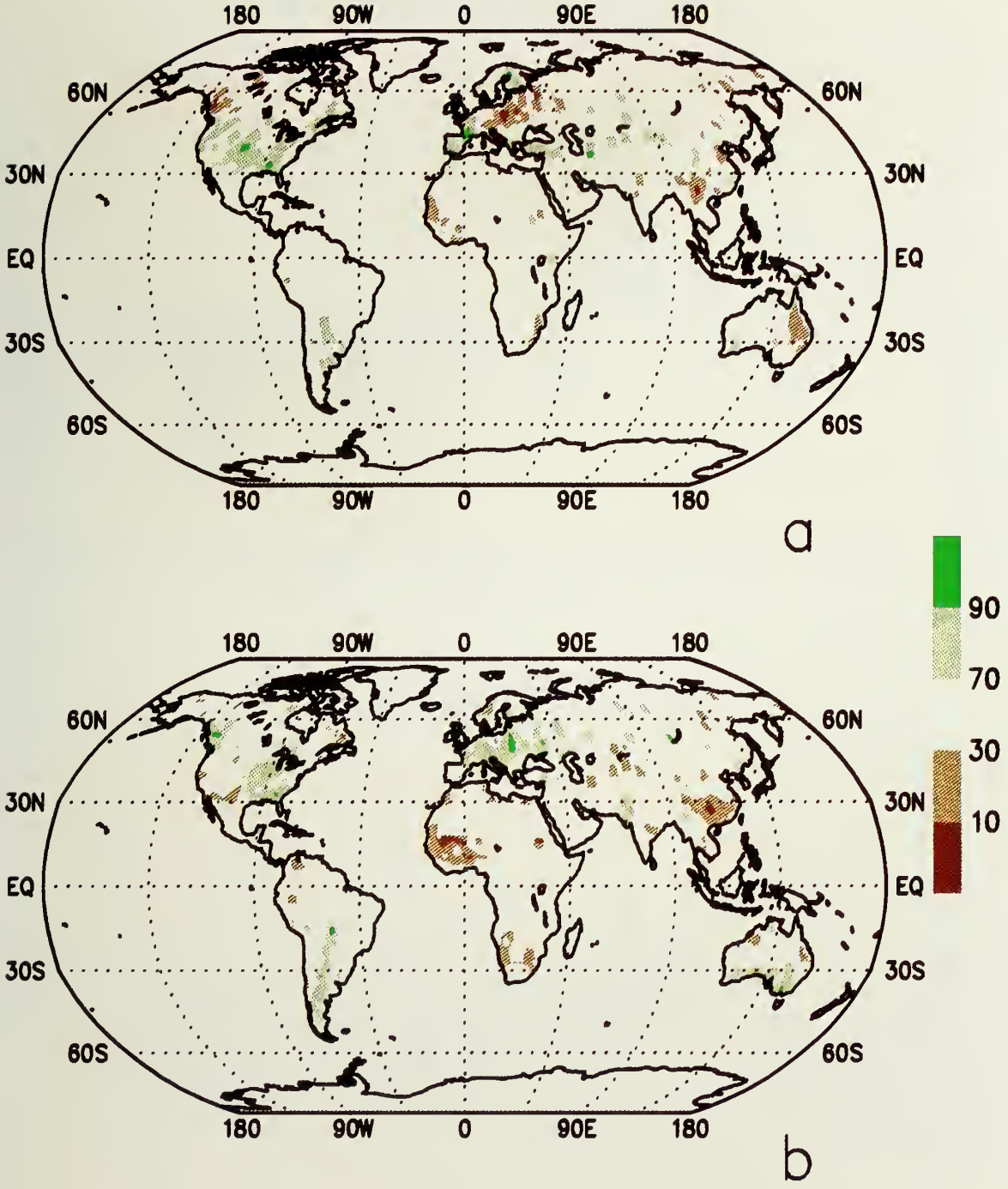

Fig. 52. Precipitation percentiles for a) June – August 1992 and b) September – November 1992 based on a gamma distribution fit to the 1961–1990 base period. Analysis not done in areas with insufficient data.

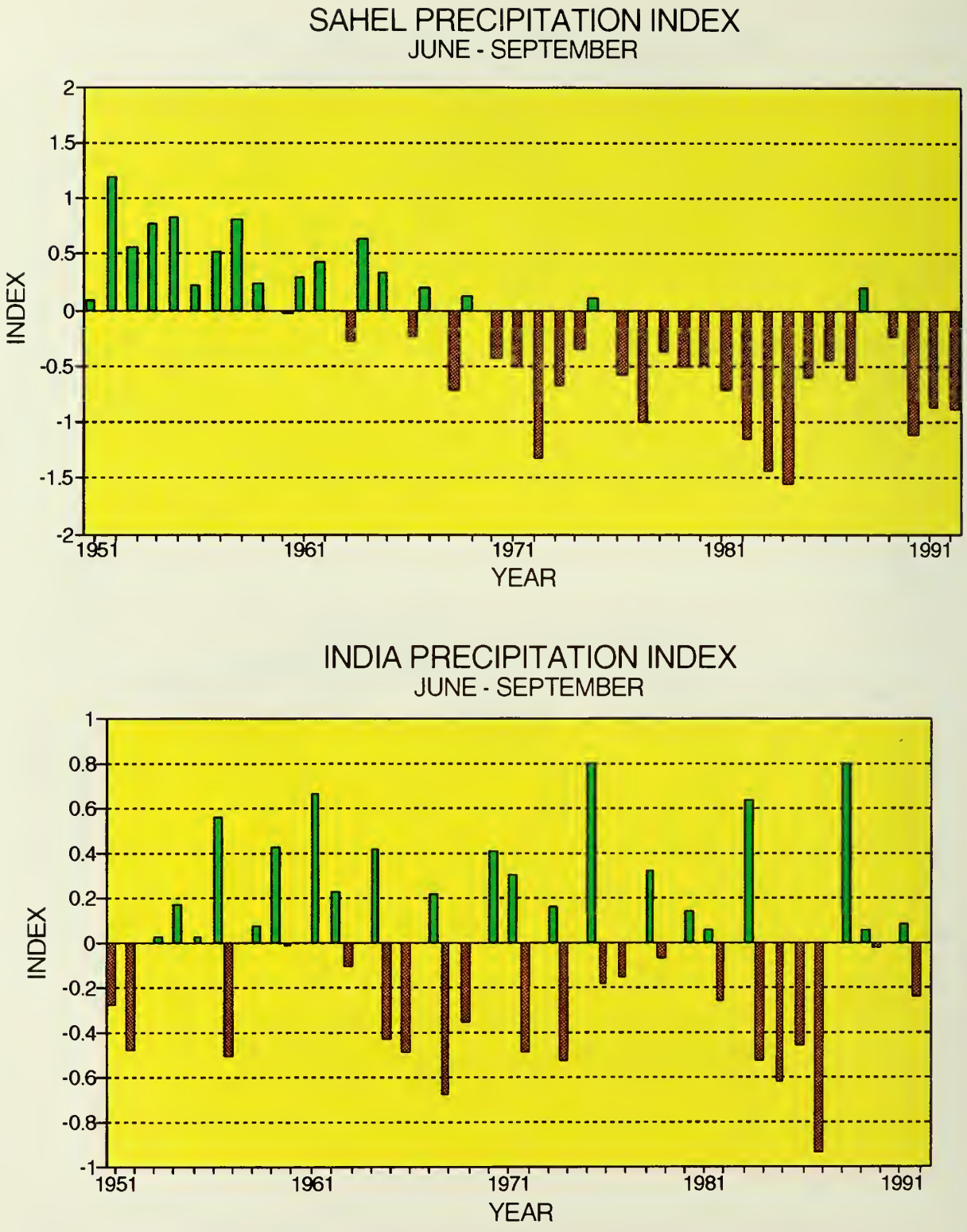

Fig. 53. Precipitation index (average gamma percentiles of station precipitation within the region) for the western Sahel, June - September (top) and India, June - September (bottom). Index computed relative to the 1951-1980 base period. (Source: CAC)

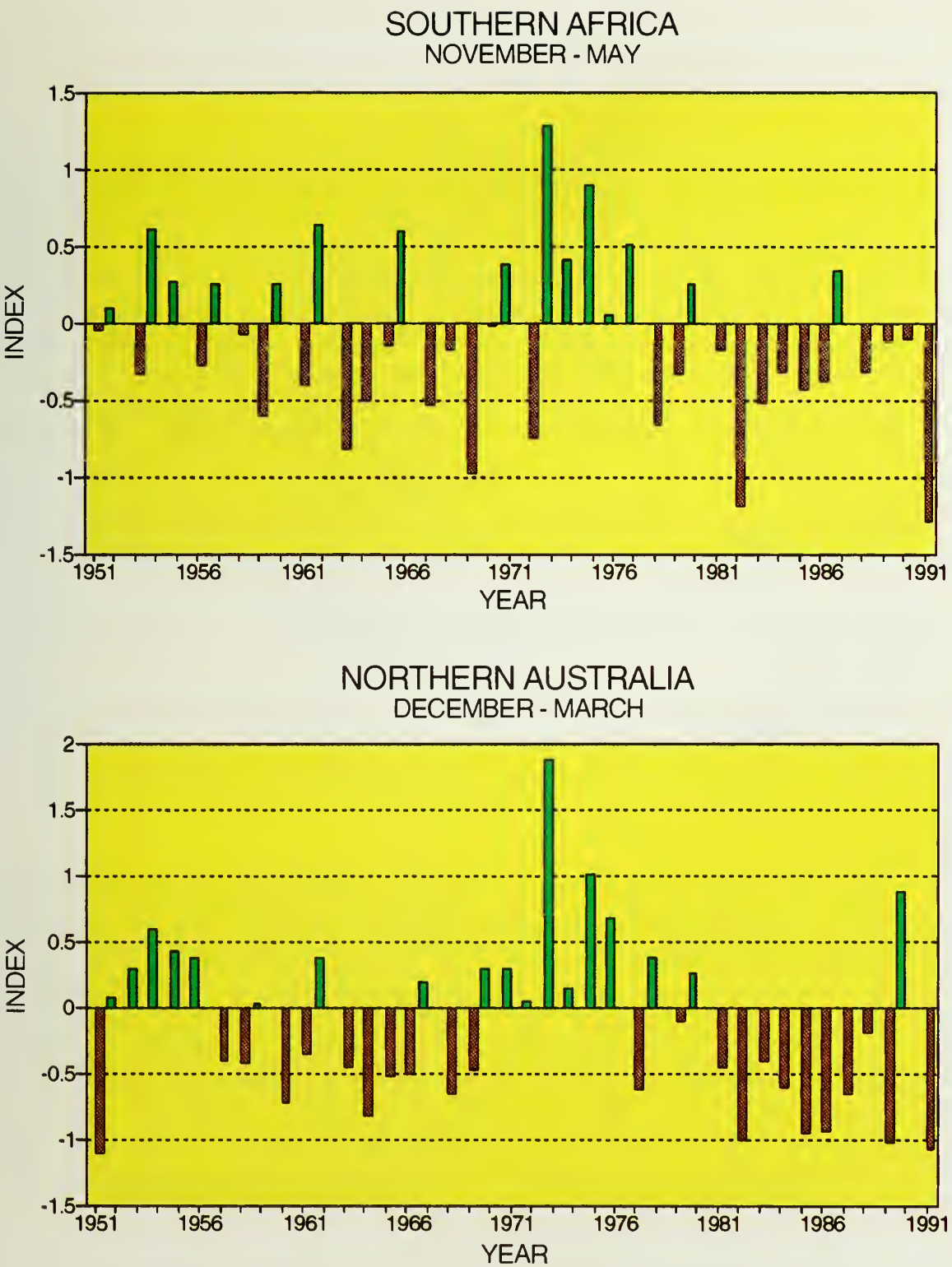

Fig. 54. Precipitation index (average gamma percentiles of station precipitation within the region) for southern Africa, November - May (top) and northern Australia, December - March (bottom). Index computed relative to the 1951-1980 base period. (Source: CAC)

b. Satellite Estimates

Anomalies (1986-92 base period) in tropical rainfall during 1992 (**Fig. 55**) were estimated using the GOES Precipitation Index (GPI) technique (*Arkin and Meisner, 1987*), which was applied to geostationary and polar orbiting infrared data provided by the Global Precipitation Climatology Project (*Janowiak and Arkin, 1991*). The GPI uses a cloud-top temperature threshold to estimate convective rainfall over reasonably large (2.5° latitude/longitude) areas, and hence, is best suited to tropical regions where rainfall is primarily convective and where surface temperatures are relatively warm. The technique erroneously depicts rainfall in regions of persistent jetstream cirrus since temperature is the only information used.

The rainfall anomaly patterns for December 1991 - February 1992 (DJF) and March - May 1992 (MAM) reflect the warm ENSO episode conditions that prevailed during that time in the central tropical Pacific. During DJF, a large region centered at the equator and east of the date line experienced positive anomalies exceeding 150 mm. Conversely, a region west of 170°E of similar size experienced rainfall deficits of about the same magnitude. An eastward shift of the South Pacific Convergence Zone (SPCZ) was also observed during this period. This estimated pattern of rainfall anomalies is consistent with warm episode conditions (Ropelewski and Halpert, 1987).

During MAM, the rainfall anomaly pattern in the central Pacific was quite similar to DJF. The Inter-Tropical Convergence Zone (ITCZ) in the eastern Pacific was stronger than normal, as ENSO-related rainfall anomalies propagated eastward toward the South American coast. Rainfall deficits of more than 100 mm were experienced in Northeast Brazil, which is also consistent with ENSO conditions.

In June-August 1992, the magnitude and extent of the rainfall anomalies in the tropical Pacific declined substantially, and near normal conditions prevailed in most other regions of the tropics. However, estimated precipitation over the Arabian Sea and Bay of Bengal was greater than normal. This observation is contrary to the expected rainfall anomaly patterns in this region since, in general, the summer monsoon rains in the Indian region are less than normal after warm ENSO episodes (*Ropelewski and Halpert, 1987*). Ground-based observations (**Fig. 53**, bottom and **Fig. 58**), show that the Indian sub-continent, as a whole, experienced a slightly drier than normal monsoon season. However, much of this dryness occurred in central India, where the satellite estimates imply near normal rainfall. Observations in India along the Arabian Sea and the Bay of Bengal show that these regions did experience above normal rainfall (**Fig. 58**).

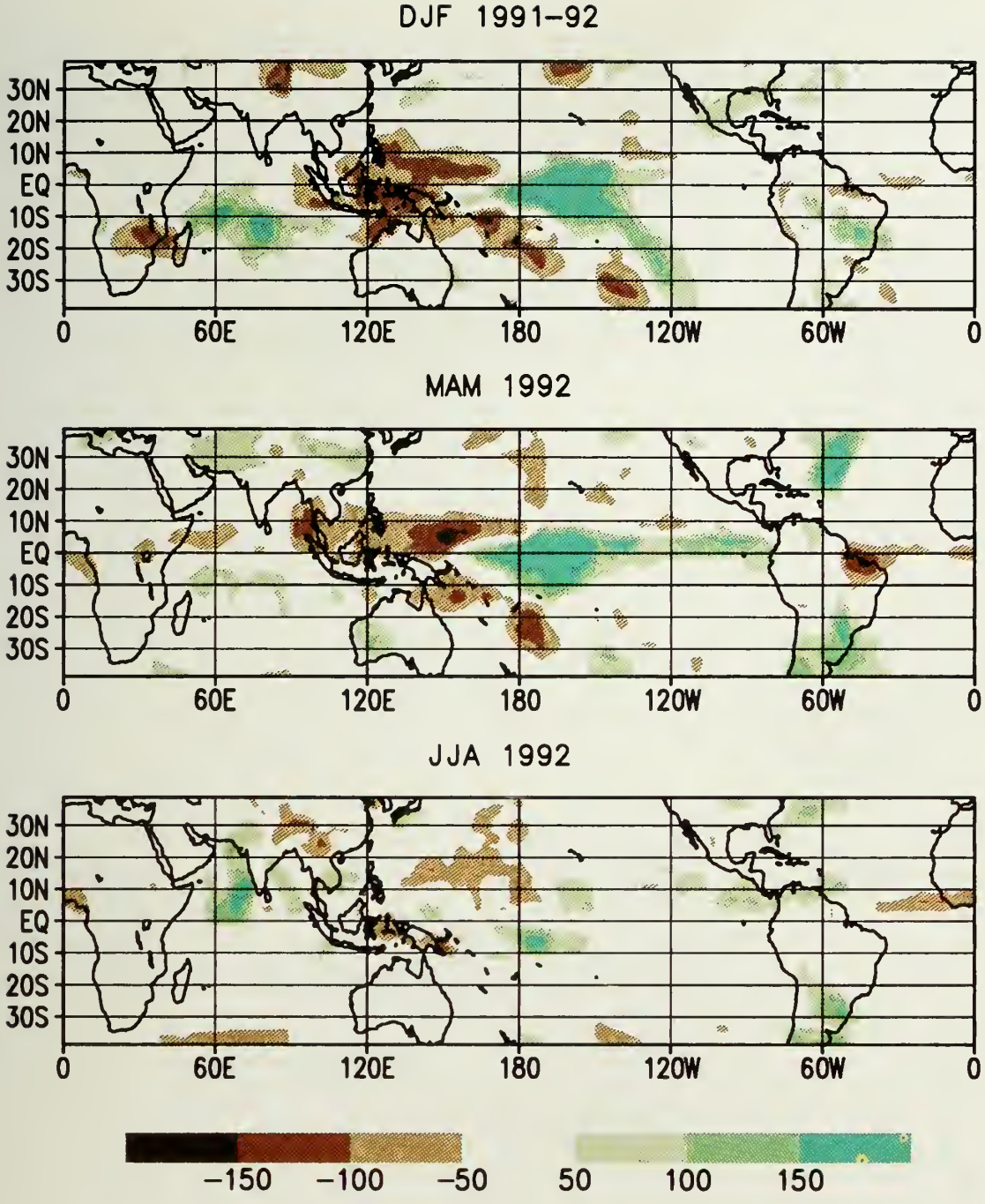

Fig. 55. Satellite-derived estimates of rainfall anomalies Units are mm. Anomalies are computed from 1986–1992 base period.

c. West African Summary

Precipitation totals across western Africa are highly variable, with amounts ranging from over 1200 mm to under 200 mm during May through September 1992 (**Fig. 56**). This time period is especially critical to the Sahel (regions north of about 8°N latitude), since more than 90% of the annual rainfall occurs in this 5 month period. During the month of May, which marks the beginning of the rainy season in the Sahel, precipitation was near normal at most locations. However, during June, when significant Sahelian rainfall traditionally commences, widespread dryness gripped much of the Sahel. Monthly rainfall amounts were among the lowest 10% of the 1951-1980 climatological distribution in the far western Sahel. Also, very little precipitation has fallen in the countries bordering the Gulf of Guinea. Little or no seasonal rains had fallen across northern Senegal, southern Mauritania, and adjacent Mali through early July.

Rainfall increased during mid-July and continued into August across much of the Sahel, bringing seasonal totals closer to normal in some regions. During early September, generous rains (between 75-200 mm) fell on northern Senegal and southern Mauritania, easing dryness there. Elsewhere, rainfall amounts and coverage followed it's normal seasonal decline, except in Niger, where the ITCZ withdrew prematurely. Overall, May-September precipitation was highly variable as most areas recorded subnormal amounts (**Figs. 57**). Less than 75% of normal rainfall (with respect to the 1951-1980 base period) occurred in northern Senegal, Mauritania, and along the Gulf of Guinea, while surplus seasonal precipitation fell on parts of southern Mali, western Burkina Faso, southern Niger. The rainy season in the western Sahel (**Fig. 53**, top) exhibited dryness similar in magnitude to both 1990 and 1991.

May 1 – September 30, 1992

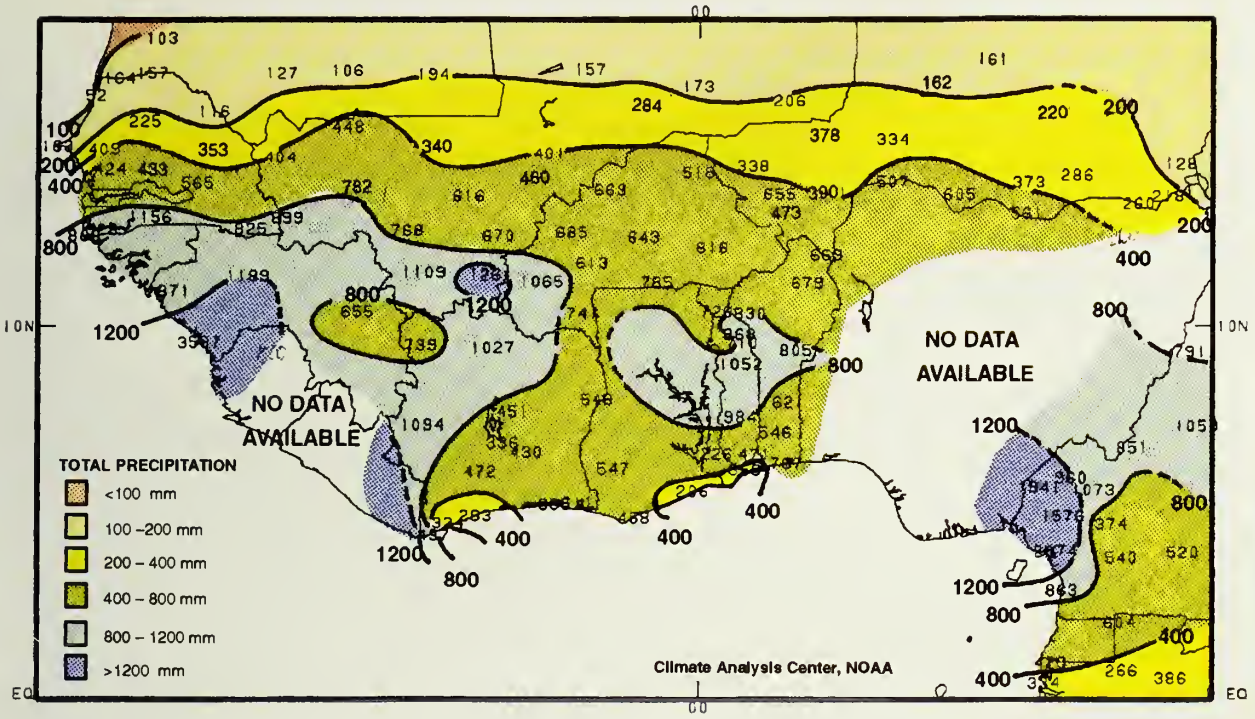

Fig. 56. Total precipitation for West Africa for May - September 1992. (Source: CAC)

May 1 – September 30, 1992

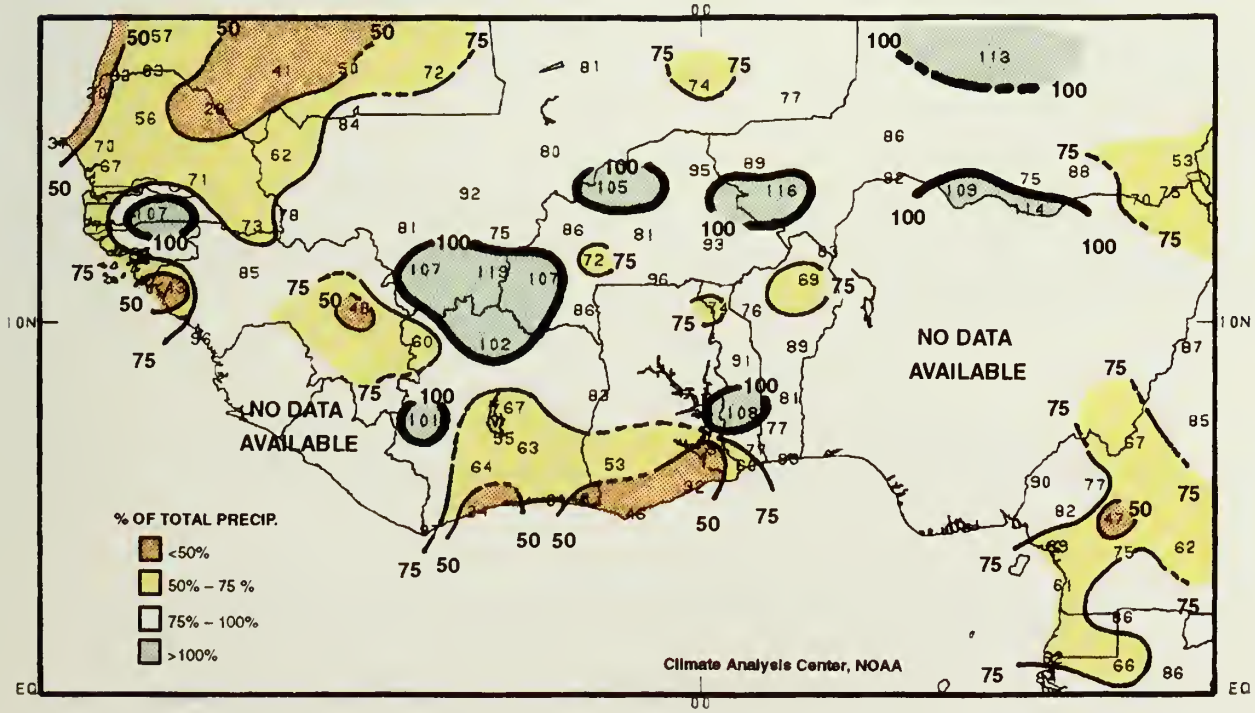

Fig. 57. Percent of normal precipitation for West Africa for May - September 1992. (Source: CAC)

d. Southwest Asian Monsoon Summary

Despite an early start to the monsoon in southern and eastern portions of the subcontinent, much of central and southeastern India experienced an abnormally dry June and first half of July, with many locations observing totals among the lowest 10% of the 1951-1980 climatological distribution. Rainfall in northeastern India was enhanced by Cyclone 3B which swept into India near Calcutta around mid-June, generating flooding throughout the coastline of Bangladesh. Farther north, near to above normal rainfall fell on northern Pakistan, Kashmir, and Nepal.

In mid-July a resurgent monsoon finally produced widespread and abundant rains over much of central, northwestern, and southwestern India, and across much of Pakistan. Unfortunately, heavy late July and early August rains caused flooding in western India's Gujarat state and southern Pakistan's Sindh province. During mid-August over 150 mm of rainfall fell in 12 hours on Karachi. Elsewhere, widespread and generous rains fell across the remainder of India and Pakistan through much of August, with the exception of light rains across southern India's Tamil Nadu state. According to the India Meteorological Department (IMD), the June-August 1992 rainfall was only 92% of the normal monsoon average. During the first three monsoon months, 27 of 35 meteorological divisions in India received normal (between 80-120%) rainfall, two had excess, and six had deficient rains. The IMD stated that the spread of the monsoon was uncharacteristic, with heavy rains in arid regions, while typically wet areas were drier than normal.

As the month of September progressed, torrential downpours inundated sections of northeastern Afghanistan, northern Pakistan, and northern India, producing catastrophic flooding. Farther east, heavy rains in September in northwestern India and northern Pakistan continued for several days, also resulting in widespread flooding. All told, this was the worst flooding in Pakistan since the country was founded in 1947.

Precipitation diminished in mid-September across much of the region. However, despite heavy rain in the Northwest, the 1992 was still below normal across much of northern, central, and eastern India, Bangladesh, and Nepal (**Figs. 58 and 59**).

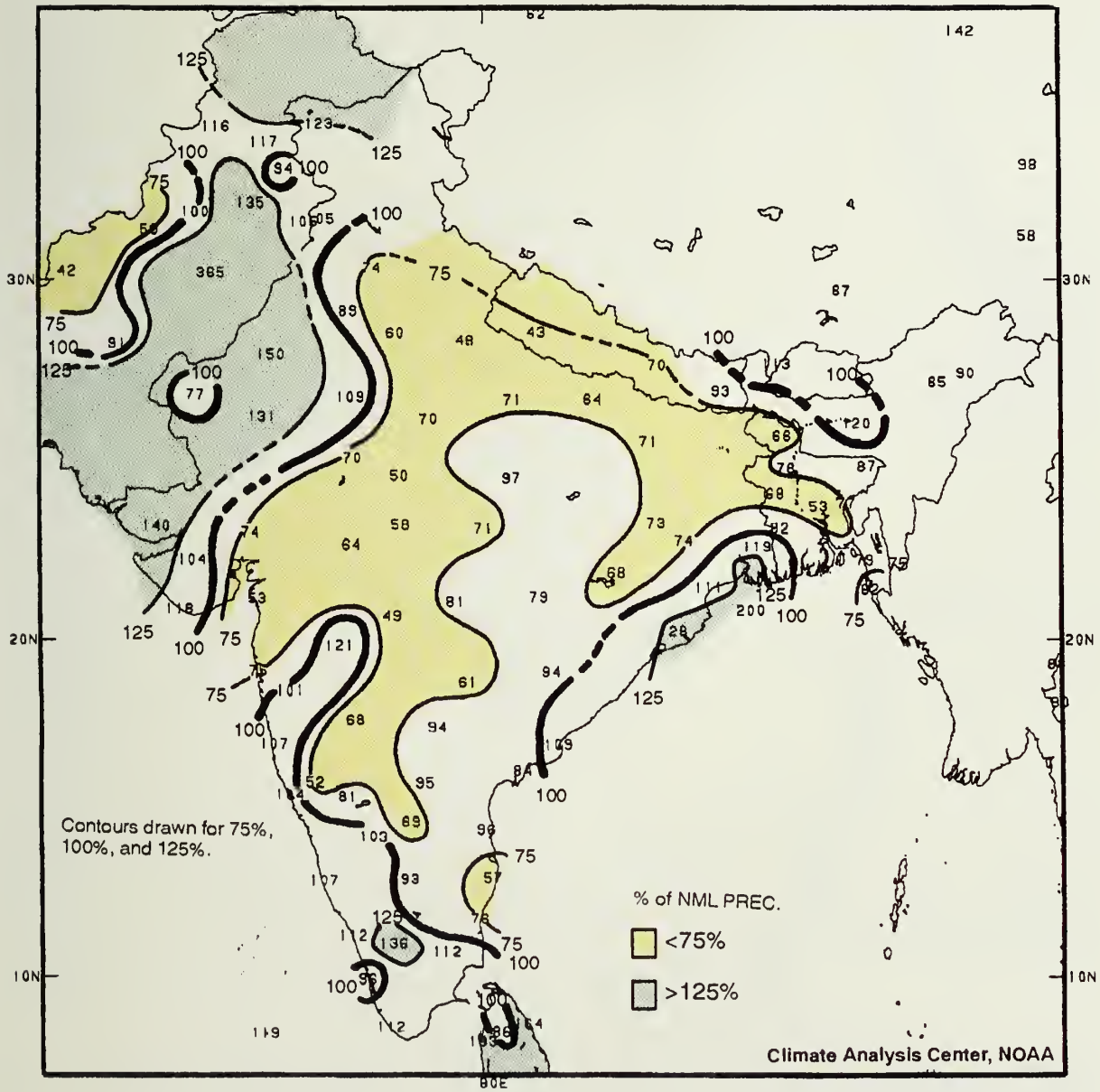

Fig. 58. Percent of normal precipitation for India for May - September 1992.

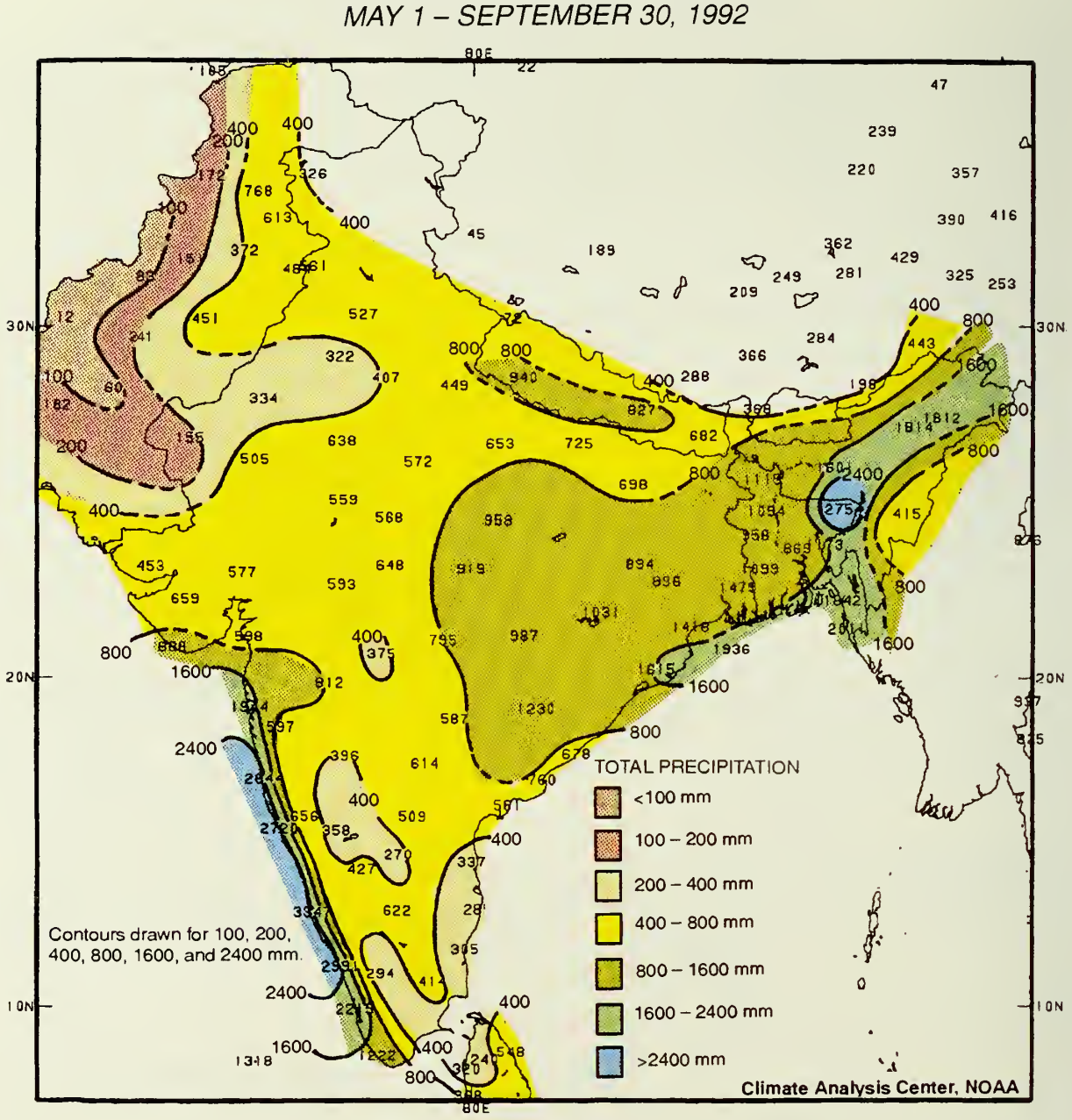

Fig. 59. Total precipitation for India for May - September 1992.

e. Western United States Summary

Precipitation falls in a very distinct pattern across the western United States, with the bulk of the annual total usually occurring during the November - March period. Below normal totals have been observed across large portions of the Far West through each of the last six "wet seasons" (1986/87 - 1991/92). Precipitation deficits of 1000 - 1800 mm have accumulated across much of the Sierra Nevada, Cascades, northwestern California, and the western halves of Washington and Oregon during this period.

October 1992 brought an early start to the wet season in most of the Far West, although totals were small compared to those normally observed later in the season. November, however, was quite dry at most locations. According to the California State Dept. of Water Resources, only 20% of normal November precipitation fell statewide while somewhat larger amounts were reported farther north. Beginning in early December, however, a series of storms brought heavy rains and snows (depending on elevation) to the Far West, especially the Sierra Nevada and Cascades. **Figure 60** compares the precipitation totals that were measured from the beginning of the 1992/1993 wet season through December 5 with those reported December 6, 1992 - January 10, 1993. The precipitation was very beneficial because a larger relative proportion of it fell as snow. Figure 61 shows the percent of normal precipitation and the percent of normal snow water equivalent reported in selected river basins across the Far West as of January 8, 1993. Most locations outside of Washington have received abundant precipitation, and snow water equivalents show even larger surpluses. In Washington, state year end precipitation totals were below normal at many locations, but snow water equivalents were at or above normal, reflecting the unusually large proportion of the precipitation that fell as snow. Across the Sierra Nevadas, snow water equivalent was 140%-145% of normal at the end of the 1992.

The 1992/1993 wet-season precipitation totals through January 1, across California's primary water storage regions are the largest of the past 8 seasons, including what has been termed a "flood year" in 1985/1986 (**Fig. 62**). Despite the recent heavy rains and snows, reservoir storage at California's primary reservoirs remain very low (below 60% of normal with little change from January 1 of 1992). An accurate assessment of the expected improvement in the state's water supply provided by these storms cannot be made until the snowpack begins to melt and the water flows into the reservoirs in late spring.

The large December 1992 precipitation total reported statewide is not unprecedented (**Fig. 63**). Similarly large amounts have fallen at other times since the commencement of drought conditions, but the wet spells did not continue long enough to provide complete relief. Through January, however, 1992/1993 is the first wet season since the beginning of the drought to bring above normal precipitation to each of California's ten hydrologic regions (**Fig. 64**). This has resulted in widespread benefits and provides the possibility of significant improvement in long-term conditions, should ample precipitation occur during the remainder of the wet season.

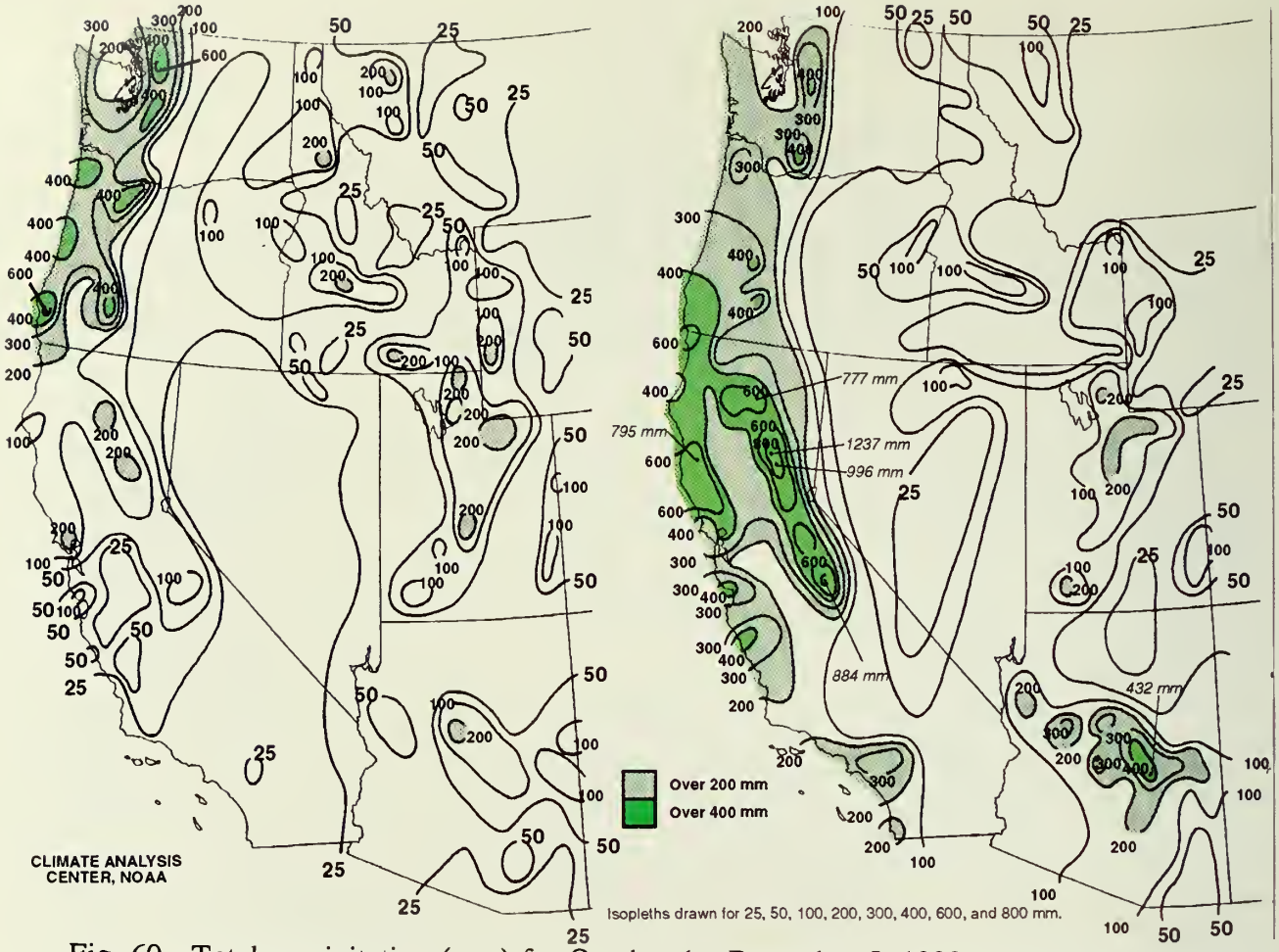

Fig. 60. Total precipitation (mm) for October 1 - December 5, 1992 and December 6, 1992 - January 15, 1993. (Source: CAC)

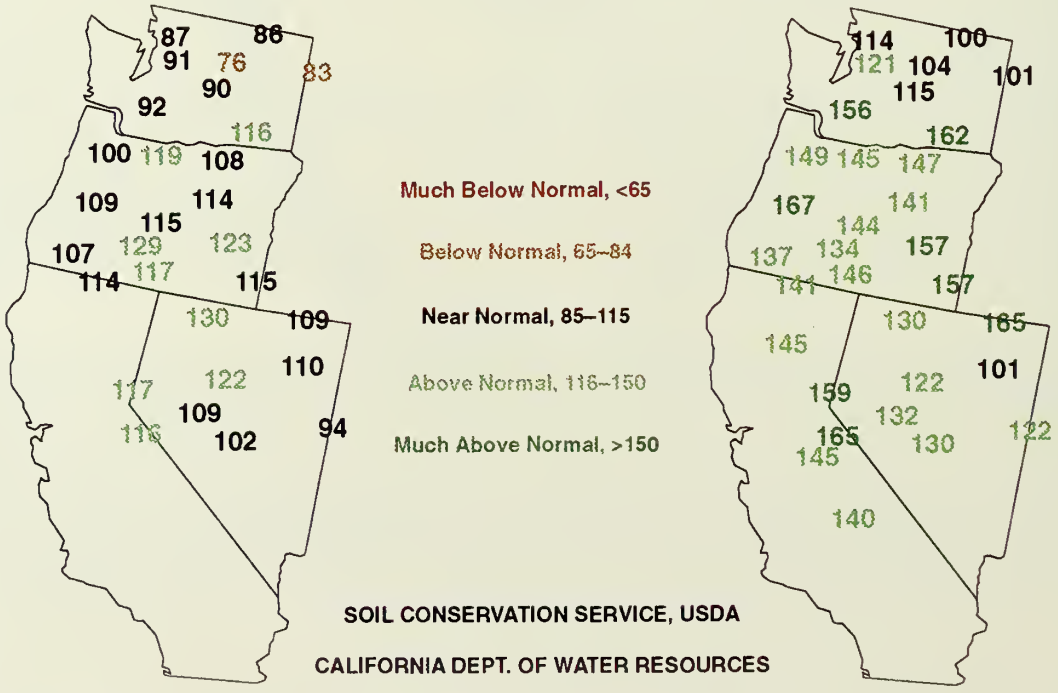

Fig. 61. Percent of normal precipitation (left) and percent of normal snow water equivalent (right) for period October 1, 1992 - January 8, 1993.

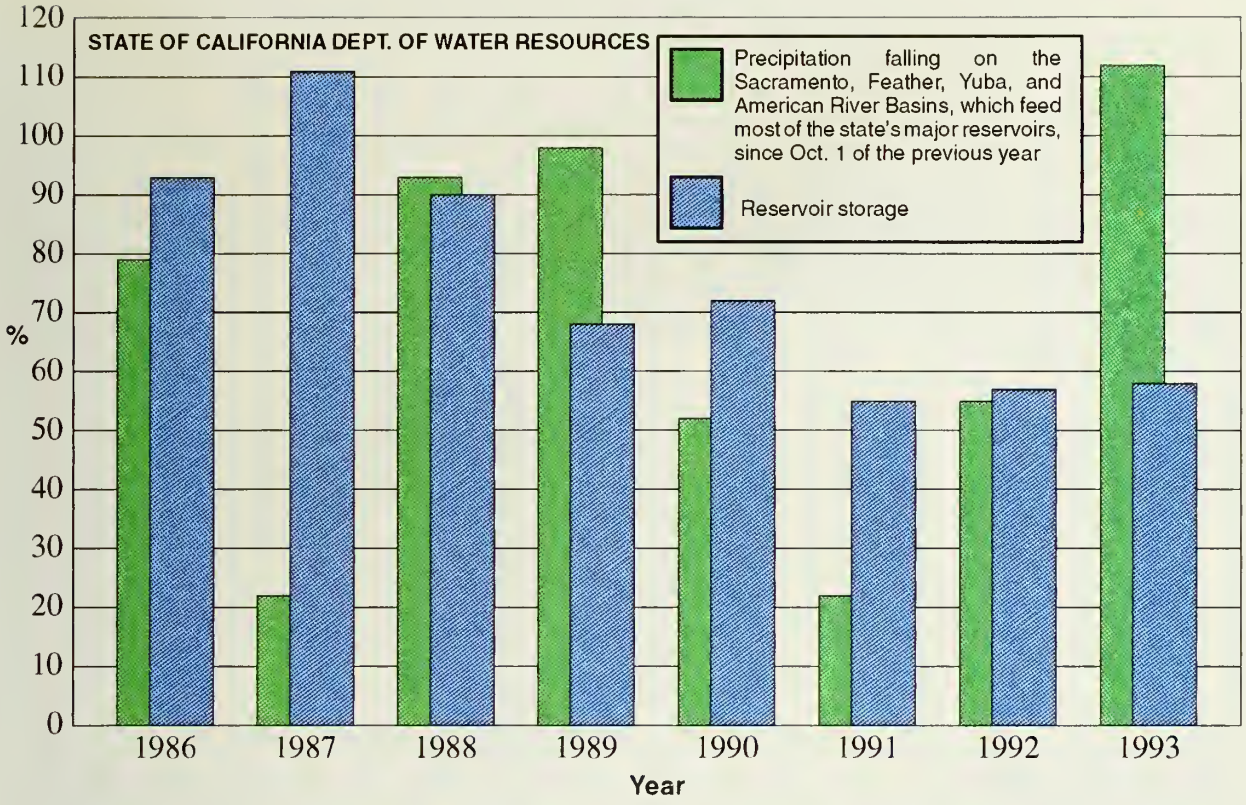

Fig. 62. Water year percent of normal precipitation in major river basins and percent of normal reservoir storage in 155 primary California reservoirs as of January 1.

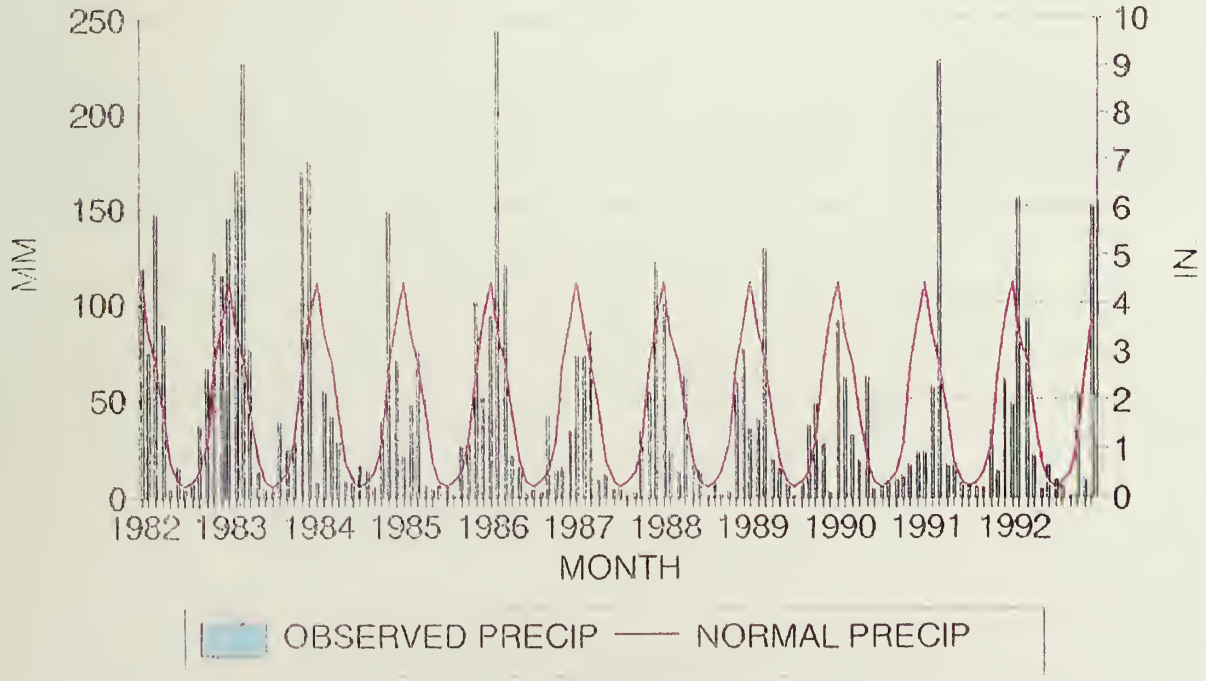

Fig. 63. Observed vs. normal monthly precipitation averaged over California. (Source: NCDC)

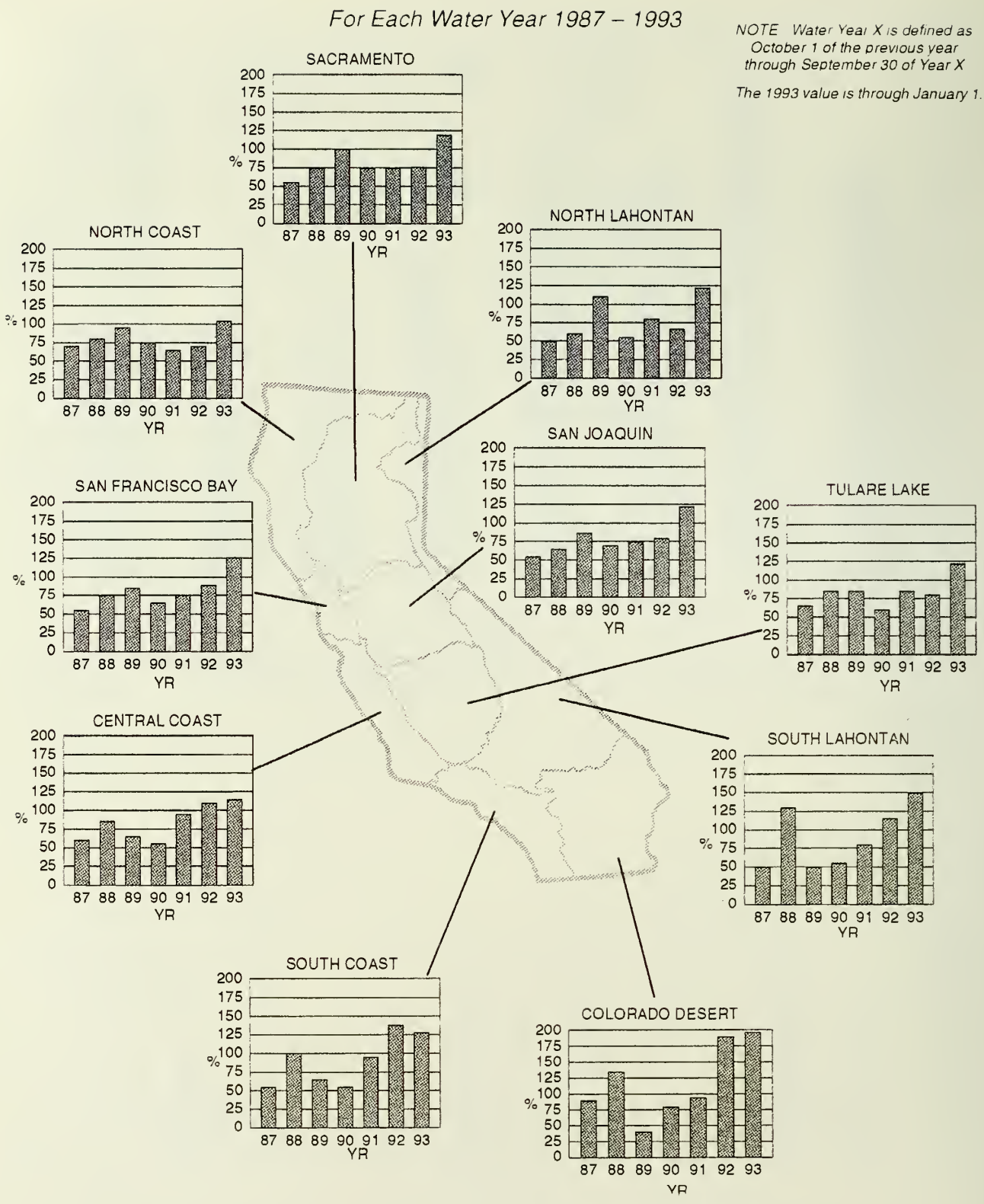

Fig. 64. Percent of normal precipitation across California averaged by hydrologic region for each water year (October - September) 1987 - 1993. 1993 value is through January 1.

7. CRYOSPHERE

a. Snow Cover

During the period of satellite observations (1966 to the present), Northern Hemisphere snow cover area has generally been anti-correlated with Northern Hemisphere surface land temperatures. This relationship also held for the year 1992, which was characterized by slightly positive temperature anomalies and below normal snow cover extent over the Northern Hemisphere.

A slightly more complex picture emerges if the year is split in two. The first half of the year, January through June 1992, represents snow cover conditions at the end of the 1991/92 snow season (**Fig. 65**). The 1992 January through June period was the seventh in a row to exhibit below normal snow cover area for North America and fifth consecutive snow-deficit season over Eurasia. Thus, this pattern is consistent with the observed tendency for anti-correlation between surface temperature anomalies, which were slightly above normal, and snow cover anomalies.

On the other hand, even though the global land surface temperatures for the second half of 1992 were slightly negative, above normal snow cover for the July to December period was present only over North America (**Fig. 66**). Eurasian snow cover remained slightly below normal during the relatively cold July through December half of the year.

b. Sea ice

After exhibiting a period of extreme variability early in the record, the fluctuations in Antarctic sea ice area have been extremely small over the past several years including 1992 (**Fig. 67**, top). Examinations of the sea ice areas in the "ice factories" of the Weddell and Ross Seas (not shown) show some tendency for increased sea ice area in the Weddell Sea and less than average ice area coverage in the Ross Sea during 1992.

In contrast, the Arctic sea ice has continued to show relatively large year-to-year excursions in area (**Fig. 67**, bottom). The largest relative variations in area tend to occur during the latter half of the year. In general, the Arctic sea ice area has been below average for most of the past two years prior to mid-1992, when the anomalies became positive. This suggests a slight tendency for anti-correlation between Arctic sea ice area and Northern Hemisphere surface temperature over the past two years.

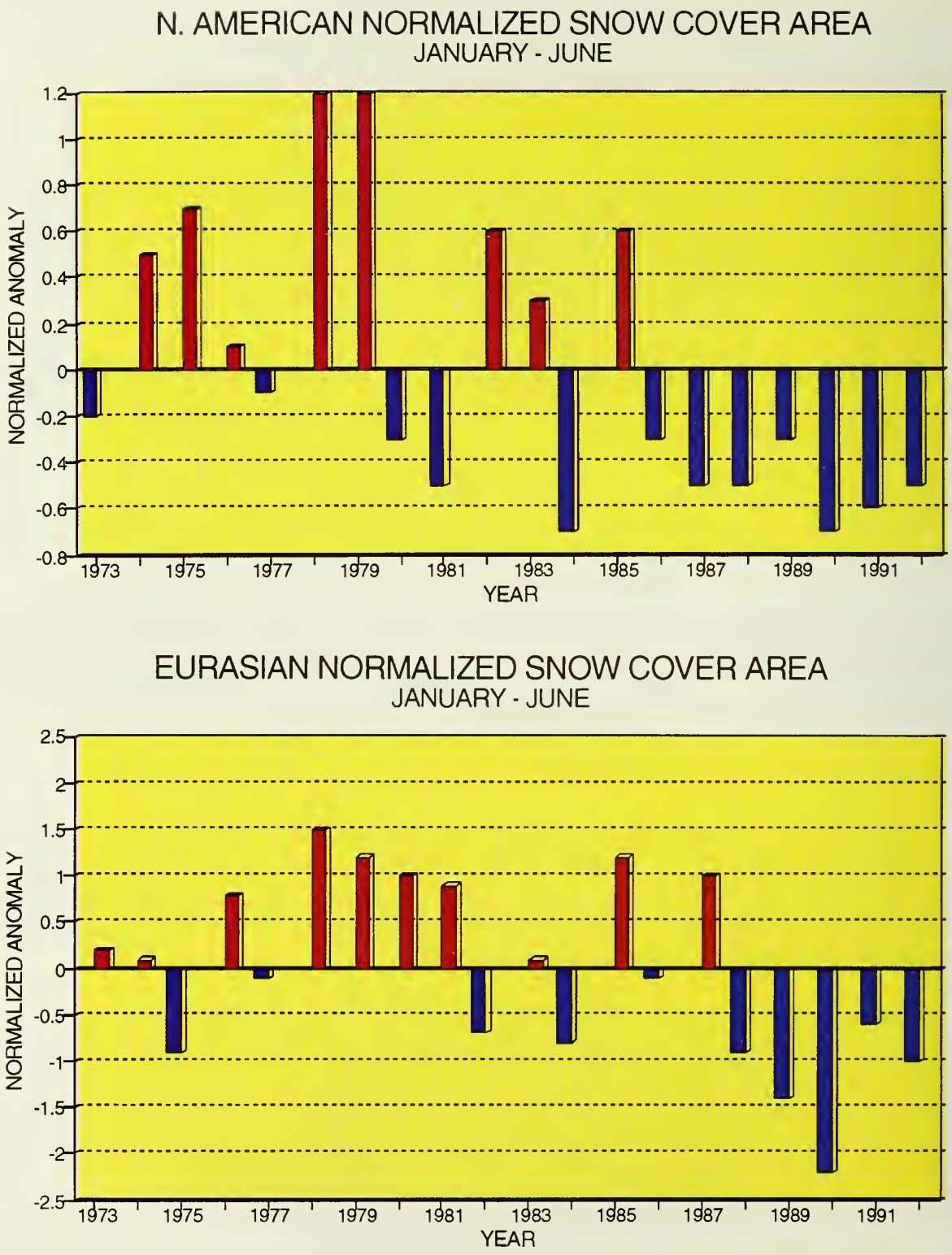

Fig. 65. Time series of normalized North American (top) and Eurasian (bottom) snow cover area for the January - June period derived from satellite data. Snow area values are normalized by the 1973-1992 base period.

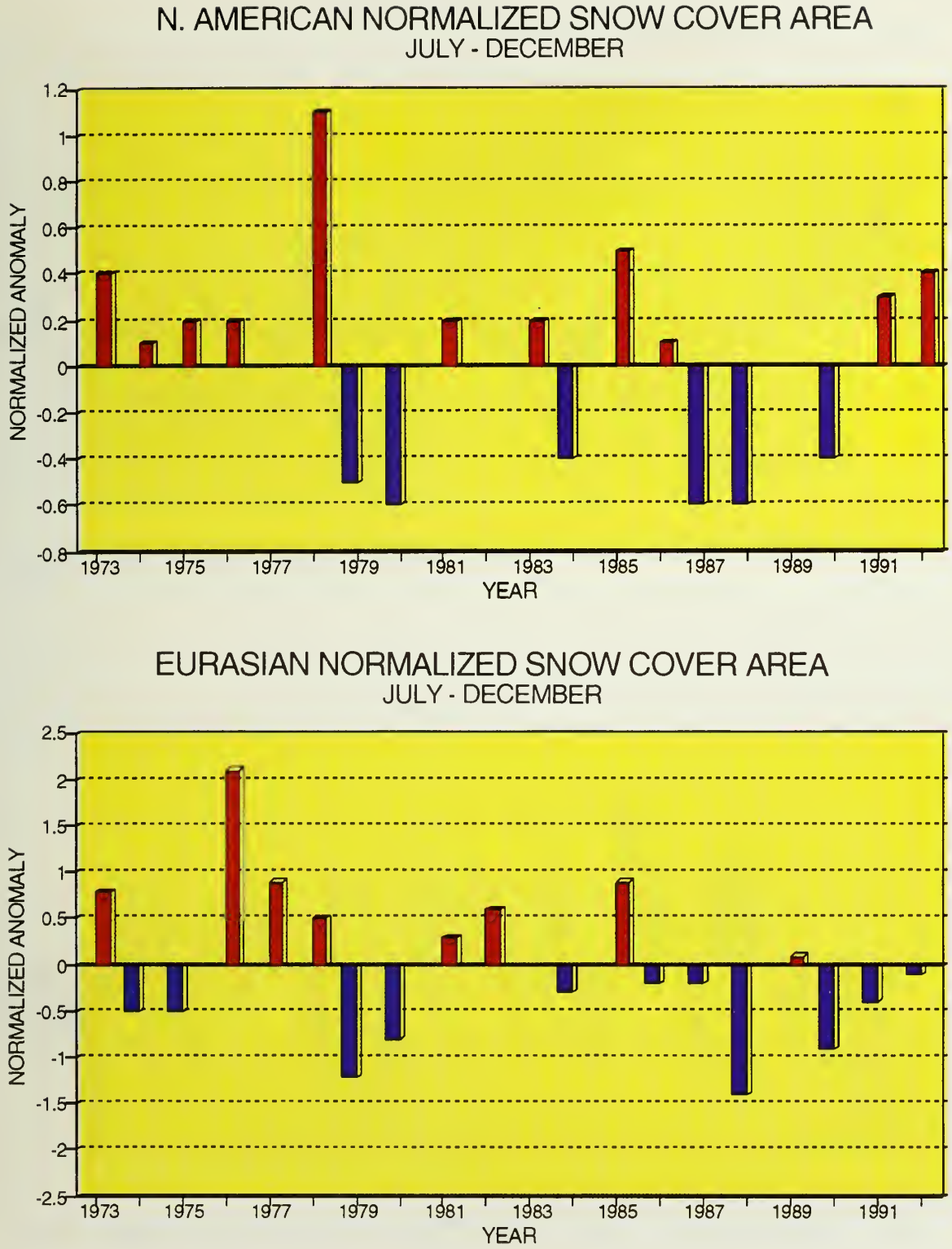

Fig. 66. Time series of normalized North American (top) and Eurasian (bottom) snow cover area for the July - December period derived from satellite data. Snow area values are normalized by the 1973-1992 base period.

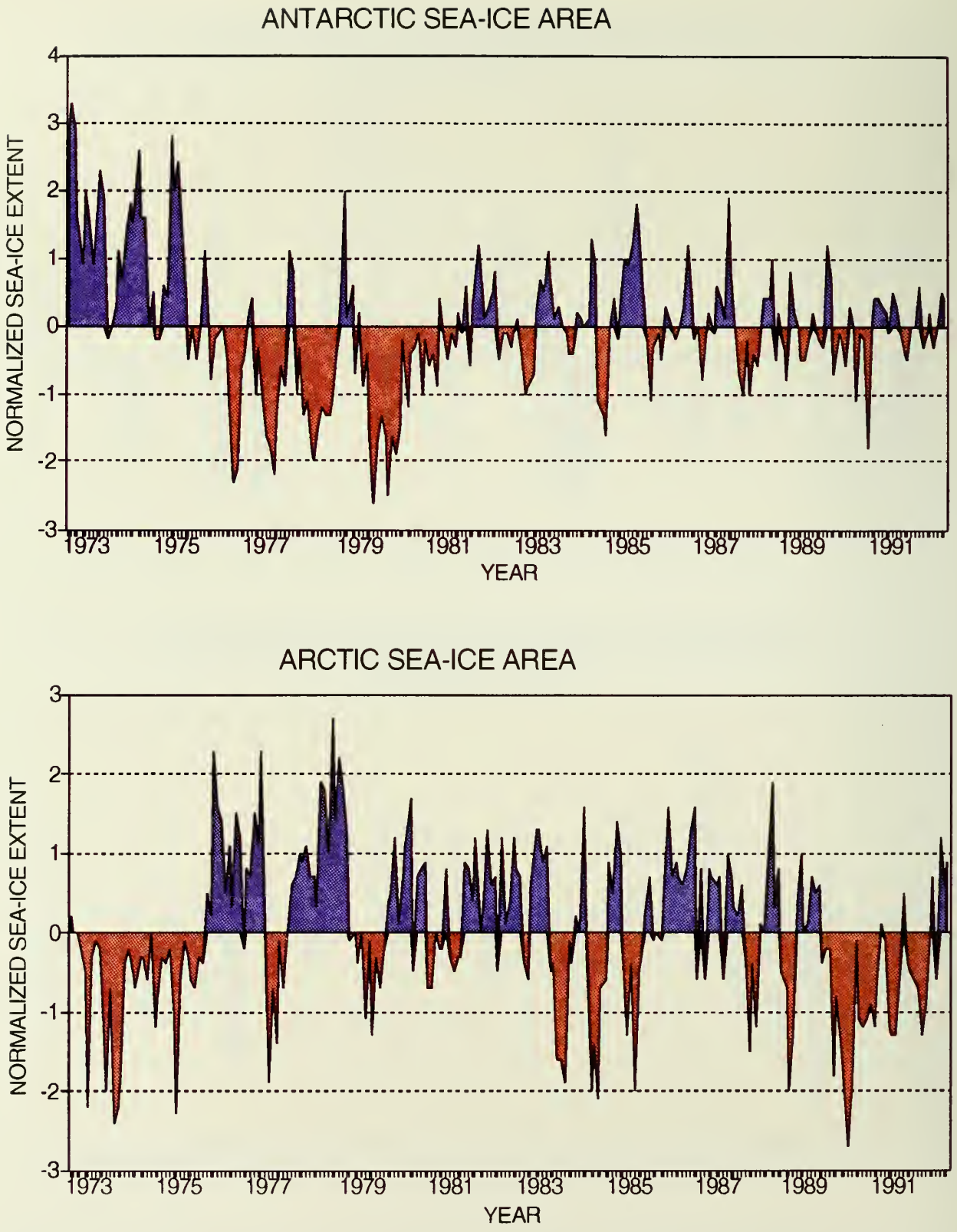

Fig. 67. Time series of normalized monthly Antarctic (top) and Arctic (bottom) sea ice area. Sea ice area is normalized by the 1973-1992 base period.

8. MAJOR SURFACE CLIMATE ANOMALIES

1. Western North America: MILD AND DRY WEATHER DOMINATES

Exceptionally mild conditions prevailed across much of western North America, especially the Pacific Northwest and southwestern Canada, during the first five months of the year. Below normal precipitation totals established a sixth consecutive year of drought across northern California, southeastern Oregon, and portions of Nevada during the 1991-92 rainy season.

2. North America: UNUSUALLY COLD CONDITIONS

Temperatures were unseasonably cold in eastern Canada beginning in February, especially along southern Hudson Bay. Unusually cool conditions became more widespread around mid-year, covering the eastern half of the U.S. and much of southern and northwestern Canada and Alaska during the summer and fall.

3. Northern Bahamas, southern Florida, southern Louisiana, and western Hawaiian Islands: INTENSE HURRICANES CAUSE MUCH DAMAGE

During late August, Hurricane Andrew intensified into an extreme Category 4 storm before tracking through the northern Bahamas and southern Florida. The storm then moved into the eastern Gulf of Mexico while maintaining most of its strength, making a second U.S. landfall along the south-central Louisiana coast. In early September, Hurricane Iniki made landfall on Kauai, Hawaii, the strongest hurricane to affect Hawaii this century.

4. East-central South America: ABNORMALLY HIGH RAINFALL

Heavy rainfall produced severe flooding in portions of northern Argentina, and downpours caused flash flooding and mudslides in the western and northern suburbs of Rio de Janeiro in early January. May proved to be an exceptionally wet month, with rainfall exceeding 400 mm in northern Rio Grande do Sul and central Santa Catarina, Brazil.

5. Western South America: UNUSUALLY WARM; HEAVY RAINS IN CHILE

Unusually warm weather, with temperatures averaging as much as 5°C above normal, prevailed along the immediate Pacific Coast of northwestern South America during January-June. Rare heavy rains caused flash flooding in the desert regions of northern Chile.

6. Central and southern South America: TEMPERATURE EXTREMES IN AREA

During July-September, temperatures averaged around 2°C below normal in central South America, with departures reaching -7°C in southeastern Bolivia. In sharp contrast, weekly temperature departures up to +7°C occurred in late August in southern South America.

7. Europe, Middle East, southwestern Asia, and northern Africa: VERY COLD WINTER

A very cold Winter (December 1991-February 1992) in southern Europe and the Mideast was characterized by repeated invasions of cold air and heavy snow. Farther east, southwestern Asia also experienced a very cold winter. Well below normal temperatures also affected northern Africa.

8. Europe: HOT AND DRY WEATHER ENVELOPS CONTINENT

Unusually dry conditions affected Europe during summer. Much of the continent received less than half of normal late Spring and early Summer precipitation. During mid-August, weekly temperatures averaged up to 7°C above normal, with highs up to 39°C in parts of Germany.

9. Europe and northwestern Africa: AUTUMN STORMS AND EARLY-WINTER COLD

A series of strong storms in late September and early October brought heavy precipitation and hurricane-force winds to much of southwestern Europe and Great Britain. As autumn progressed, bitterly cold weather overspread northern Scandinavia and northwestern Russia in late October and persisted through mid-November.

10. Sahel Region: DRIER THAN NORMAL RAINY SEASON

Despite widespread abundant rainfall during late July and August, precipitation amounts over the Sahel were generally lower than normal. The driest conditions occurred in the far western part of the Sahel, where less than 75% of normal rainfall fell.

11. Southern Africa: WORST DROUGHT THIS CENTURY

A severe drought affected much of southern Africa during the 1991- 92 rainy season. The year began with an intensifying drought across the region, and brief late January rains failed to ease long-term deficits. Hot and dry weather persisted from February until May when the normal dry season commences.

12. Pakistan and western India: A DELAYED MONSOON ENDS WITH FLOODING

Although the early part of the monsoon season was abnormally dry, heavy late-season showers dropped widespread, abundant rains on much of central, northwestern, and southwestern India and much of Pakistan, easing early-season dryness, but causing severe flooding in portions of the aforementioned areas.

13. Sri Lanka and southern India: SEVERE DRYNESS ENVELOPS REGION

A severe drought affected Sri Lanka during the first three months of 1992, with moisture deficits approaching 360 mm by the end of March.

14. Eastern China and western Japan: HEAVY RAINS CAUSE WIDESPREAD FLOODING

Moderate to heavy February, March, and early April precipitation soaked much of eastern China, Taiwan, the Ryukyus, South Korea, and western Japan. Heavy rains caused severe flooding in Jiangxi, Guizhou, and Zhejiang provinces in southeastern China from mid-June to mid-July.

15. Interior southeastern China: PROLONGED SPELL OF VERY DRY WEATHER

Well below normal rainfall affected interior southeastern China during late summer and autumn. Much of Jiangxi, Hunan, eastern Guangxi and Guizhou, and southern Hubei provinces recorded under half of normal rainfall from mid-July through early October.

16. Southeast Asia: TROPICAL CYCLONES AND HEAVY RAINS PREVAIL

Between July and October, numerous typhoons and tropical storms brought heavy rains to parts of Vietnam, southern Japan, Taiwan, the northern Philippines and eastern China.

17. Western Pacific, southeast Asia, and the northern Philippines: VERY HOT AND DRY

Very hot weather dominated much of southeastern Asia and the northern Philippines during the spring, with temperatures averaging as much as 4°C above normal in parts of Myanmar and Thailand. In addition, tropical shower and thundershower activity was unusually quiet across the western Pacific and the Philippines during the first half of the year.

18. Northern and eastern Australia: EARLY DRYNESS, THEN HEAVY RAINS

The 1991-1992 rainy season in northern Australia started slowly as abnormal dryness covered northern and eastern portions of the continent. By February, however, heavier rains began to fall on the east-central and northeastern sections of the country. Unseasonably heavy rains fell across the region in mid-May, particularly in western Queensland and the eastern Northern Territory.

19. Southern and western Australia: UNUSUALLY WET, THEN UNSEASONABLY COLD.

Abnormally high precipitation dominated much of southern Australia from August through October. Between two and four times the normal amounts were measured in northwestern Victoria and much of southern South Australia during the period. During November and December, southwestern Australia experienced much below normal temperatures.

20. New Zealand: VERY DRY CONDITIONS REPORTED.

In New Zealand, four months (mid-February to mid-June) of abnormally low precipitation (45-85% of normal) created deficits of 75- 250 mm throughout the nation.

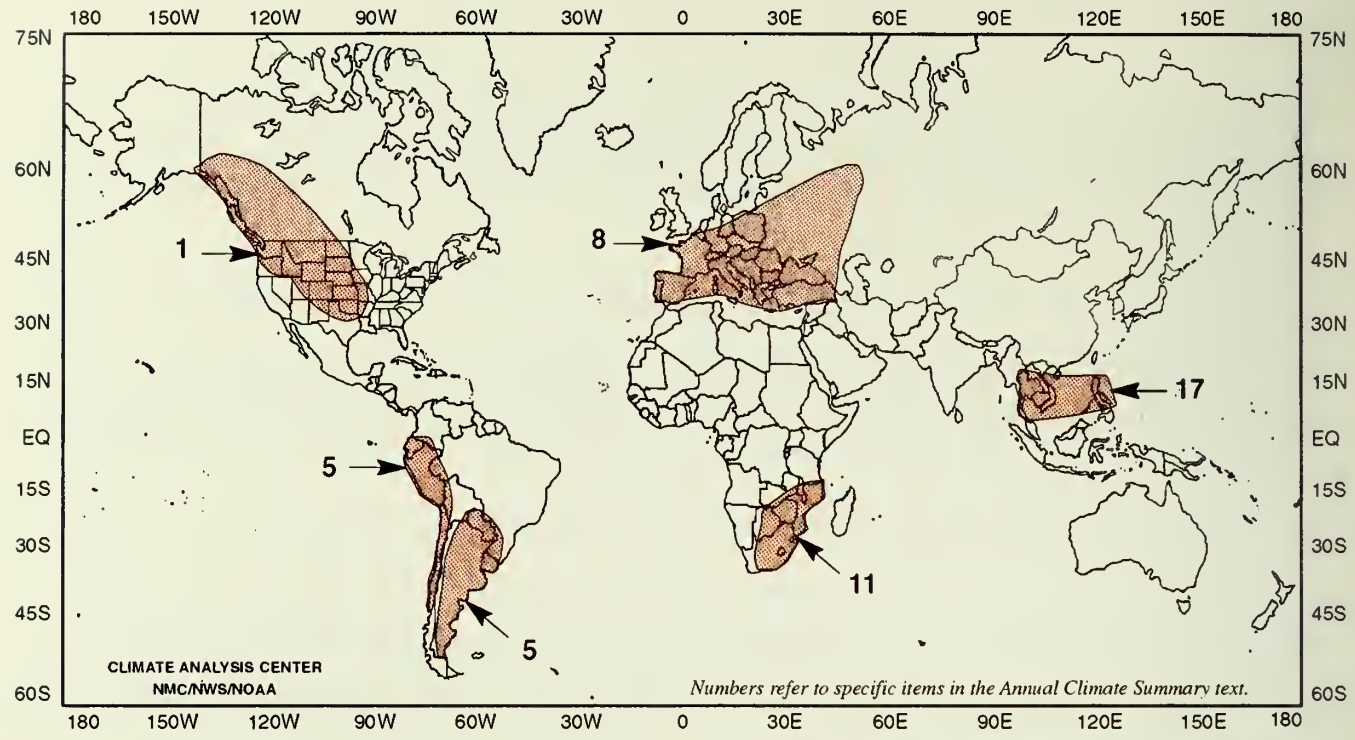

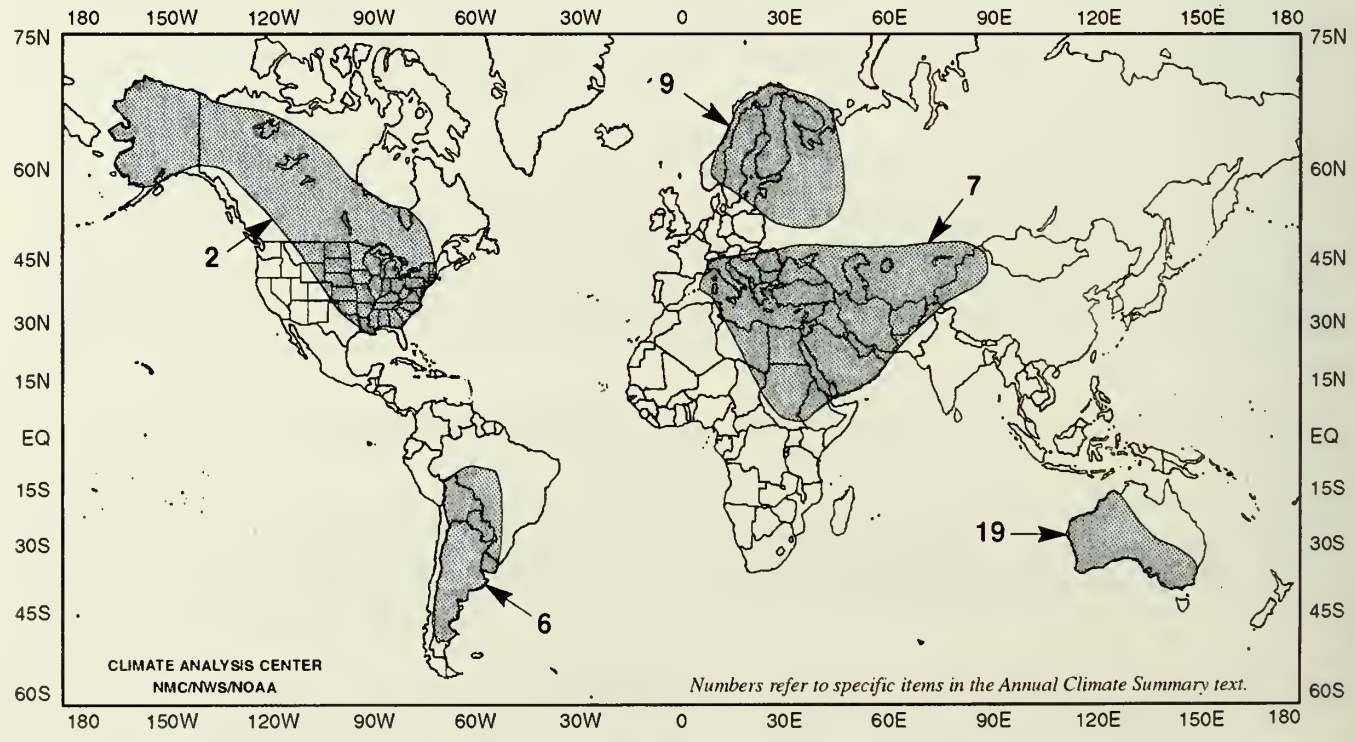

Fig. 68. Significant above normal temperature anomalies (top) and below normal temperatures anomalies (bottom) during 1992. (Source: CAC)

SIGNIFICANT ABOVE NORMAL PRECIPITATION ANOMALIES DURING 1992

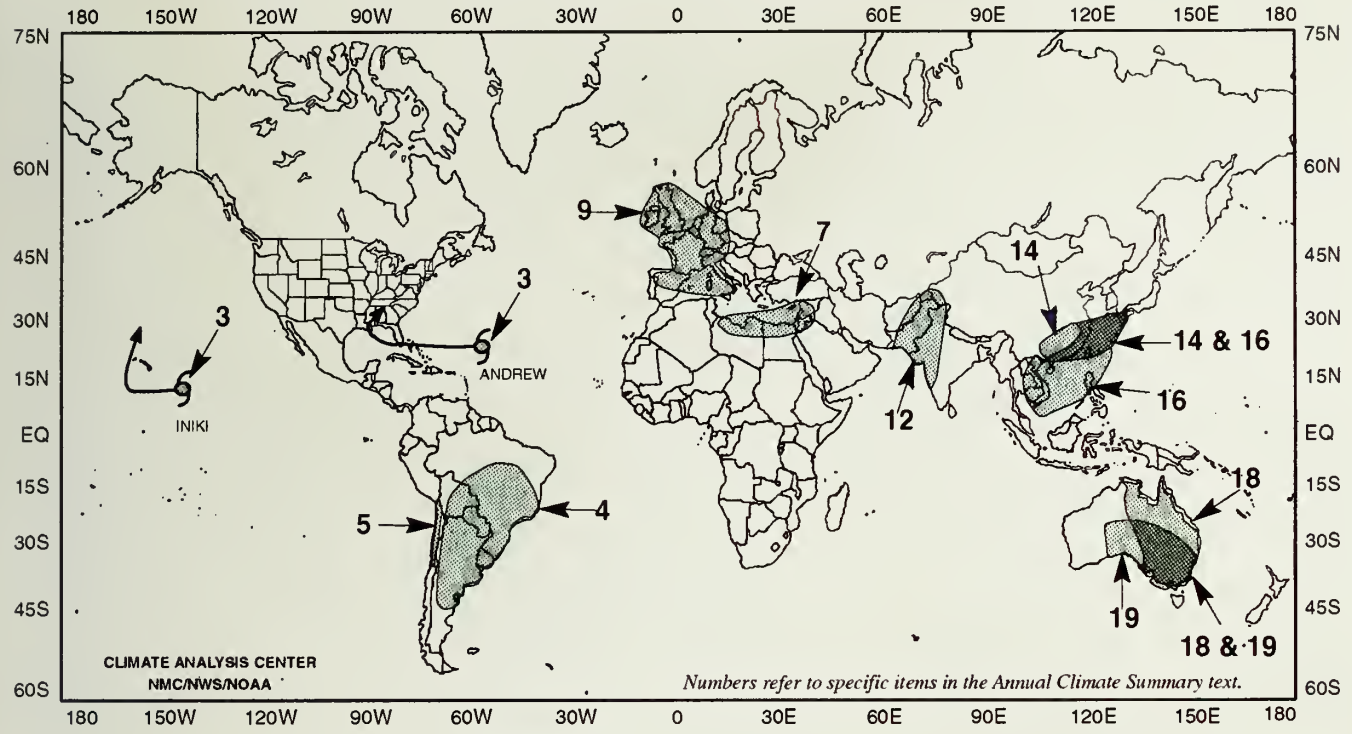

SIGNIFICANT BELOW NORMAL PRECIPITATION ANOMALIES DURING 1992

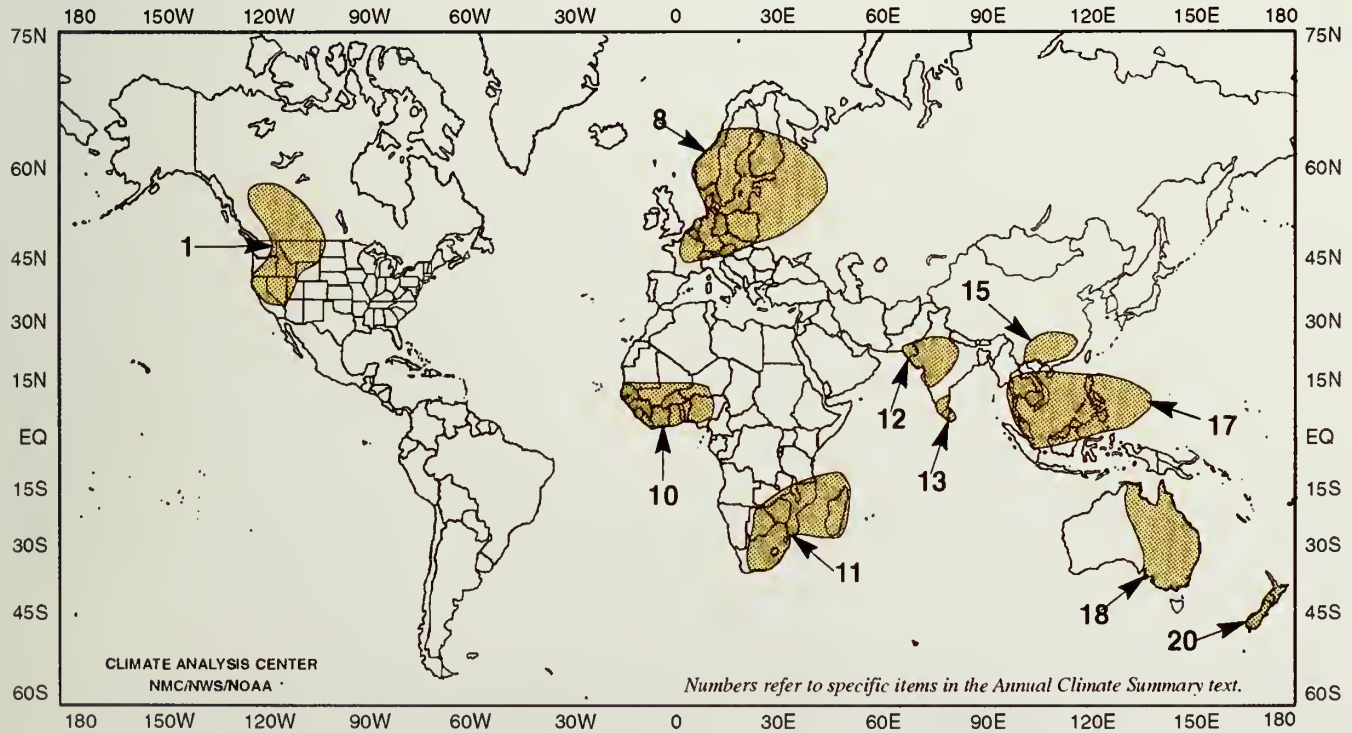

Fig. 69. Significant above normal precipitation anomalies (top) and below normal precipitation anomalies (bottom) during 1992. (Source: CAC)

REFERENCES

Angell, J., 1990: Variations in global tropospheric temperature after adjustment for the El Niño influence, 1958-1989. **J. Geophys. Res. Letters, 17,** 1093-1096.

Arkin, P.A. and B.N. Meisner, 1987: The relationship between large-scale convective rainfall and cold cloud over the western hemisphere during 1982-1984. **Mon. Wea. Rev., 115,** 51-74.

Ellis, H. T. and R. F. Pueschel, 1971: Solar radiation: Absence of air pollution trends at Manua Loa, **Science, 172,** 845-846.

Halpert, M. S. and C. F. Ropelewski [Eds.], 1991, Climate Assessment: A Decadal Review, 1981-1990. [U. S. Govt. Printing Office: 1991 - 281-557/40426], 109 pp.

Halpert, M. S. and C. F. Ropelewski [Eds.], 1992, Third Annual Climate Assessment: 1991. [U. S. Govt. Printing Office: 1992], 74 pp.

Janowiak, J.E. and P.A. Arkin, 1991: Rainfall variations in the tropics during 1986-1989, as estimated from observations of cloud-top temperature. **J. Geophys. Res., 96,** 3359-3373.

Keeling, C. D., R. B. Bacastow, and T. P. Whorf, 1982: Measurements of the concentration of carbon dioxide at Manua Loa Observatory, Hawaii. **Carbon Dioxide Review: 1982,** [W. C. Clark, Ed.], Oxford University Press, New York, pp. 377-385.

Klein, W. H., 1983: Objective specification of monthly mean surface temperature from mean 700 mb heights in winter. **Mon. Wea. Rev., 111,** 674-691.

Ropelewski, C.F. and M.S. Halpert, 1987: Global and regional scale precipitation patterns associated with the El Niño/Southern Oscillation. **Mon. Wea. Rev., 115,** 1606-1626.

Spencer, R. W. and J. R. Christy, 1992: Precision and radiosonde validation of satellite gridpoint temperature anomalies. Part II: A tropospheric retrieval and trends during 1979-1990, **J. of Clim., 5,** 858-866.

Steele, L. P., E. J. Dlugokencky, P. M. Lang, P. P. Tans, R. C. Martin, and K. A. Masarie, 1992: Slowing down of the global accumulation of atmospheric methane during the 1980s. **Nature, 358,** 313-316.

Thoning, K. W., P. P. Tans, and W. D. Komhyr, 1989: Atmospheric carbon dioxide at Manua Loa Observatory 2. Analysis of the NOAA/GMCC data, 1974-1985. **Journal of Geophysical Research, 94,** 8549-8565.